

Chapter 5

Electron Collisions with Atoms and Ions

In this chapter we commence our discussion of multichannel R -matrix theory by considering its application in the study of low-energy electron collisions with atoms and atomic ions. As well as describing an important application of the theory, this chapter provides an introduction to the basic concepts of multichannel R -matrix theory which will be applied in later chapters to a wide range of other atomic, molecular and optical collision processes. We restrict our consideration in this chapter to low-energy electron collisions, where only elastic scattering and excitation processes are energetically allowed or play a significant role in the collision process. We consider electron collisions with atoms and atomic ions at intermediate energies, which range from close to the ionization threshold to several times this threshold, in [Chap. 6](#).

We introduce multichannel R -matrix theory in [Sect. 5.1](#) by considering first electron collisions with light multi-electron atoms and atomic ions where an accurate representation of the collision process can be obtained by solving the time-independent non-relativistic Schrödinger equation. We commence in [Sect. 5.1.1](#) with a general introduction to R -matrix theory describing the partitioning of configuration space adopted in this theory. We then give a brief overview of the computer programs that have been developed to implement this theory, where we mention further developments of these programs to include relativistic effects which can be described using the Breit–Pauli Hamiltonian. In the rest of this section we describe in detail the solution of the Schrödinger equation, first in an internal region in [Sect. 5.1.2](#), then in an external region in [Sect. 5.1.3](#) and finally in an asymptotic region in [Sect. 5.1.4](#), yielding the K -matrix and S -matrix from which the collision cross sections can be determined.

In [Sect. 5.2](#), we derive a variational principle for the R -matrix defined on the boundary of the internal region. We consider explicitly low-energy electron collisions with atoms and atomic ions although the variational principle that we obtain will be applicable for any multichannel collision process which can be described in the internal region by coupled second-order integrodifferential equations. In [Sect. 5.3](#) we consider methods for determining zero-order radial continuum basis orbitals which represent the scattered electron in the expansion of the total wave function in the internal region. We also discuss methods for calculating corrections

to the R -matrix and wave function. We consider first in Sect. 5.3.1 an approach using basis orbitals which satisfy homogeneous boundary conditions on the surface of the internal region. We then show in Sect. 5.3.2 that when the radial continuum basis orbitals satisfy homogeneous boundary conditions a Buttler correction to the R -matrix must be included to obtain accurate results. We also discuss how a Buttler-type correction to the wave function near the boundary of the internal region can be calculated, which may be required in some applications. In Sect. 5.3.3, we summarize methods for determining analytic continuum basis orbitals which satisfy arbitrary boundary conditions on the surface of the internal region, where these methods have been reviewed in Sect. 4.4. In recent years these basis orbitals have found increasing use in many applications of R -matrix theory, ranging from electron collisions with atoms and molecules to photoionization and multiphoton ionization processes. Then, in Sect. 5.3.4 we describe a partitioned R -matrix method where the calculation of the R -matrix is sub-divided into two parts: a low-energy part which is accurately determined and a high-energy part for which an approximation is derived which enables much larger problems to be treated.

Next, in Sect. 5.4 we consider electron collisions with atoms and ions with higher nuclear charge number Z where relativistic effects must be included in the calculation. Initially as Z increases these effects are small and in this case the collision calculation can first be carried out in $LS\pi$ -coupling, using the non-relativistic Hamiltonian. The K -matrices, obtained from this calculation, are then recoupled to give K -matrices, cross sections and collision strengths including relativistic effects. We consider this approach in Sect. 5.4.1. Then as the nuclear charge number Z increases further, relativistic effects must be included in both the target wave function and the collision wave function. Provided Z is not too large, this can be achieved by replacing the non-relativistic Hamiltonian in these calculations by the Breit-Pauli Hamiltonian. We consider this approach in Sect. 5.4.2. Next, in Sect. 5.4.3, we consider a frame-transformation theory approach where relativistic effects are omitted, or only partly included, in the internal region with considerable saving in computational effort. However, for the heaviest atomic targets it is necessary to treat both the target and the collision wave functions using the Dirac Hamiltonian. We consider this approach in Sect. 5.5 where we follow our analysis of non-relativistic collisions, in Sect. 5.1, by considering the solution in internal, external and asymptotic regions in turn, enabling the K -matrix, S -matrix and cross sections to be determined.

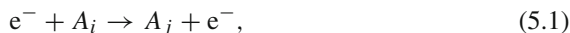
Finally, in Sect. 5.6 we describe the results of some representative low-energy electron-atom and electron-ion collision calculations.

5.1 Multichannel R -Matrix Theory

In this section we introduce R -matrix theory by considering low-energy electron collisions with multi-electron atoms and ions which are accurately described by the non-relativistic Schrödinger equation.

5.1.1 Introduction and Computer Programs

We consider the following low-energy electron collision process:



where A_i and A_j are the initial and final bound states of the target atom or ion which we assume contains N electrons and has nuclear charge number Z . For light atoms and ions this process can be accurately described by the time-independent Schrödinger equation

$$H_{N+1}\Psi = E\Psi, \quad (5.2)$$

where Ψ is the collision wave function and H_{N+1} is the non-relativistic Hamiltonian defined in atomic units by

$$H_{N+1} = \sum_{i=1}^{N+1} \left(-\frac{1}{2} \nabla_i^2 - \frac{Z}{r_i} \right) + \sum_{i>j=1}^{N+1} \frac{1}{r_{ij}}. \quad (5.3)$$

In this equation we have taken the origin of coordinates to be the target nucleus, which we assume has infinite mass, and we have written $r_{ij} = |\mathbf{r}_i - \mathbf{r}_j|$ where \mathbf{r}_i and \mathbf{r}_j are the vector coordinates of the i th and j th electrons.

In order to solve (5.2), and the corresponding equations in relativistic R -matrix theory discussed in Sects. 5.4 and 5.5, the theory commences, as briefly discussed in our introduction to Chap. 4, by partitioning configuration space into an internal region, an external region and an asymptotic region as shown in Fig. 5.1. The three regions are separated, as shown in this figure, by spheres of radius $r = a_0$ and a_p which are centered on the target nucleus where r is the radial coordinate of the scattered electron. We now consider the calculation of the solutions in each of these regions in turn.

In the internal region $0 \leq r \leq a_0$, where r is the radial coordinate of the scattered electron relative to the target nucleus, electron exchange and electron–electron

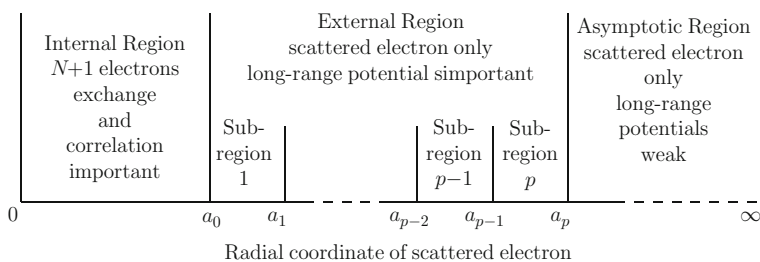


Fig. 5.1 Partitioning of configuration space in R -matrix theory of electron–atom and electron–ion collisions

correlation effects between the scattered electron and the N electrons in the target are important and the $(N + 1)$ -electron collision complex behaves in a similar way to a bound state. Consequently, a configuration interaction expansion of this complex, similar to that used in Sect. 2.2 for target eigenstates and pseudostates, is adopted. We discuss the solution in this region in Sect. 5.1.2 and we consider the continuum basis orbitals which are used to represent the scattered electron in this region in Sect. 5.3.

In the external region $a_0 \leq r \leq a_p$, electron exchange and correlation effects between the scattered electron and the target are negligible if the radius a_0 of the sphere is chosen, as discussed in Sect. 2.3.2, so that the charge distributions of the target eigenstates and pseudostates retained in the configuration interaction expansion in the internal region are negligible for $r \geq a_0$. This is achieved if we choose the radius a_0 so that

$$P_{n\ell}(r) \approx 0, \quad r \geq a_0, \quad (5.4)$$

where the $P_{n\ell}(r)$ are the reduced radial physical and pseudo-orbitals used to construct the target eigenstates and pseudostates. With this definition, the scattered electron then moves in the external region in the long-range multipole potential of the target, defined by (2.73) and (2.74), and the corresponding reduced radial wave functions describing the motion of this electron satisfy the coupled second-order differential equations (2.76). The solution in this region can be obtained by sub-dividing it into p sub-regions, as illustrated in Fig. 5.1, and using a standard method for solving ordinary coupled second-order differential equations. We discuss the solution in the external region in Sect. 5.1.3 and we consider R -matrix and log-derivative methods for propagating the solution of these equations across the p sub-regions in Appendix E.

Finally, in the asymptotic region $r \geq a_p$, the solution is represented by an asymptotic expansion where a_p is chosen large enough that the expansion yields accurate results on this boundary. We show how the solution can be fitted to this expansion at $r = a_p$ in Sect. 5.1.4, yielding the K -matrix, S -matrix and cross sections and we consider asymptotic expansion methods in Appendix F.1.

Hence we see that by a suitable choice of radii a_0 and a_p , the wave function in the internal, external and asymptotic regions have very different properties and thus it is appropriate both from a physical and from a computational point of view to obtain the solutions in these regions independently and then to link these solutions by the R -matrix on their common boundaries. It is also important to appreciate that this sub-division of configuration space is appropriate even in the presence of long-range Coulomb potentials, since electron exchange and correlation effects are confined to a volume defined by the range of the target states and pseudostates included in the calculation which decay exponentially at large distances.

To conclude this introductory section we briefly summarize in Fig. 5.2 the computer programs developed to obtain accurate target states and electron–atom and electron–ion phase shifts and collision cross sections, when relativistic effects are either not important or can be accurately described using the Breit–Pauli

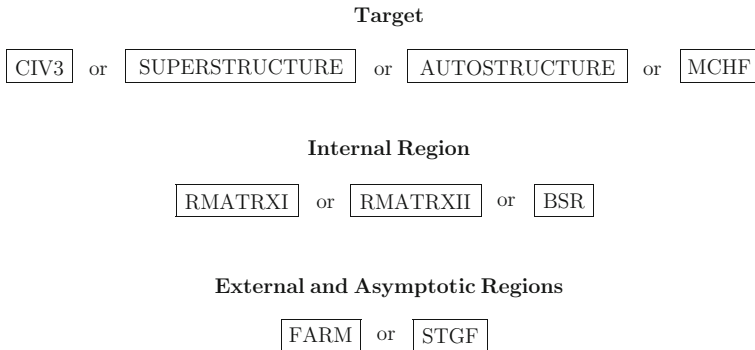


Fig. 5.2 Computer programs which have been developed and used in R -matrix electron–atom and electron–ion collision calculations classified into three stages corresponding to (i) target state calculations; (ii) internal region calculations yielding the R -matrix on the boundary $r = a_0$; (iii) external and asymptotic region calculations yielding the K -matrix, S -matrix and collision cross sections

Hamiltonian, discussed in Sect. 5.4.2. We will briefly summarize the corresponding computer programs used when the solution of the Dirac equation is appropriate in Sect. 5.5.1.

In the first stage of the calculation shown in Fig. 5.2 we mention four programs that have been written to obtain accurate target state energies and wave functions, which are used in the following stages of the R -matrix calculations. These are

- i. CIV3 written by Hibbert [464] and extended by Glass and Hibbert [381, 383]
- ii. SUPERSTRUCTURE written by Eissner et al. [290]
- iii. AUTOSTRUCTURE written by Badnell [30, 31], which incorporates SUPERSTRUCTURE
- iv. MCHF written by Froese Fischer et al. [344–350].

An important component of these atomic structure calculations are general programs to calculate angular integrals written by Hibbert and Froese Fischer [463, 466].

In the second stage of the calculation shown in Fig. 5.2 we mention three programs written to solve the electron–atom collision problem in the R -matrix internal region shown in Fig. 5.1. These are

- i. RMATRXI written by Berrington et al. [95, 98] and extended to include relativistic effects using the Breit–Pauli Hamiltonian by Scott and Burke [843], Scott and Taylor [844] and Berrington et al. [102]. A parallel version of RMATRXI has been developed by Mitnik et al. [654, 655] which is summarized by Ballance and Griffin [43], and a no-exchange program RMATRX NX has been developed by V.M. Burke et al. [192], which enables R -matrix calculations at higher energies and for higher angular momenta to be carried out efficiently.
- ii. RMATRXII written by Burke et al. [185], which extended the procedure adopted in RMATRXI for evaluating the angular integrals. Relativistic effects

are not included in RMATRIXII. Instead, an extra stage FINE, transforms the non-relativistic R -matrix surface amplitudes calculated on the internal region boundary $r = a_0$ to include relativistic fine-structure effects, ready for the inclusion of these effects in the external region calculation.

- iii. BSR written by Zatsariny [992], which includes relativistic effects using the Breit–Pauli Hamiltonian. It describes the target states using non-orthogonal term-dependent orbitals and represents the bound and continuum orbitals by expansions in B-splines, discussed in Sect. 4.4.7.

In the third stage of the calculation shown in Fig. 5.2 we mention two programs that have been written to solve the electron–atom collision problem in the R -matrix external and asymptotic regions shown in Fig. 5.1. These are

- i. FARM, written by V.M. Burke and Noble [191], which uses R -matrix propagator methods, discussed in Appendices E.1 and E.3. A parallel version of FARM (PFARM) has been developed by Sunderland et al. [896] as part of the electron–atom and electron–ion collision program PRMAT which combines PFARM with the internal region program RMATRIXII.
- ii. STGF, written by Seaton [860], which calculates solutions which are correct to second order in the long-range potentials. A parallel version PSTGF which runs on massively parallel computers has been developed by Mitnik et al. [654].

These programs enable the K -matrix, S -matrix and hence collision cross sections to be determined.

5.1.2 Internal Region Solution

We consider first the solution of the non-relativistic Schrödinger equation (5.2) in the internal region defined in Fig. 5.1 for each set of conserved quantum numbers Γ defined by (2.58). The R -matrix expansion of the collision wave function Ψ in this region at a total energy E takes the form

$$\Psi_{jE}^{\Gamma}(\mathbf{X}_{N+1}) = \sum_{k=1}^{n_t} \psi_k^{\Gamma}(\mathbf{X}_{N+1}) A_{kj}^{\Gamma}(E), \quad (5.5)$$

where j labels the linearly independent solutions of (5.2), ψ_k^{Γ} are energy-independent basis functions and $A_{kj}^{\Gamma}(E)$ are energy-dependent expansion coefficients, which depend on the asymptotic boundary conditions satisfied by the wave function Ψ_{jE}^{Γ} at the energy E . Following our discussion in Sect. 2.3, we expand the basis functions ψ_k^{Γ} in an R -matrix expansion, which has the same general form as the close coupling with pseudostates expansion (2.57), which we write here as

$$\begin{aligned} \psi_k^\Gamma(\mathbf{X}_{N+1}) = & \mathcal{A} \sum_{i=1}^n \sum_{j=1}^{n_c} \bar{\Phi}_i^\Gamma(\mathbf{X}_N; \hat{\mathbf{r}}_{N+1} \sigma_{N+1}) r_{N+1}^{-1} u_{ij}^0(r_{N+1}) a_{ij}^\Gamma \\ & + \sum_{i=1}^m \chi_i^\Gamma(\mathbf{X}_{N+1}) b_{ik}^\Gamma, \quad k = 1, \dots, n_t, \end{aligned} \quad (5.6)$$

where n is the number of channels retained in the expansion, n_c is the number of radial continuum basis orbitals retained in each channel, m is the number of quadratically integrable functions and $n_t = nn_c + m$ is the total number of linearly independent basis functions in this expansion. The channel functions $\bar{\Phi}_i^\Gamma$ and the quadratically integrable functions χ_i^Γ in (5.6) are defined following (2.57) and do not need to be discussed further here except to note that condition (5.4) satisfied by the physical and pseudo-orbitals implies that these functions are negligible by the boundary $r = a_0$ of the internal region. However, the radial continuum basis orbitals $u_{ij}^0(r)$, $j = 1, \dots, n_c$ in (5.6), which replace the reduced radial functions $F_{ij}^\Gamma(r)$ in (2.57), are now defined only over the range $0 \leq r \leq a_0$. They represent the radial motion of the scattered electron in the internal region and are chosen to vanish at the origin and are in general non-zero on the boundary $r = a_0$ of the internal region, thus providing a link between the solutions in the internal and external regions. We will consider their explicit form in Sect. 5.3. Also we note that the coefficients b_{ik}^Γ multiplying the quadratically integrable functions in (5.6) are related to the corresponding coefficients in (2.57) through the expansion of the collision wave function Ψ_{jE}^Γ in terms of the basis functions ψ_k^Γ given by (5.5). Finally we determine the coefficients a_{ij}^Γ and b_{ik}^Γ in (5.6) by diagonalizing $H_{N+1} + \mathcal{L}_{N+1}$ in this basis as follows:

$$\langle \psi_k^\Gamma | H_{N+1} + \mathcal{L}_{N+1} | \psi_{k'}^\Gamma \rangle_{\text{int}} = E_k^\Gamma \delta_{kk'}, \quad k, k' = 1, \dots, n_t, \quad (5.7)$$

where \mathcal{L}_{N+1} is a Bloch operator [118], discussed below, and where the integration in this equation is carried out over the space and spin coordinates of all $N+1$ electrons and where the radial integrals are confined to the internal region.

The Bloch operator \mathcal{L}_{N+1} in (5.7) has been introduced, following our discussion in potential scattering in Sect. 4.2, since the kinetic energy operators $-\frac{1}{2}\nabla_i^2$, $i = 1, \dots, N+1$, in H_{N+1} are not hermitian over the internal region in the space of functions satisfying arbitrary boundary conditions on the surface of the sphere of radius $r = a_0$ enveloping this region. The appropriate Bloch operator which ensures that $H_{N+1} + \mathcal{L}_{N+1}$ is hermitian is defined by the equation

$$\mathcal{L}_{N+1} = \frac{1}{2} \sum_{i=1}^{N+1} \delta(r_i - a_0) \left(\frac{d}{dr_i} - \frac{b_0 - 1}{r_i} \right), \quad (5.8)$$

where, as in potential scattering, b_0 is an arbitrary constant which can depend on the channel of the scattered electron and which is set zero in most applications. We

can prove that $H_{N+1} + \mathcal{L}_{N+1}$ is hermitian in the internal region by showing that the following integral is zero:

$$\langle \psi^{(1)} | H_{N+1} + \mathcal{L}_{N+1} | \psi^{(2)} \rangle_{\text{int}} - \langle \psi^{(2)} | H_{N+1} + \mathcal{L}_{N+1} | \psi^{(1)} \rangle_{\text{int}} = 0, \quad (5.9)$$

where $\psi^{(1)}$ and $\psi^{(2)}$, which are defined over the internal region, are arbitrary quadratically integrable functions of the space and spin coordinates $\mathbf{x}_1, \dots, \mathbf{x}_{N+1}$ of the $N + 1$ interacting electrons which vanish at the origin and satisfy arbitrary boundary conditions on the surface $r = a_0$ of the internal region. Also in (5.9) the integrations are carried out over all $N + 1$ electronic space and spin coordinates, where the integration over radial coordinates r_i of the electrons is restricted to the internal region so that

$$0 \leq r_i \leq a_0, \quad i = 1, \dots, N + 1. \quad (5.10)$$

In the evaluation of (5.9) we have to consider radial integrals of the form

$$I = \int_0^{a_0} \left\{ r^{-1} v(r) \left[-\frac{1}{2r^2} \frac{d}{dr} r^2 \frac{d}{dr} + \frac{1}{2} \delta(r - a_0) \left(\frac{d}{dr} - \frac{b_0 - 1}{r} \right) \right] r^{-1} w(r) \right\} \times r^2 dr, \quad (5.11)$$

where $v(r)$ and $w(r)$ are arbitrary differentiable functions of r , which are quadratically integrable over the internal region and which vanish at the origin and satisfy arbitrary boundary conditions at $r = a_0$. Also the first term in the square brackets in (5.11) is the radial part of the kinetic energy operator $-\frac{1}{2} \nabla^2$. It is straightforward to show that (5.11) reduces to

$$I = \int_0^{a_0} v(r) \left[-\frac{1}{2} \frac{d^2}{dr^2} + \frac{1}{2} \delta(r - a_0) \left(\frac{d}{dr} - \frac{b_0}{r} \right) \right] w(r) dr. \quad (5.12)$$

It then follows that, as in potential scattering, see (4.32), the operator in square brackets in (5.12) is hermitian over the internal region for arbitrary b_0 and hence the integral I in (5.11) can be rewritten as

$$I = \int_0^{a_0} \left\{ r^{-1} w(r) \left[-\frac{1}{2r^2} \frac{d}{dr} r^2 \frac{d}{dr} + \frac{1}{2} \delta(r - a_0) \left(\frac{d}{dr} - \frac{b_0 - 1}{r} \right) \right] r^{-1} v(r) \right\} \times r^2 dr. \quad (5.13)$$

This shows that the operator in the square brackets in (5.11) and (5.13) is hermitian over the internal region and hence, from (5.9), that the operator

$$H_{N+1} + \mathcal{L}_{N+1} \quad (5.14)$$

is hermitian over the internal region.

We can now solve (5.2) in the internal region, for each set of conserved quantum numbers Γ and for each linearly independent solution labelled by j , by including the Bloch operator term $\mathcal{L}_{N+1}\Psi$ on both sides of this equation giving

$$(H_{N+1} + \mathcal{L}_{N+1} - E)\Psi_{jE}^\Gamma = \mathcal{L}_{N+1}\Psi_{jE}^\Gamma, \quad (5.15)$$

where the solution Ψ_{jE}^Γ corresponds to (5.5), (5.6) and (5.7). Equation (5.15) then has the formal solution in the internal region

$$\Psi_{jE}^\Gamma = (H_{N+1} + \mathcal{L}_{N+1} - E)^{-1} \mathcal{L}_{N+1}\Psi_{jE}^\Gamma. \quad (5.16)$$

The spectral representation of the Green's function $(H_{N+1} + \mathcal{L}_{N+1} - E)^{-1}$ in (5.16) can be obtained in terms of the R -matrix basis functions ψ_k^Γ defined by (5.6) and (5.7). Equation (5.16) then becomes

$$|\Psi_{jE}^\Gamma\rangle = \sum_{k=1}^{n_t} |\psi_k^\Gamma\rangle \frac{1}{E_k^\Gamma - E} \langle \psi_k^\Gamma | \mathcal{L}_{N+1} | \Psi_{jE}^\Gamma \rangle. \quad (5.17)$$

We then project (5.17) onto the n channel functions $\overline{\Phi}_i^\Gamma(\mathbf{X}_N; \hat{\mathbf{r}}_{N+1}\sigma_{N+1})$ and evaluate it on the boundary $r_{N+1} = a_0$ of the internal region. We find using (5.5) and (5.6) that the reduced radial wave functions $F_{ij}^\Gamma(r)$ describing the motion of the scattered electron in the i th channel at the energy E satisfy the equation

$$F_{ij}^\Gamma(a_0) = \sum_{i'=1}^n R_{ii'}^\Gamma(E) \left(a_0 \frac{dF_{i'j}^\Gamma}{dr} - b_0 F_{i'j}^\Gamma \right)_{r=a_0}, \quad i = 1, \dots, n, \quad (5.18)$$

where the elements of the R -matrix $R_{ii'}^\Gamma(E)$ are defined by

$$R_{ii'}^\Gamma(E) = \frac{1}{2a_0} \sum_{k=1}^{n_t} \frac{w_{ik}^\Gamma w_{i'k}^\Gamma}{E_k^\Gamma - E}, \quad i, i' = 1, \dots, n, \quad (5.19)$$

the functions $F_{ij}^\Gamma(r)$ are defined by

$$F_{ij}^\Gamma(r_{N+1}) = \langle r_{N+1}^{-1} \overline{\Phi}_i^\Gamma | \Psi_{jE}^\Gamma \rangle', \quad i = 1, \dots, n \quad (5.20)$$

and the surface amplitudes w_{ik}^Γ are defined by

$$\begin{aligned} w_{ik}^\Gamma &= \langle r_{N+1}^{-1} \overline{\Phi}_i^\Gamma | \psi_k^\Gamma \rangle'_{r_{N+1}=a_0} \\ &= \sum_{j=1}^{n_c} u_{ij}^0(a_0) a_{ij}^\Gamma, \quad i = 1, \dots, n, \quad k = 1, \dots, n_t. \end{aligned} \quad (5.21)$$

We can also write down an alternative expression for the reduced radial wave functions $F_{ij}^\Gamma(r)$ in the internal region by substituting for Ψ_{jE}^Γ from (5.5) into (5.20) giving

$$F_{ij}^\Gamma(r_{N+1}) = \sum_{k=1}^{n_t} \langle r_{N+1}^{-1} \bar{\Phi}_i^\Gamma | \psi_k^\Gamma \rangle' A_{kj}^\Gamma(E), \quad i = 1, \dots, n. \quad (5.22)$$

The primes on the Dirac brackets in (5.20), (5.21) and (5.22) mean that the integrations are carried out over the space and spin coordinates of all $N + 1$ electrons in the internal region, except the radial coordinate r_{N+1} of the scattered electron, where the r_{N+1}^{-1} factors in these and later integrands correspond to the r_{N+1}^{-1} factor on the right-hand side of (5.6). Also the number of linearly independent solutions, denoted by the subscript j in (5.18), (5.20) and (5.22), is discussed below.

Equations (5.18) and (5.19) are the basic equations describing electron collisions with atoms and atomic ions in the internal region. The R -matrix, defined by (5.19), is determined at all energies by a single diagonalization of $H_{N+1} + \mathcal{L}_{N+1}$ in (5.7) in the basis defined by (5.6) for each set of conserved quantum numbers Γ , which yields the surface amplitudes w_{ik}^Γ and the corresponding eigenenergies E_k^Γ . The logarithmic derivatives of the reduced radial wave functions $F_{ij}^\Gamma(r)$ on the boundary of the internal region are then given by (5.18). This equation provides the boundary condition for the solution of the electron-atom collision problem in the external region considered in the next section.

We consider next the determination of the reduced radial wave functions $F_{ij}^\Gamma(r)$, defined in the internal region by (5.20) and (5.22), and the full collision wave function $\Psi_{jE}^\Gamma(\mathbf{X}_{N+1})$, defined in the internal region by (5.5), which we will see are required in many applications. We first observe that while (5.20) defines $F_{ij}^\Gamma(r)$ for all r , it is only when the exchange and quadratically integrable functions in (5.6) are negligible, that $F_{ij}^\Gamma(r)$ has a simple form. This occurs in the external and asymptotic regions, discussed in Sects. 5.1.3 and 5.1.4, respectively, and near the boundary $r = a_0$ in the internal region. It follows from (5.5), (5.6) and (5.22) that near the boundary $r = a_0$ in the internal region, the expression for $F_{ij}^\Gamma(r)$ reduces to the following simple form:

$$F_{ij}^\Gamma(r) = \sum_{k=1}^{n_t} w_{ik}^\Gamma(r) A_{kj}^\Gamma(E), \quad i = 1, \dots, n, \quad r \lesssim a_0, \quad (5.23)$$

where the functions $w_{ik}^\Gamma(r)$ can be expanded in terms of the continuum basis orbitals $u_{ik}^0(r)$ in (5.6) by

$$w_{ik}^\Gamma(r) = \sum_{j=1}^{n_c} u_{ij}^0(r) a_{ijk}^\Gamma, \quad i = 1, \dots, n, \quad k = 1, \dots, n_t. \quad (5.24)$$

Comparing this result with (5.21) we see that $w_{ik}^\Gamma = w_{ik}^\Gamma(a_0)$. It follows that in order to determine $F_{ij}^\Gamma(r)$ near the boundary $r = a_0$ in the internal region and the full collision wave function $\Psi_{jE}^\Gamma(\mathbf{X}_{N+1})$ in the internal region, we have to determine the expansion coefficients $A_{kj}^\Gamma(E)$ in (5.5). This can be achieved by comparing (5.17) with (5.5) giving

$$A_{kj}^\Gamma(E) = \frac{1}{E_k^\Gamma - E} \langle \psi_k^\Gamma | \mathcal{L}_{N+1} | \Psi_{jE}^\Gamma \rangle, \quad k = 1, \dots, n_t. \quad (5.25)$$

We then substitute in this equation for ψ_k^Γ from (5.6) and for the Bloch operator \mathcal{L}_{N+1} from (5.8). We also use the result

$$\Psi_{jE}^\Gamma(\mathbf{X}_{N+1}) = \sum_{i=1}^n \bar{\Phi}_i^\Gamma(\mathbf{X}_N; \hat{\mathbf{r}}_{N+1} \sigma_{N+1}) r_{N+1}^{-1} F_{ij}^\Gamma(r_{N+1}), \quad r_{N+1} = a_0, \quad (5.26)$$

which follows from (5.20). Equation (5.25) then reduces to

$$A_{kj}^\Gamma(E) = \frac{1}{2a_0(E_k^\Gamma - E)} \sum_{i=1}^n w_{ik}^\Gamma \left(a_0 \frac{dF_{ij}^\Gamma}{dr} - b_0 F_{ij}^\Gamma \right)_{r=a_0}, \quad k = 1, \dots, n_t. \quad (5.27)$$

We see from this equation that in order to determine the expansion coefficients $A_{kj}^\Gamma(E)$ we have to determine dF_{ij}^Γ/dr and $F_{ij}^\Gamma(r)$ on the boundary $r = a_0$ of the internal region. This is achieved by solving the relevant coupled second-order differential equations in the external and asymptotic regions, as discussed in Sects. 5.1.3 and 5.1.4, respectively, subject to the R -matrix boundary condition at $r = a_0$ defined by (5.18) and (5.19). These solutions can be combined to yield the relevant asymptotic boundary conditions, enabling $A_{kj}^\Gamma(E)$ to be determined. We will see that the number of linearly independent solutions labelled by j depends on these asymptotic boundary conditions and will usually correspond to the number of open channels n_a at the energy E considered. In this way we can determine the reduced radial wave functions $F_{ij}^\Gamma(r)$ in the external and asymptotic regions. We also show in Sect. 5.3.2 that when the radial continuum basis orbitals $u_{ij}^0(r)$, retained in expansion (5.6), satisfy homogeneous boundary conditions a Buttler correction to the reduced radial wave function is required near the boundary $r = a_0$ in the internal region. Hence we can determine the full collision wave function $\Psi_{jE}^\Gamma(\mathbf{X}_{N+1})$, defined by (5.5) in the internal region, which is important in applications such as photoionization, discussed in Chap. 8, where the collision wave function in the internal region as well as the R -matrix is required.

We conclude this section by remarking that the R -matrix, defined by (5.18) and (5.19), together with the basis functions ψ_k^Γ , defined by (5.6), and the expansion coefficients $A_{kj}^\Gamma(E)$, defined by (5.27), provide a complete description of the collision process in the internal region. Furthermore, it follows from (5.19) that the

R -matrix is a real symmetric analytic function of energy with simple poles only on the real energy axis. This property has been used as the basis of the development of multichannel effective range theories in Sect. 3.3 which enable the analytic properties of the K -matrix and T -matrix to be determined in the neighbourhood of thresholds.

5.1.3 External Region Solution

We now consider the solution of the Schrödinger equation (5.2) in the external region, corresponding to $a_0 \leq r \leq a_p$ in Fig. 5.1, for each required energy E . We have seen that a_0 is chosen so that electron exchange and correlation effects between the scattered electron and the target atom or atomic ion can be neglected in this region. The close coupling expansion (2.57) of the total wave function at energy E for each set of conserved quantum numbers Γ then reduces to

$$\Psi_{jE}^{\Gamma}(\mathbf{X}_{N+1}) = \sum_{i=1}^n \bar{\Phi}_i^{\Gamma}(\mathbf{X}_N; \hat{\mathbf{r}}_{N+1} \sigma_{N+1}) r_{N+1}^{-1} F_{ij}^{\Gamma}(r_{N+1}), \quad r_{N+1} \geq a_0, \quad (5.28)$$

where j labels the linearly independent solutions. Also the channel functions $\bar{\Phi}_i^{\Gamma}$ retained in this expansion are the same as those retained in the internal region expansion (5.6) and $F_{ij}^{\Gamma}(r)$ are energy-dependent reduced radial wave functions, defined by (5.20). In comparing (5.28) with (5.5) and (5.6), we see that we no longer include the antisymmetrization operator \mathcal{A} in (5.28), since the scattered and target electrons occupy different regions of space and hence exchange effects are negligible, enabling more efficient algorithms to be used in solving the coupled equations in this region, as discussed in Appendix E. In addition, the quadratically integrable functions χ_i^{Γ} , which are included in expansion (5.6), vanish in the external region since the boundary a_0 is chosen so that the target physical and pseudo-orbitals $P_{n\ell}(r)$, used to construct these functions, satisfy (5.4).

The coupled second-order differential equations, satisfied by the reduced radial wave functions $F_{ij}^{\Gamma}(r)$ in (5.28), are obtained by substituting (5.28) into the Schrödinger equation (5.2) and projecting onto the channel functions $\bar{\Phi}_i^{\Gamma}$. We then find that the functions $F_{ij}^{\Gamma}(r)$ satisfy the following set of coupled equations:

$$\left(\frac{d^2}{dr^2} - \frac{\ell_i(\ell_i + 1)}{r^2} + \frac{2(Z - N)}{r} + k_i^2 \right) F_{ij}^{\Gamma}(r) = 2 \sum_{i'=1}^n V_{ii'}^{\Gamma}(r) F_{i'j}^{\Gamma}(r), \quad i = 1, \dots, n, \quad r \geq a_0, \quad (5.29)$$

where ℓ_i is the orbital angular momentum of the scattered electron, Z is the nuclear charge number, N is the number of target electrons and k_i^2 is the square of the wave number of the scattered electron defined by (2.64) and (2.65). Also the potential matrix $V_{ii'}^{\Gamma}(r)$, which is defined by (2.66), can be written as a summation over inverse powers of r given by (2.73), that is by

$$V_{ii'}^\Gamma(r) = \sum_{\lambda=1}^{\lambda_{\max}} \alpha_{ii'\lambda}^\Gamma r^{-\lambda-1}, \quad r \geq a_0, \quad i, i' = 1, \dots, n. \quad (5.30)$$

The long-range potential coefficients $\alpha_{ii'\lambda}^\Gamma$ in (5.30) are defined by (2.74) and a general expression for them is derived in Appendix D.1. We see that the coupled second-order differential equations (5.29) can be obtained from (2.63) by setting the non-local exchange potential $W_{ii'}^\Gamma$ and the non-local correlation potential $X_{ii'}^\Gamma$ zero, and omitting the Lagrange multiplier terms which vanish in the external region.

The solution of (5.29) in the external region for each required energy E can be obtained by sub-dividing this region into p sub-regions, as illustrated in Fig. 5.1. In Appendices E.1, E.2 and E.3 we describe methods for propagating the R -matrix, or the log-derivative matrix, and the reduced radial wave functions across this region, where the R -matrix at $r = a_0$ is usually defined by setting the arbitrary constant $b_0 = 0$ in (5.18) which, as pointed out following (5.8), is the value adopted in most applications.

However, if b_0 is not set equal to zero in the internal region calculation, we can relate the corresponding R -matrix to that obtained by setting $b_0 = 0$. To obtain this relation we rewrite (5.18), where b_0 is non-zero, in matrix form as follows:

$$\mathbf{F}(a_0) = \mathbf{R}_{b_0}(E) \left(a_0 \frac{d\mathbf{F}}{dr} - b_0 \mathbf{F} \right)_{r=a_0}, \quad (5.31)$$

where we have shown explicitly in this equation the dependence of the R -matrix $\mathbf{R}_{b_0}(E)$ on the value of b_0 . The boundary condition corresponding to setting $b_0 = 0$ in (5.31) is then

$$\mathbf{F}(a_0) = \mathbf{R}_0(E) a_0 \left. \frac{d\mathbf{F}}{dr} \right|_{r=a_0}. \quad (5.32)$$

Eliminating $\mathbf{F}(a_0)/(d\mathbf{F}/dr)_{r=a_0}$ between (5.31) and (5.32) then yields the following relation between the R -matrices

$$\mathbf{R}_0(E) = \frac{\mathbf{R}_{b_0}(E)}{\mathbf{I} + b_0 \mathbf{R}_{b_0}(E)}, \quad (5.33)$$

which can be inverted giving

$$\mathbf{R}_{b_0}(E) = \frac{\mathbf{R}_0(E)}{\mathbf{I} - b_0 \mathbf{R}_0(E)}. \quad (5.34)$$

Equations (5.33) and (5.34) are the required relations between the R -matrix $\mathbf{R}_{b_0}(E)$, defined when b_0 is non-zero, and the R -matrix $\mathbf{R}_0(E)$, defined when b_0 is zero. It is interesting to note that this transformation shifts the pole positions in the R -matrix, where the poles of $\mathbf{R}_{b_0}(E)$ now occur where

$$\det[\mathbf{I} - b_0 \mathbf{R}_0(E)] = 0. \quad (5.35)$$

This can be useful in situations where calculations close to a pole in the R -matrix lead to inaccuracies. In the present context we set the arbitrary constant $b_0 = 0$ in the rest of Sect. 5.1, as well as in [Appendix E](#).

Finally, we observe that since the expression for the long-range potential coefficients $\alpha_{ii'\lambda}^F$, derived in [Appendix D.1](#), is diagonal in the target spin quantum number S_i for non-relativistic collisions and the non-local exchange and correlation potentials vanish in the external region, it follows that the coupled second-order differential equations (5.29) sub-divide into two uncoupled sets of equations depending on whether the target spin $S_i = S - 1/2$ or $S_i = S + 1/2$. This enables more efficient R -matrix propagator methods to be used, as discussed in [Appendix E.6](#). Using one of these methods, the R -matrix at $r = a_0$ can be propagated from $r = a_0$ to a_p to yield the R -matrix at $r = a_p$, thus providing the boundary condition satisfied by the solution in the asymptotic region $r \geq a_p$.

5.1.4 Asymptotic Region Solution

The final step in solving the Schrödinger equation (5.2) is to determine the solution in the asymptotic region, corresponding to $r \geq a_p$ in Fig. 5.1, and hence to calculate the K -matrix, S -matrix and cross sections for each required energy E . In this region the close coupling expansion again reduces to (5.28) where the reduced radial wave functions $F_{ij}^F(r)$ satisfy the coupled second-order differential equations (5.29). We will assume that the radius a_p is chosen large enough that one of the asymptotic expansion methods discussed in [Appendix F.1](#) gives an accurate solution of (5.29) for r satisfying $a_p \leq r \leq \infty$.

Following our discussion in [Appendix F.1](#) we assume that the channels are ordered so that

$$k_1^2 \geq k_2^2 \geq \dots \geq k_n^2, \quad (5.36)$$

where, at the energy E of interest, the first n_a channels are open with $k_i^2 \geq 0$ and the last n_b channels are closed with $k_i^2 < 0$, where $n_a + n_b = n$. We show in [Appendix F.1](#) that we can determine $n + n_a$ linearly independent asymptotic solutions of (5.29) which are regular as $r \rightarrow \infty$. In this section we find it convenient to define these $n + n_a$ solutions to satisfy the following asymptotic boundary conditions:

$$\begin{aligned} s_{ij}(r) &\underset{r \rightarrow \infty}{\sim} k_i^{-1/2} \sin \theta_i \delta_{ij}, & i = 1, \dots, n, \quad j = 1, \dots, n_a, \\ c_{ij}(r) &\underset{r \rightarrow \infty}{\sim} k_i^{-1/2} \cos \theta_i \delta_{ij}, & i = 1, \dots, n, \quad j = 1, \dots, n_a, \\ c_{ij}(r) &\underset{r \rightarrow \infty}{\sim} \exp(-\phi_i) \delta_{ij}, & i = 1, \dots, n, \quad j = n_a + 1, \dots, n, \end{aligned} \quad (5.37)$$

where

$$\theta_i = k_i r - \frac{1}{2} \ell_i \pi - \eta_i \ln 2k_i r + \sigma_{\ell_i}, \quad i = 1, \dots, n_a, \quad (5.38)$$

with

$$\eta_i = -\frac{Z - N}{k_i}, \quad i = 1, \dots, n_a \quad (5.39)$$

and

$$\sigma_{\ell_i} = \arg(\ell_i + 1 + i\eta_i), \quad i = 1, \dots, n_a, \quad (5.40)$$

and where

$$\phi_i = |k_i|r - \frac{Z - N}{|k_i|} \ln(2|k_i|r), \quad i = n_a + 1, \dots, n. \quad (5.41)$$

When n_a channels are open we showed in [Sect. 2.4](#) that there are n_a linearly independent physical solutions which vanish at the origin and are finite at infinity. These physical solutions, defined by (2.85), can be written in terms of the $n + n_a$ asymptotic solutions defined by (5.37) as follows:

$$\mathbf{F}^\Gamma(r) = \mathbf{s}(r) + \mathbf{c}(r)\mathbf{N}^\Gamma, \quad r \geq a_p, \quad (5.42)$$

where $\mathbf{F}^\Gamma(r)$ has dimension $n \times n_a$, $\mathbf{s}(r)$ has dimension $n \times n_a$, $\mathbf{c}(r)$ has dimension $n \times n$ and \mathbf{N}^Γ has dimension $n \times n_a$. The matrix \mathbf{N}^Γ can be written in the form

$$\mathbf{N}^\Gamma = \begin{bmatrix} \mathbf{K}^\Gamma \\ \mathbf{L}^\Gamma \end{bmatrix}, \quad (5.43)$$

where \mathbf{K}^Γ is the usual $n_a \times n_a$ -dimensional K -matrix defined by (2.85) and \mathbf{L}^Γ is a subsidiary $n_b \times n_a$ -dimensional matrix which multiplies the decaying solutions $\mathbf{c}(r)$ defined by the last equation in (5.37). We see from (5.42) that \mathbf{K}^Γ postmultiplies the first n_a columns of the matrix $\mathbf{c}(r)$ while \mathbf{L}^Γ postmultiplies the last n_b columns of the matrix $\mathbf{c}(r)$.

We can now express the $n_a \times n_a$ -dimensional K -matrix \mathbf{K}^Γ in terms of the $n \times n$ -dimensional R -matrix $\mathbf{R}_p^\Gamma(E)$ at $r = a_p$. Since we have set the arbitrary constant $b_0 = 0$ then these matrices are related by the equation

$$\mathbf{F}^\Gamma(a_p) = \mathbf{R}_p^\Gamma(E)a_p\dot{\mathbf{F}}^\Gamma(a_p), \quad (5.44)$$

where $\dot{\mathbf{F}}^\Gamma(r)$ is the derivative of $\mathbf{F}^\Gamma(r)$, which from (5.42) can be written as

$$\dot{\mathbf{F}}^\Gamma(r) = \frac{d\mathbf{F}^\Gamma}{dr} = \dot{\mathbf{s}}(r) + \dot{\mathbf{c}}(r)\mathbf{N}^\Gamma, \quad r \geq a_p. \quad (5.45)$$

We then substitute the expressions for $\mathbf{F}^\Gamma(a_p)$ and $\dot{\mathbf{F}}^\Gamma(a_p)$, given respectively by (5.42) and (5.45), into (5.44). After rearranging the terms we obtain

$$\left[\mathbf{c}(a_p) - a_p \mathbf{R}_p^{\Gamma}(E) \dot{\mathbf{c}}(a_p) \right] \mathbf{N}^{\Gamma} = -\mathbf{s}(a_p) + a_p \mathbf{R}_p^{\Gamma}(E) \dot{\mathbf{s}}(a_p), \quad (5.46)$$

which is a set of n linear simultaneous equations with n_a right-hand sides. The solution of these equations for each required energy E yields the $n \times n_a$ -dimensional matrix \mathbf{N}^{Γ} , from which the $n_a \times n_a$ -dimensional K -matrix \mathbf{K}^{Γ} can be determined from (5.43). It follows from (5.37) and (5.42) that the required physical solution matrix $\mathbf{F}^{\Gamma}(r)$ satisfies the asymptotic boundary conditions

$$\mathbf{F}^{\Gamma}(r) \underset{r \rightarrow \infty}{\sim} \mathbf{k}^{-1/2} [\sin \theta + \cos \theta \mathbf{K}^{\Gamma}] \quad (5.47)$$

in the open channels, since the decaying solutions in (5.37) vanish asymptotically.

We also find it convenient to define a solution matrix satisfying the asymptotic boundary conditions

$$\mathbf{G}^{\Gamma}(r) \underset{r \rightarrow \infty}{\sim} \mathbf{k}^{-1/2} [\exp(-i\theta) - \exp(i\theta) \mathbf{S}^{\Gamma}], \quad (5.48)$$

which is obtained by taking linear combinations of the solutions defined by (5.47). The $n_a \times n_a$ -dimensional S -matrix \mathbf{S}^{Γ} in (5.48) is defined in terms of the $n_a \times n_a$ -dimensional K -matrix by the matrix equation

$$\mathbf{S}^{\Gamma} = \frac{\mathbf{I} + i\mathbf{K}^{\Gamma}}{\mathbf{I} - i\mathbf{K}^{\Gamma}}. \quad (5.49)$$

The T -matrix and cross sections can then be determined using the procedure described in Sect. 2.5. The solutions in the internal, external and asymptotic regions can be determined in a similar way for all relevant $LS\pi$ values enabling the corresponding total cross sections, angular distributions and rate coefficients to be calculated, as described in Sect. 2.5.

5.2 Variational Principle for the R -Matrix

In this section we derive a variational principle for the multichannel R -matrix defined on the boundary $r = a_0$ of the internal region. We consider explicitly low-energy electron collisions with atoms and atomic ions. However, the variational principle that we obtain will be applicable for any multichannel collision process which can be described in an internal region by coupled second-order integro-differential equations with the form defined by (2.63). Variational principles for the R -matrix have been considered by many workers, as discussed in Sect. 4.3. Our approach is a generalization of the variational principles derived by Kohn [542] and Jackson [495], which we considered in Sect. 4.3 in the special case of potential scattering.

Following our treatment of multichannel collisions in Sects. 2.3 and 5.1.2, we expand the wave function describing the collision of an electron with an N -electron atom or atomic ion in the internal R -matrix region as follows:

$$\begin{aligned} \Psi_{jE}^\Gamma(\mathbf{X}_{N+1}) = & \mathcal{A} \sum_{i=1}^n \bar{\Phi}_i^\Gamma(\mathbf{X}_N; \hat{\mathbf{r}}_{N+1} \sigma_{N+1}) r_{N+1}^{-1} F_{ij}^\Gamma(r_{N+1}) \\ & + \sum_{i=1}^m \chi_i^\Gamma(\mathbf{X}_{N+1}) c_{ij}^\Gamma, \quad j = 1, \dots, n. \end{aligned} \quad (5.50)$$

In this equation we have adopted the same notation for the channel functions $\bar{\Phi}_i^\Gamma$ and the quadratically integrable functions χ_i^Γ as in (2.57) and (5.6) and we observe that the coefficients c_{ij}^Γ in (5.50) can be written in terms of the coefficients b_{ik}^Γ in (5.6) and the coefficients $A_{kj}^\Gamma(E)$ in (5.5) by the equation

$$c_{ij}^\Gamma = \sum_{k=1}^{n_t} b_{ik}^\Gamma A_{kj}^\Gamma(E), \quad i = 1, \dots, m, \quad j = 1, \dots, n. \quad (5.51)$$

Also the subscript j in (5.50) labels the complete set of n linearly independent solutions of the corresponding coupled second-order integrodifferential equations (2.63), where the reduced radial functions $F_{ij}^\Gamma(r)$ vanish at the origin $r = 0$. Since we are considering a variational principle for the $n \times n$ -dimensional R -matrix on the surface $r = a_0$ of the internal region, we are not restricted in this analysis to the n_a solutions which are regular at infinity as in Sect. 5.1.4. We now derive a variational principle for the solutions of (2.63) in the internal region $0 \leq r \leq a_0$, where a_0 is such that electron exchange and correlation effects between the scattered electron and the target atom or ion can be neglected for $r \geq a_0$.

We commence by defining the integral

$$I_{jj'} = \langle \Psi_j | H_{N+1} + \mathcal{L}_{N+1} - E | \Psi_{j'} \rangle_{\text{int}}, \quad j, j' = 1, \dots, n, \quad (5.52)$$

where we have omitted the superscript Γ and the subscript E on the wave functions Ψ_{jE}^Γ and $\Psi_{j'E}^\Gamma$ for notational convenience, where Γ represents the conserved quantum numbers and E is the total energy being considered. The integrations in (5.52) are carried out over the space and spin coordinates of all $N + 1$ electrons, where the radial integrations are confined to the internal region. Also \mathcal{L}_{N+1} is the Bloch operator, defined by (5.8), which ensures that $H_{N+1} + \mathcal{L}_{N+1}$ is hermitian in the internal region for functions satisfying arbitrary boundary conditions on the surface $r = a_0$ of the internal region. The first-order variations of $\delta I_{jj'}$ in $I_{jj'}$ corresponding to first-order variations $\delta \Psi_j$ in Ψ_j and $\delta \Psi_{j'}$ in $\Psi_{j'}$ about the exact solutions of the coupled second-order integrodifferential equations (2.63) in the internal region are then given by

$$\delta I_{jj'} = \langle \Psi_j | H_{N+1} + \mathcal{L}_{N+1} - E | \delta \Psi_{j'} \rangle_{\text{int}} + \langle \delta \Psi_j | H_{N+1} + \mathcal{L}_{N+1} - E | \Psi_{j'} \rangle_{\text{int}}. \quad (5.53)$$

Using the hermiticity of $H_{N+1} + \mathcal{L}_{N+1}$, (5.53) can be written as

$$\delta I_{jj'} = \langle \delta \Psi_{j'} | H_{N+1} + \mathcal{L}_{N+1} - E | \Psi_j \rangle_{\text{int}} + \langle \delta \Psi_j | H_{N+1} + \mathcal{L}_{N+1} - E | \Psi_{j'} \rangle_{\text{int}}. \quad (5.54)$$

On the boundary $r = a_0$ of the internal region the exchange terms and the quadratically integrable functions in (5.50) vanish and hence this equation reduces to

$$\Psi_j(\mathbf{X}_{N+1}) = \sum_{i=1}^n \bar{\Phi}_i(\mathbf{X}_N; \hat{\mathbf{r}}_{N+1} \sigma_{N+1}) r_{N+1}^{-1} F_{ij}(r_{N+1}), \quad j = 1, \dots, n. \quad (5.55)$$

Substituting (5.55) into (5.54) and remembering that $F_{ij}(r)$ and $F_{ij'}(r)$ are both exact solutions of (2.63) in the internal region, we obtain

$$\begin{aligned} \delta I_{jj'} = \frac{1}{2} \sum_{i=1}^n \left[\delta F_{ij'}(a_0) \left(\frac{dF_{ij}}{dr} - \frac{b_0}{a_0} F_{ij} \right)_{r=a_0} \right. \\ \left. + \delta F_{ij}(a_0) \left(\frac{dF_{ij'}}{dr} - \frac{b_0}{a_0} F_{ij'} \right)_{r=a_0} \right], \end{aligned} \quad (5.56)$$

where we have used definition (5.8) for the Bloch operator.

Following our discussion of the variational principle introduced by Jackson [495] in Sect. 4.3, we now consider the variational functional

$$\begin{aligned} \mathcal{F}[\Psi_j^t, \Psi_{j'}^t] = \langle \Psi_j^t | H_{N+1} + \mathcal{L}_{N+1} - E | \Psi_{j'}^t \rangle_{\text{int}} \\ - \frac{1}{2a_0} \left[F_{jj'}^t(a_0) + F_{j'j}^t(a_0) \right], \end{aligned} \quad (5.57)$$

where Ψ_j^t is a trial function and $F_{j'j}^t(r)$ is the corresponding reduced radial wave function. We consider first-order variations $\delta \Psi_j$ in Ψ_j and $\delta \Psi_{j'}$ in $\Psi_{j'}$ about the exact solutions of (2.63) in the internal region, subject to the boundary conditions

$$\left(a_0 \frac{dF_{ij}^t}{dr} - b_0 F_{ij}^t \right)_{r=a_0} = \delta_{ij}, \quad i, j = 1, \dots, n. \quad (5.58)$$

It follows from (5.52) and (5.56) that this functional is stationary for first-order variations about the exact solutions so that

$$\delta \mathcal{F}[\Psi_j, \Psi_{j'}] = 0, \quad (5.59)$$

where we note that the boundary condition (5.58) defines n particular linear combinations of the n linearly independent solutions of (2.63) which vanish at the origin. We see that (5.57), (5.58) and (5.59) are the multichannel generalization of the variational principle for potential scattering given by (4.55), (4.56) and (4.59), respectively.

When the exact solutions of (2.63) are substituted into (5.57) we find that

$$\begin{aligned} \mathcal{F}[\Psi_j, \Psi_{j'}] &= \frac{1}{2} [\langle \Psi_j | \mathcal{L}_{N+1} | \Psi_{j'} \rangle + \langle \Psi_{j'} | \mathcal{L}_{N+1} | \Psi_j \rangle] \\ &\quad - \frac{1}{2a_0} [F_{jj'}(a_0) + F_{j'j}(a_0)]. \end{aligned} \quad (5.60)$$

Substituting for the Bloch operator and using the boundary condition (5.58) then yields

$$\mathcal{F}[\Psi_j, \Psi_{j'}] = -\frac{1}{4a_0} [F_{jj'}(a_0) + F_{j'j}(a_0)]. \quad (5.61)$$

However, the R -matrix on the boundary $r = a_0$ of the internal region is defined by (5.18) which, when combined with the boundary condition (5.58), reduces to

$$F_{ij}(a_0) = R_{ij}(E). \quad (5.62)$$

Hence, it follows from (5.61) and (5.62) and the symmetry of the R -matrix that

$$\mathcal{F}[\Psi_j, \Psi_{j'}] = -\frac{1}{2a_0} R_{jj'}(E). \quad (5.63)$$

This shows that the R -matrix can be determined from the stationary value of the functional $\mathcal{F}[\Psi_j, \Psi_{j'}]$.

We now demonstrate that this variational principle provides a variational procedure for calculating the R -matrix. Following (5.6), we introduce a basis in the internal region defined by

$$\begin{aligned} \psi_k(\mathbf{X}_{N+1}) &= \mathcal{A} \sum_{i=1}^n \sum_{j=1}^{n_c} \bar{\Phi}_i(\mathbf{X}_N; \hat{\mathbf{r}}_{N+1} \sigma_{N+1}) r_{N+1}^{-1} u_{ij}^0(r_{N+1}) a_{ijk} \\ &\quad + \sum_{i=1}^m \chi_i(\mathbf{X}_{N+1}) b_{ik}, \quad k = 1, \dots, n_t, \end{aligned} \quad (5.64)$$

where, as in (5.6), $n_t = nn_c + m$ is the number of linearly independent basis functions. Also in (5.64) $u_{ij}^0(r)$ are radial continuum basis orbitals defined over the internal region $0 \leq r \leq a_0$ and the functions $\bar{\Phi}_i$ and χ_i are defined as in (2.57) and (5.6). The coefficients a_{ijk} and b_{ik} are obtained by diagonalizing $H_{N+1} + \mathcal{L}_{N+1}$ in this basis as follows:

$$\langle \psi_k | H_{N+1} + \mathcal{L}_{N+1} | \psi_{k'} \rangle_{\text{int}} = E_k \delta_{kk'}, \quad k, k' = 1, \dots, n_t, \quad (5.65)$$

where, as in (5.52), the integration is carried out over the internal region. Following (5.5) we now expand the wave functions Ψ_j^t and $\Psi_{j'}^t$ in the functional $\mathcal{F}[\Psi_j^t, \Psi_{j'}^t]$ in this basis giving

$$\begin{aligned}\Psi_j^t(\mathbf{X}_{N+1}) &= \sum_{k=1}^{n_t} \psi_k(\mathbf{X}_{N+1}) A_{kj}(E), \quad j = 1, \dots, n, \\ \Psi_{j'}^t(\mathbf{X}_{N+1}) &= \sum_{k=1}^{n_t} \psi_k(\mathbf{X}_{N+1}) A_{kj'}(E), \quad j' = 1, \dots, n,\end{aligned}\quad (5.66)$$

where $A_{kj}(E)$ and $A_{kj'}(E)$ are variational coefficients which depend on the total energy E of interest. Substituting these expansions into (5.57) then gives the following equation for this functional

$$\begin{aligned}\mathcal{F}[\Psi_j^t, \Psi_{j'}^t] &= \sum_{kk'} (E_k - E) A_{kj}(E) A_{k'j'}(E) \delta_{kk'} \\ &\quad - \frac{1}{2a_0} \sum_k [w_{jk} A_{kj'}(E) + w_{j'k} A_{kj}(E)],\end{aligned}\quad (5.67)$$

where the surface amplitudes w_{jk} are defined by

$$w_{jk} = \sum_{i=1}^{n_c} u_{ji}^0(a_0) a_{jik}, \quad j = 1, \dots, n, \quad k = 1, \dots, n_t. \quad (5.68)$$

Writing $\mathcal{F}_{jj'} \equiv \mathcal{F}[\Psi_j^t, \Psi_{j'}^t]$, for notational convenience, and using the stationary property of this functional with respect to variations in the wave functions Ψ_j^t and $\Psi_{j'}^t$, we obtain

$$\frac{\partial \mathcal{F}_{jj'}}{\partial A_{kj}} = (E_k - E) A_{kj'}(E) - \frac{1}{2a_0} w_{j'k} = 0 \quad (5.69)$$

and

$$\frac{\partial \mathcal{F}_{jj'}}{\partial A_{kj'}} = (E_k - E) A_{kj}(E) - \frac{1}{2a_0} w_{jk} = 0. \quad (5.70)$$

Both these equations give the following result:

$$A_{kj}(E) = \frac{1}{2a_0} \frac{w_{jk}}{E_k - E}, \quad j = 1, \dots, n, \quad k = 1, \dots, n_t. \quad (5.71)$$

The stationary value of the functional $\mathcal{F}_{jj'}$ is obtained by substituting (5.71) into (5.67) yielding

$$\begin{aligned}
\mathcal{F}_{jj'} &= \frac{1}{4a_0^2} \sum_{k=1}^{n_t} \frac{w_{jk}w_{j'k}}{E_k - E} - \frac{1}{2a_0^2} \sum_{k=1}^{n_t} \frac{w_{jk}w_{j'k}}{E_k - E} \\
&= -\frac{1}{4a_0^2} \sum_{k=1}^{n_t} \frac{w_{jk}w_{j'k}}{E_k - E}, \quad j, j' = 1, \dots, n.
\end{aligned} \tag{5.72}$$

We then combine this result with (5.63), which relates the stationary value of the functional $\mathcal{F}_{jj'} \equiv \mathcal{F}[\Psi_j^t, \Psi_{j'}^t]$ to the R -matrix, to give the following variational expression for the R -matrix:

$$R_{jj'}(E) = \frac{1}{2a_0} \sum_{k=1}^{n_t} \frac{w_{jk}w_{j'k}}{E_k - E}, \quad j, j' = 1, \dots, n. \tag{5.73}$$

We see that this equation for the R -matrix is identical to (5.19) showing that our procedure for calculating the R -matrix described in Sect. 5.1.2 yields a variational result.

We can also obtain a variational expression for the wave function Ψ_j by substituting the expansion for $A_{kj}(E)$ given by (5.71) into (5.66). This gives

$$\Psi_j(\mathbf{X}_{N+1}) = \frac{1}{2a_0} \sum_{k=1}^{n_t} \psi_k(\mathbf{X}_{N+1}) \frac{w_{jk}}{E_k - E}, \quad j = 1, \dots, n, \tag{5.74}$$

where the reduced wave functions $F_{ij}(r)$ in expansion (5.50) of Ψ_j satisfy the boundary condition (5.58) at $r = a_0$. This result corresponds to the expression for the full collision wave function given by (5.5) and (5.27) when we impose the boundary conditions (5.58). As pointed out in Sect. 5.1.2, where we determined the solution in the internal region, this result is important in applications such as photoionization, discussed in Chap. 8, where the wave function as well as the R -matrix is required.

5.3 Continuum Basis Orbitals and Correction Methods

In this section we consider methods for determining the zero-order radial continuum basis orbitals $u_{ij}^0(r)$ in (5.6) which represent the radial motion of the scattered electron in the expansion of the wave function in the internal region $0 \leq r \leq a_0$. We also consider methods for calculating and correcting the R -matrix. In principle, as discussed in the case of potential scattering in Sect. 4.4, members of any linearly independent set of orbitals which vanish at the origin and are complete over the range $0 \leq r \leq a_0$ can be used. However, a careful choice of basis orbitals will enable the convergence of expansion (5.6) to be made more rapid. We consider first in Sect. 5.3.1 an approach using radial continuum basis orbitals which satisfy homogeneous boundary conditions on the surface of the internal region. We then show in Sect. 5.3.2 that a Buttler correction to the R -matrix must be included to

obtain accurate results. We also consider in this section how a Buttler-type correction to the wave function can be determined. We will see later that this approach has been widely used in calculations of electron collisions with atoms, ions and molecules. Then in Sect. 5.3.3 we summarize methods where the radial continuum basis orbitals satisfy arbitrary boundary conditions on the surface of the internal region. Some of these methods have been reviewed in Sect. 4.4, where we showed that in general they avoid the need for a Buttler correction to the R -matrix and to the wave function and, as a consequence, the resultant solution can be derived from a variational principle. However, it is found that for electron collisions with multi-electron atomic targets the number of continuum orbitals required to obtain converged results can often be larger than when homogeneous boundary conditions are used with a Buttler correction. Finally, in Sect. 5.3.4 we consider a method for partitioning the R -matrix into a part which can be accurately determined and a part which is approximated, enabling accurate results to be efficiently obtained when the Hamiltonian matrix becomes large.

5.3.1 Homogeneous Boundary Condition Method

We consider first a procedure for calculating the radial continuum basis orbitals $u_{ij}^0(r)$ in (5.6) in the R -matrix internal region, which was described by Robb [791] and adopted by Burke et al. [155, 178] in their study of low-energy electron collisions with multi-electron atoms and atomic ions.

In this method, the radial continuum basis orbitals $u_{ij}^0(r)$ in (5.6) are chosen to be solutions of the following zero-order differential equation for each continuum orbital angular momentum ℓ_i

$$\begin{aligned} & \left(\frac{d^2}{dr^2} - \frac{\ell_i(\ell_i + 1)}{r^2} - U_0(r) + k_{ij}^2 \right) u_{ij}^0(r) \\ &= \sum_{n_b = \ell_i + 1}^{\ell_i + n_{\ell_i}} \lambda_{ijn_b} P_{n_b \ell_i}(r), \quad i = 1, \dots, n, \quad j = 1, \dots, n_c, \end{aligned} \quad (5.75)$$

satisfying the homogeneous boundary conditions

$$u_{ij}^0(0) = 0, \quad i = 1, \dots, n, \quad j = 1, \dots, n_c \quad (5.76)$$

and

$$\frac{a_0}{u_{ij}^0(a_0)} \frac{du_{ij}^0}{dr} \Big|_{r=a_0} = b_0, \quad i = 1, \dots, n, \quad j = 1, \dots, n_c, \quad (5.77)$$

where b_0 is an arbitrary constant which can depend on the orbital angular momentum ℓ_i , although in most applications b_0 is set equal to zero. Also in (5.75), the summation n_b goes over the n_{ℓ_i} reduced radial physical bound orbitals $P_{n_b \ell_i}(r)$,

which are included in the representation of the atomic target states for each ℓ_i . However, any pseudo-orbitals retained in the configuration interaction representation of the target states are not included in this summation, since their inclusion would slow the convergence of the expansion over the radial continuum basis orbitals, as described below. Finally, the $\lambda_{ij n_b}$ in (5.75) are Lagrange multipliers which are chosen so that the continuum basis orbitals are orthogonal to the physical bound orbitals with the same orbital angular momentum symmetry, so that

$$\int_0^{a_0} u_{ij}^0(r) P_{n_b \ell_i}(r) dr = 0, \quad j = 1, \dots, n_c, \quad n_b = \ell_i + 1, \dots, \ell_i + n_{\ell_i} \quad (5.78)$$

are satisfied for each ℓ_i . It follows that the continuum basis orbitals, generated in this way for each ℓ_i , are mutually orthogonal and in addition can be normalized so that

$$\int_0^{a_0} u_{ij}^0(r) u_{ij'}^0(r) dr = \delta_{jj'}, \quad j, j' = 1, \dots, n_c. \quad (5.79)$$

It also follows that for each ℓ_i the reduced radial orbitals

$$P_{n_b \ell_i}(r), \quad n_b = \ell_i + 1, \dots, \ell_i + n_{\ell_i}; \quad u_{ij}^0(r), \quad j = 1, \dots, n_b \quad (5.80)$$

form a complete set over the range $0 \leq r < a_0$ in the limit $n_c \rightarrow \infty$ for any b_0 and zero-order potential $U_0(r)$ in (5.75).

In order to obtain rapid convergence of the R -matrix expansion (5.19), including the Buttler correction discussed below, the zero-order potential $U_0(r)$ in (5.75) should provide a good representation of the charge distribution of the target atom or ion. In many applications the simple form

$$U_0(r) = -\frac{2N}{r} \exp(-Z^{1/3}r) - \frac{2(Z - N)}{r} \quad (5.81)$$

suggested by the Thomas–Fermi statistical model of the atom (see, for example, [817]) has proved suitable, in that it has the correct form near the nucleus and asymptotically and a reasonably accurate charge distribution radius. A more sophisticated potential which also satisfies these criteria is the static potential of the target atom or ion in its ground state with possibly the addition of a local polarization potential. Such a form becomes increasingly appropriate for high Z atoms and ions. It is important to note that in practical electron–atom and electron–ion collision calculations, the solution of (5.75), (5.76), (5.77), (5.78) and (5.79) to generate the radial continuum basis orbitals takes a very small part of the overall computer time. Hence the use of a more sophisticated zero-order potential is fully justified if it increases the rate of convergence of the R -matrix expansion.

The inclusion of Lagrange multiplier terms on the right-hand side of (5.75) is related to the inclusion of Lagrange multiplier terms in (2.63) which ensure that the orthogonality constraints (2.62) are satisfied. In the present situation the inclusion

of these terms in (5.75) has the following further justification. It is well known that in the static exchange approximation in electron–atom collisions, the difference between the phase shift at zero energy and at infinite energy for each orbital angular momentum satisfies the equation

$$\delta(0) - \delta(\infty) = (n_{bs} + n_p)\pi, \quad (5.82)$$

which is a generalization of Levinson’s theorem [587] first studied by Swan [899]. In (5.82), n_{bs} is the number of bound states of the electron–atom system and n_p is the number of states excluded by the Pauli principle corresponding to the orbital angular momentum symmetry being considered. For example, in the case of electron collisions with Ne which has the Hartree–Fock ground-state configuration $1s^2 2s^2 2p^6 \ ^1S^e$ and where $n_{bs} = 0$, we have $n_p = 2$ for s-wave scattering, since the scattered electron is excluded from the fully occupied $1s$ and $2s$ shells, and $n_p = 1$ for p-wave scattering, since the scattered electron is excluded from the fully occupied $2p$ shell. The effect of including the $1s$ and $2s$ orbitals on the right-hand side of (5.75) for s-wave scattering, and the $2p$ orbital for p-wave scattering and using a suitable zero-order potential $U_0(r)$ ensures that the zero-order solution also satisfies (5.82). We see therefore that the inhomogeneous term on the right-hand side of (5.75) plays the role of an exchange potential, while at the same time ensuring that the continuum basis orbitals are orthogonal to the physical orbitals. Hence the inclusion of the Lagrange multiplier terms on the right-hand side of (5.75) in the generation of the zero-order radial continuum basis orbitals usually means that the R -matrix expansion over these orbitals will converge rapidly. We note that an inhomogeneous term of this type was used by Lippmann and Schey [601] in their model study of elastic e^- –H collisions. Finally, as observed in our discussion following (2.57), the imposition of orthogonality constraints on the radial continuum basis orbitals means that additional quadratically integrable functions must be included in the second expansion in (5.6) to ensure completeness of the collision wave function.

5.3.2 Buttle Correction to the R -Matrix and Wave Function

Since the radial continuum basis orbitals $u_{ij}^0(r)$, retained in expansion (5.6) in the homogeneous boundary condition method, satisfy the zero-order differential equation (5.75) subject to homogeneous boundary conditions (5.76) and (5.77) it is necessary to add a Buttle correction to the R -matrix to obtain accurate results. This procedure, first introduced by Buttle [195] and discussed in the case of potential scattering in Sect. 4.4.2, corrects for the omission of high-lying pole terms in expansion (5.19) of the R -matrix $R_{ij}^{\Gamma}(E)$. In our discussion here, which is a straightforward generalization of potential scattering theory given in Sect. 4.4.2 to multichannel collisions, we consider in turn the Buttle correction to the R -matrix and to the wave function.

5.3.2.1 Buttler Correction to the R -Matrix

An important simplification which arises in applying the Buttler correction to the multichannel R -matrix expansion (5.19) is that usually only the diagonal elements of the R -matrix need to be corrected. This can be seen by examining the elements of the Hamiltonian matrix which is diagonalized to yield the basis functions ψ_k^Γ in (5.7). If the zero-order differential equation (5.75) provides a good representation of the electron–atom or electron–ion collision process at high energies, then the Hamiltonian matrix corresponding to the high-lying zero-order radial continuum basis orbitals $u_{ij}^0(r)$ will be dominated by the diagonal elements. In this case we can augment the internal region expansion (5.6) of the basis functions ψ_k^Γ by the following zero-order basis functions:

$$B_k^\Gamma(\mathbf{X}_{N+1}) = \mathcal{A}\bar{\Phi}_i^\Gamma(\mathbf{X}_N; \hat{\mathbf{r}}_{N+1}\sigma_{N+1})r_{N+1}^{-1}u_{ij}^0(r_{N+1}), \quad i = 1, \dots, n, \\ j = n_c + 1, \dots, \infty, \quad k = n_t + 1, \dots, \infty, \quad (5.83)$$

where the integers i , j and k are related by

$$k = n_t + i + (j - n_c - 1)n. \quad (5.84)$$

Hence, in each channel $i = 1, \dots, n$, an infinite number of zero-order basis functions $j = n_c + 1, \dots, \infty$ are included in the internal region expansion, where n_c is the number of radial continuum basis orbitals retained in expansion (5.6) for each channel.

The Buttler correction to the diagonal elements of the R -matrix defined by (5.19) corresponding to the inclusion of the additional zero-order basis functions (5.83) is then given by

$$R_{ii}^{\Gamma(\text{BC})}(E) = \frac{1}{2a_0} \sum_{j=n_c+1}^{\infty} \frac{[u_{ij}^0(a_0)]^2}{E_{ij}^0 - E}, \quad i = 1, \dots, n, \quad (5.85)$$

where the summation over j goes over the zero-order continuum basis orbitals included in (5.83) for each channel i , and the zero-order energies E_{ij}^0 are obtained from the corresponding zero-order eigenvalues k_{ij}^2 in (5.75) which, using (2.7), gives

$$E_{ij}^0 = e_i + \frac{1}{2}k_{ij}^2. \quad (5.86)$$

As in potential scattering, see (4.79), this correction can be rewritten as

$$R_{ii}^{\Gamma(\text{BC})}(E) = u_i^0(a_0) \left(a_0 \frac{du_i^0}{dr} - b_0 u_i^0 \right)_{r=a_0}^{-1} - \frac{1}{2a_0} \sum_{j=1}^{n_c} \frac{[u_{ij}^0(a_0)]^2}{E_{ij}^0 - E}, \\ i = 1, \dots, n, \quad (5.87)$$

where the first term on the right-hand side of this equation is obtained by solving the zero-order equation (5.75), subject to the boundary condition (5.76) and the orthogonality constraint (5.78) at the given energy E of interest, while the second term is obtained from the zero-order continuum basis orbitals included in expansion (5.6). Both terms can be rapidly calculated and the correction added to the diagonal elements of the R -matrix given by (5.19). Indeed, since the Buttler correction is smoothly varying without poles in the low-energy region of interest, it can usually be calculated at a few energies in this region and interpolated to give the correction at any required energy.

5.3.2.2 Buttler Correction to the Wave Function

We now discuss how a Buttler correction to the wave function near the boundary in the internal region can be determined. We have already remarked in our discussion of potential scattering that such a correction may be required to obtain accurate results in, for example, atomic photoionization calculations where the accuracy of the wave function near the boundary $r = a_0$ of the internal region may be important. In order to derive a correction to the wave function in multichannel collisions, we commence from (5.17) which we rewrite here as

$$|\Psi_{jE}^{\Gamma}\rangle = \sum_{k=1}^{n_t} |\psi_k^{\Gamma}\rangle \frac{1}{E_k^{\Gamma} - E} \langle \psi_k^{\Gamma} | \mathcal{L}_{N+1} | \Psi_{jE}^{\Gamma} \rangle, \quad j = 1, \dots, n, \quad (5.88)$$

where the subscript j on the functions Ψ_{jE}^{Γ} now labels the n linearly independent solutions that can be formed in the internal region. We project this equation onto the n channel functions $\bar{\Phi}_i^{\Gamma}(\mathbf{x}_1, \dots, \mathbf{x}_N; \hat{\mathbf{r}}_{N+1} \sigma_{N+1})$ yielding the following expression for the reduced radial wave functions $F_{ij}^{\Gamma}(r)$ near the boundary $r = a_0$ of the internal region

$$F_{ij}^{\Gamma}(r) = \frac{1}{2a_0} \sum_{k=1}^{n_t} \sum_{i'=1}^n \frac{w_{ik}^{\Gamma}(r) w_{i'k}^{\Gamma}(a_0)}{E_k^{\Gamma} - E} \left(a_0 \frac{dF_{i'j}^{\Gamma}}{dr} - b_0 F_{i'j}^{\Gamma} \right)_{r=a_0}, \quad i, j = 1, \dots, n, \quad (5.89)$$

where the amplitudes $w_{ik}^{\Gamma}(r)$ are defined by (5.24). It is convenient to choose these n solutions to satisfy the boundary condition

$$\left(a_0 \frac{dF_{ij}^{\Gamma}}{dr} - b_0 F_{ij}^{\Gamma} \right)_{r=a_0} = \delta_{ij}, \quad i, j = 1, \dots, n, \quad (5.90)$$

where we note that any other linearly independent set of solutions in the internal region can be expressed as a linear combination of these solutions. Substituting this boundary condition into (5.89) then yields the following expression for the reduced radial wave function near the boundary of the internal region:

$$F_{ij}^{\Gamma}(r) = \frac{1}{2a_0} \sum_{k=1}^{n_r} \frac{w_{ik}^{\Gamma}(r)w_{jk}^{\Gamma}(a_0)}{E_k^{\Gamma} - E}, \quad i, j = 1, \dots, n. \quad (5.91)$$

In determining the correction to the reduced radial wave function defined by (5.91) we observe that the simplification adopted in our derivation of the Buttler correction to the R -matrix, that only the diagonal elements need correcting, also applies in the present case. Hence the correction to the wave function (5.91) can be written, in analogy with the correction to the R -matrix (5.85), as

$$F_{ii}^{\Gamma(\text{BC})}(r) = \frac{1}{2a_0} \sum_{j=n_c+1}^{\infty} \frac{u_{ij}^0(r)u_{ij}^0(a_0)}{E_{ij}^0 - E}, \quad i = 1, \dots, n, \quad (5.92)$$

where the summation j goes over the additional zero-order continuum basis orbitals included in (5.83) and the zero-order energies E_{ij}^0 are again given by (5.86). Equation (5.92) can then be rewritten as

$$F_{ii}^{\Gamma(\text{BC})}(r) = \frac{1}{2a_0} \sum_{j=1}^{\infty} \frac{u_{ij}^0(r)u_{ij}^0(a_0)}{E_{ij}^0 - E} - \frac{1}{2a_0} \sum_{j=1}^{n_c} \frac{u_{ij}^0(r)u_{ij}^0(a_0)}{E_{ij}^0 - E}, \quad i = 1, \dots, n, \quad (5.93)$$

where the first term on the right-hand side of this equation can be written in terms of the solution of the zero-order equation (5.75) as

$$\frac{1}{2a_0} \sum_{j=1}^{\infty} \frac{u_{ij}^0(r)u_{ij}^0(a_0)}{E_{ij}^0 - E} = u_i^0(r) \left(a_0 \frac{du_i^0}{dr} - b_0 u_i^0 \right)_{r=a_0}^{-1}, \quad i = 1, \dots, n, \quad (5.94)$$

which follows from (5.89) by replacing $F_{ij}^{\Gamma}(r)$ with the solution of the zero-order equation (5.75) at the energy E . Hence the correction to the wave function near the boundary of the internal region is given by

$$F_{ii}^{\Gamma(\text{BC})}(r) = u_i^0(r) \left(a_0 \frac{du_i^0}{dr} - b_0 u_i^0 \right)_{r=a_0}^{-1} - \frac{1}{2a_0} \sum_{j=1}^{n_c} \frac{u_{ij}^0(r)u_{ij}^0(a_0)}{E_{ij}^0 - E}, \quad i = 1, \dots, n. \quad (5.95)$$

Both terms on the right-hand side of this equation can be rapidly calculated in terms of the solutions of (5.75).

In the above derivation we have seen that with our special choice of boundary condition defined by (5.90) only the diagonal elements of the reduced radial wave function near the boundary $r = a_0$ need correcting. However, the general solution of the Schrödinger equation, defined by (5.89), is a linear combination of the solutions satisfying (5.90). Hence each element of the general solution will be corrected.

We conclude this section by remarking that including a Buttle correction to the R -matrix and the wave function, obtained using the homogeneous boundary condition method, means that these quantities are no longer derivable from the variational principle discussed in Sect. 5.2. However, this does not mean that the resultant R -matrix and wave function are less accurate than the R -matrix and wave function which are derived from a variational principle. Indeed in many practical situations the inclusion of a Buttle correction enables accurate results to be obtained using fewer terms in the R -matrix expansion.

5.3.3 Arbitrary Boundary Condition Methods

In this section we summarize methods where the radial continuum basis orbitals $u_{ij}^0(r)$ in the R -matrix expansion (5.6) are represented by functions which satisfy arbitrary boundary conditions at $r = a_0$. The application of some of these methods in potential scattering has been reviewed in Sect. 4.4.

In recent years R -matrix calculations using arbitrary boundary condition bases have found increasing application in the study of electron collisions with atoms and molecules as well as photoionization and multiphoton ionization processes. Non-orthogonal continuum basis orbitals satisfying arbitrary boundary conditions have also been found to give rapid convergence in studies of atomic vibrations in self-consistent field models of condensed matter by Liberman and Bennett [593] and in studies of electron transport in semiconductor devices discussed in Sect. 12.2.

The use of orbitals satisfying arbitrary boundary conditions removes the need to include a Buttle correction to the R -matrix, as well as to the wave function, as discussed in Sect. 5.3.2. In addition, the resultant solution can be derived from the multichannel variational principle for the R -matrix, as discussed in Sect. 5.2. Although homogeneous boundary condition methods with an appropriate choice of the zero-order differential equation (5.75) can often give fast convergence, for example, for electron collisions with atoms and atomic ions with many open and closed channels at low and intermediate energies, the use of arbitrary boundary condition basis orbitals is required to obtain accurate results in some applications. This is particularly true for time-dependent R -matrix theory of multiphoton processes discussed in Chap. 10, where the time evolution operator requires an accurate representation of the wave function on and near the boundary of the internal region.

A wide variety of basis orbitals satisfying arbitrary boundary conditions have been used in R -matrix calculations including Gaussian-type orbitals, Slater-type orbitals, Legendre functions, Lagrange meshes and B-splines. In early work on electron collisions with diatomic molecules, discussed further in Sect. 11.1, Schneider [821, 822] and Schneider and Hay [826] expanded the continuum orbitals in terms of Gaussian orbitals, yielding low-energy static-exchange cross sections for electron collisions with H_2 and F_2 . Also, the convergence properties of Slater-type orbital bases were explored by Noble et al. [690] for electron collisions with H_2 and N_2 , where it was found that accurate results can be efficiently obtained at low electron impact energies, but because of linear dependence problems numerical continuum

basis functions satisfying homogeneous boundary conditions were to be preferred at higher energies. A procedure for generating these continuum orbitals for electron–molecule collisions, analogous to that used in Sect. 5.3.1, was later developed by Tennyson et al. [922]. More recently, a considerable body of work has been carried out using Gaussian-type orbitals to represent both the bound and continuum orbitals in electron collisions with polyatomic molecules, in particular by Nestmann and Peyerimhoff [680], Pfingst et al. [732, 733], Nestmann et al. [682], Morgan et al. [661, 662] and Faure et al. [313]. This work showed that Gaussian-type orbitals can give accurate phase shifts and cross sections at low electron impact energies with relatively small bases.

Legendre basis functions have also been used in *R*-matrix collision calculations. For example, shifted Legendre polynomials have been used by Baluja et al. [47] and Sunderland et al. [896] in their implementation of the BBM propagator method for solving the coupled differential equations (5.29) in the external *R*-matrix region, discussed in Appendix E.3. These basis functions were also used in time-dependent *R*-matrix theory calculations of multiphoton processes in potential scattering by Burke and Burke [172]. Lagrange mesh methods have also been used in *R*-matrix calculations and work using these methods is reviewed in Sect. 4.4.6.

Recently, B-spline methods, which are reviewed in Sect. 4.4.7, have been increasingly used in *R*-matrix calculations. For example, van der Hart [930] used B-spline bases in *R*-matrix calculations for two-electron processes, obtaining accurate results for low-energy electron collisions with atomic hydrogen. This work was later extended by van der Hart [931] to electron impact excitation and ionization of He^+ , by van der Hart and Feng [318, 319, 935] to study double-electron ionization of He and by McKenna and van der Hart [623] to study single- and two-photon ionization of Ca. B-spline bases have also been used in time-dependent multiphoton ionization calculations by van der Hart et al. [937, 938] and by Lysaght et al. [603–606], which are discussed in Chap. 10.

Also, Zatsarinny [991] and Zatsarinny and Froese Fischer [993] have developed a general computer program for calculating matrix elements in atomic structure with non-orthogonal orbitals, which has been extended by Zatsarinny and Froese Fischer [994] to enable B-splines to be used in *R*-matrix calculations, with an application to Li photoionization. This program, which has been further extended to enable a wide range of atomic continuum processes to be calculated using non-orthogonal orbitals represented by B-splines, has been published by Zatsarinny [992]. This has enabled accurate calculations to be carried out for a number of collision processes including investigations by Zatsarinny et al. on photodetachment of He^- [1002], by Zatsarinny and Tayal on low-energy electron collisions with atomic oxygen [995] and sulphur [996, 997] and by Zatsarinny and Bartschat on electron collisions with neon [998], argon [999], zinc [1000] and Fe^+ [1001]. Finally we mention the use of B-spline bases in time-dependent multiphoton ionization calculations by Guan et al. [429, 431, 432] which are discussed in Chap. 10.

In conclusion, we will present results from *R*-matrix calculations using both homogeneous and arbitrary boundary condition methods in Sect. 5.6 and in later chapters.

5.3.4 Partitioned R -Matrix Method

We have seen in Sect 5.1 that in order to calculate the R -matrix, defined by (5.19), which determines the boundary condition (5.18) satisfied by the external region solution at $r = a_0$, it is necessary to diagonalize the Hamiltonian matrix H_{N+1} plus Bloch operator \mathcal{L}_{N+1} in a set of basis functions ψ_k^Γ yielding the eigenenergies E_k^Γ , defined by (5.7), and surface amplitudes w_{ik}^Γ defined by (5.21). We will see when we discuss recent low-energy electron collision calculations in Sect. 5.6 that the dimension of the Hamiltonian matrix can become very large and hence the time taken to diagonalize this matrix may dominate the total computation time. For example, in our discussion of electron collisions with Fe II in Sect. 5.6.5, we will see that the number of coupled channels can exceed many thousands and hence the dimension of the corresponding Hamiltonian matrix will be many tens of thousands. Also, in electron–molecule collisions the number of coupled channels can become very large. In this section we consider a partitioned R -matrix method, introduced for electron–atom and electron–ion collisions by Berrington and Ballance [94] which alleviates this difficulty. In this method, the eigenvalues and eigenvectors of the Hamiltonian matrix are partitioned into two groups, the first consisting of those with low eigenvalues which are accurately determined and the remainder with higher eigenvalues for which an approximation is derived. This enables accurate results to be obtained more efficiently, particularly when the Hamiltonian becomes large.

The partitioned R -matrix method commences from (5.6), which we rewrite using matrix notation as

$$\boldsymbol{\psi} = \boldsymbol{\phi}\mathbf{X}, \quad (5.96)$$

where we have defined the quantities in this equation as follows:

- $\boldsymbol{\psi}$ – row vector with dimension n_t , corresponding to ψ_k^Γ in (5.6);
- $\boldsymbol{\phi}$ – row vector with dimension n_t , corresponding to $\overline{\Phi}_i^\Gamma r_{N+1}^{-1} u_{ij}^0$ and χ_i^Γ in (5.6);
- \mathbf{X} – matrix with dimensions $n_t \times n_t$, corresponding to the coefficients a_{ijk}^Γ and b_{ik}^Γ in (5.6).

The coefficient matrix \mathbf{X} is determined by diagonalizing the Hamiltonian matrix H_{N+1} plus Bloch operator \mathcal{L}_{N+1} in the basis $\boldsymbol{\phi}$ where we define

$$H_{ij} = \langle \phi_i | H_{N+1} + \mathcal{L}_{N+1} | \phi_j \rangle_{\text{int}}, \quad i, j = 1, \dots, n_t. \quad (5.97)$$

It then follows from (5.96) that (5.7) can be rewritten as

$$\mathbf{X}^T \mathbf{H} \mathbf{X} = \mathbf{E}, \quad (5.98)$$

where \mathbf{E} is a diagonal $n_t \times n_t$ -dimensional matrix with diagonal elements E_k , $k = 1, \dots, n_t$. Also, since \mathbf{H} defined by (5.97) is a real symmetric matrix, then \mathbf{X} is a real orthogonal matrix.

The partitioned R -matrix method assumes that we have accurately determined only the l lowest eigenvalues E_j and the corresponding eigenvectors of the matrix \mathbf{H} . It follows from (5.98) that

$$\sum_{k=1}^{n_t} H_{ik} X_{kj} = X_{ij} E_j, \quad i = 1, \dots, n_t, \quad j = 1, \dots, l. \quad (5.99)$$

The remaining eigenvalues are then approximated by a single degenerate energy E_0 such that

$$\sum_{k=1}^{n_t} H_{ik} X_{kj} \approx X_{ij} E_0, \quad i = 1, \dots, n_t, \quad j = l+1, \dots, n_t, \quad (5.100)$$

where the combined $n_t \times n_t$ -dimensional eigenvector matrix \mathbf{X} is still real and orthogonal satisfying

$$\mathbf{X}^T \mathbf{X} = \mathbf{X} \mathbf{X}^T = \mathbf{I}. \quad (5.101)$$

In order to determine E_0 we minimize the following functional formed from (5.100)

$$\mathcal{X}(E_0) = \sum_{i=1}^{n_t} \sum_{j=l+1}^{n_t} \left(X_{ij} E_0 - \sum_{k=1}^{n_t} H_{ik} X_{kj} \right)^2, \quad (5.102)$$

which gives

$$\frac{\partial \mathcal{X}}{\partial E_0} = 2 \sum_{i=1}^{n_t} \sum_{j=l+1}^{n_t} X_{ij} \left(X_{ij} E_0 - \sum_{k=1}^{n_t} H_{ik} X_{kj} \right). \quad (5.103)$$

After using (5.101) we obtain

$$\frac{\partial \mathcal{X}}{\partial E_0} = 2 \left(\sum_{j=l+1}^{n_t} E_0 - \sum_{i=1}^{n_t} \sum_{j=l+1}^{n_t} \sum_{k=1}^{n_t} H_{ik} X_{ij} X_{kj} \right). \quad (5.104)$$

Then, setting $\partial \mathcal{X} / \partial E_0 = 0$ and using (5.101) gives

$$E_0 = \frac{(\text{Tr} \mathbf{H} - \sum_{i=1}^l E_i)}{(n_t - l)}, \quad (5.105)$$

where

$$\text{Tr}\mathbf{H} = \sum_{i=1}^{n_t} H_{ii}. \quad (5.106)$$

The partitioned R -matrix which replaces $R_{ij}^{\Gamma}(E)$ in (5.19) is then given by

$$R_{ij}^{\text{p}}(E) = \sum_{k=1}^l \frac{w_{ik}w_{jk}}{E_k - E} + \frac{1}{E_0 - E} \sum_{k=l+1}^{n_t} w_{ik}w_{jk}, \quad i, j = 1, \dots, n, \quad (5.107)$$

which can be rewritten as

$$R_{ij}^{\text{p}}(E) = \sum_{k=1}^l \frac{w_{ik}w_{jk}}{E_k - E} - \frac{1}{E_0 - E} \sum_{k=1}^l w_{ik}w_{jk} + \frac{1}{E_0 - E} \sum_{k=1}^{n_t} w_{ik}w_{jk}, \quad i, j = 1, \dots, n. \quad (5.108)$$

The first two terms on the right-hand side of (5.108) can be calculated since we know the surface amplitudes w_{ik} , $i = 1, \dots, n_t$, $k \leq l$ from the solution of (5.99). The last term on the right-hand side of (5.108) can be calculated using expansion (5.21) for the surface amplitudes w_{ik} . We obtain

$$\sum_{k=1}^{n_t} w_{ik}w_{jk} = \sum_{k'=1}^{n_c} \sum_{k''=1}^{n_c} u_{ik'}^0(a_0)u_{jk''}^0(a_0) \sum_{k=1}^{n_t} a_{ik'k}a_{jk''k}. \quad (5.109)$$

It then follows from the orthogonality relation (5.101) that the following summation in (5.109) is given by

$$\sum_{k=1}^{n_t} a_{ik'k}a_{jk''k} = \delta_{ij}\delta_{k'k''}, \quad (5.110)$$

and hence

$$\sum_{k=1}^{n_t} w_{ik}w_{jk} = \sum_{k=1}^{n_c} \left[u_{ik}^0(a_0) \right]^2 \delta_{ij} = S_i \delta_{ij}, \quad (5.111)$$

which defines S_i . Substituting this result into (5.108) gives the following expression for the partitioned R -matrix

$$R_{ij}^{\text{p}}(E) = \sum_{k=1}^l w_{ik} \left(\epsilon_k^{-1} - \epsilon_0^{-1} \right) w_{jk} + \left[S_i \epsilon_0^{-1} + R_i^c(E) \right] \delta_{ij}, \quad (5.112)$$

where we have written

$$\epsilon_k = E_k - E, \quad k = 0, \dots, l, \quad (5.113)$$

and where $R_i^c(E)$ is an estimate of the partitioning error. It follows from (5.19) and (5.107) that this error is given by

$$R_{ij}^c(E) = \sum_{k=l+1}^{n_l} w_{ik} w_{jk} \left(\frac{1}{E_k - E} - \frac{1}{E_0 - E} \right). \quad (5.114)$$

We can obtain an estimate for this error by replacing the surface amplitudes w_{ik} in (5.114) by the corresponding zero-order radial continuum basis orbitals $u_{ij}^0(a_0)$ in (5.21) obtained by neglecting the off-diagonal terms in diagonalizing $H_{N+1} + \mathcal{L}_{N+1}$ in the internal region. This is analogous to our choice of radial continuum basis orbitals used in the Buttle correction described in Sect. 5.3.2. With this approximation (5.114) yields the following estimate of the partitioning error:

$$R_i^c(E) = \sum_{j=N_i+1}^{n_c} \left[u_{ij}^0(a_0) \right]^2 \left(\frac{1}{E_{ij} - E} - \frac{1}{E_0 - E} \right), \quad (5.115)$$

where E_{ij} is the energy of the radial continuum basis orbital and N_i is such that the radial continuum basis orbitals in the i th channel above N_i lie above the highest eigenvalue explicitly included in (5.108).

The above theory has been extended to electron–molecule collisions by Tennyson [916]. In this case several modifications of the above theory were found to be necessary, which also apply to a lesser extent in electron–atom collisions. The first modification arises from the procedure used to generate the continuum orbitals for the electron–molecule collision problem. The need to orthogonalize the continuum orbitals to the bound orbitals used to represent the target [662, 922] means that the energies of the resultant continuum orbitals are not well defined, which requires a modification to the energies E_{ij} of the radial continuum basis orbitals in (5.115). The second and more important modification concerns the definition of E_0 in (5.105). This definition averages over all diagonal elements of the Hamiltonian matrix regardless of whether the configuration involved makes any contribution to the boundary amplitude. This means that many high-lying L^2 configurations included in the second expansion on the right-hand side of (5.6), which make no contribution to the boundary amplitude, contribute to the value of E_0 . As a result, a systematic improvement in the configuration interaction representation of the target and the consequent increase in the number of L^2 configurations included in the expansion leads to an undesirable increase in E_0 , even if all the other parameters of the calculation remain the same. It is therefore preferable to define E_0 using only those configurations which contribute directly to the boundary amplitude and hence to the R -matrix; a procedure for achieving this is given by Tennyson [916]. A final problem arises from the error correction procedure leading to (5.115). The use of

the entire boundary amplitude of the higher lying radial continuum basis orbitals $[u_{ij}^0(a_0)]^2$ in the error correction will lead to an over correction if these orbitals contribute to any significant extent to the lower l surface amplitudes retained explicitly in the first summation in (5.112). It is straightforward to estimate the contribution of these orbitals to the surface amplitudes not explicitly included in the summation in (5.112) and to make a corresponding modification to the error correction formula (5.114).

Finally, we observe that, if the radial continuum basis orbitals $u_{ij}^0(r)$ retained in expansion (5.6) satisfy homogeneous boundary conditions (5.76) and (5.77), as discussed in Sect. 5.3.1, then it is necessary to add a Buttler correction to the partitioned R -matrix defined by (5.112). However, if these orbitals satisfy arbitrary boundary conditions, as discussed in Sect. 5.3.3, then this correction will usually not be required although it will still be appropriate to include the partitioning error correction defined by (5.115).

5.4 Inclusion of Relativistic Effects

As the charge number Z on the atomic nucleus increases, relativistic effects become progressively more important in the collision process. In this section and in Sect. 5.5 we consider how these effects can be accurately represented in low-energy electron collisions with heavy atoms and atomic ions. There are two main ways in which relativistic effects play a role in low-energy electron collisions. First, there is a direct effect which is due to the relativistic distortion of the wave function of the scattered electron induced by the strong nuclear potential, when this electron is in the neighbourhood of the nucleus. Second, there is an indirect effect caused by the change in the charge distribution of the target electrons due to relativity which in turn affects the motion of the scattered electron. Our objective in this section and the next is to show how these two effects can be included in multichannel R -matrix theory, in addition to electron exchange and electron–electron correlation effects which we considered earlier in this chapter.

There are several procedures for including relativistic effects in low-energy electron collisions with atoms and atomic ions. For relatively light targets, these effects are small so that the energy intervals between the fine-structure levels of the target are small compared both with the energy intervals between the $LS\pi$ -coupled energy levels of the target and with the energy of the scattered electron. In this case the collision calculation can first be carried out in $LS\pi$ -coupling using the non-relativistic Hamiltonian, as described earlier in this chapter. The K -matrices obtained from this calculation are then recoupled to give the K -matrices, and hence the corresponding cross sections, for transitions between the fine-structure levels of the target. This approach was introduced by Saraph [810, 811] and extended by Griffin et al. [426] and Badnell and Griffin [34] using multichannel quantum defect theory. We discuss this approach in Sect. 5.4.1.

As the nuclear charge number Z increases, relativistic effects must be included both in the calculation of the N -electron wave function describing the target and

in the calculation of the $(N + 1)$ -electron wave function describing the collision process. Provided Z is not too large, this can be achieved by replacing the non-relativistic Hamiltonian, defined by (5.3), by the Breit–Pauli Hamiltonian discussed, for example, by Bethe and Salpeter [105], Akhiezer and Berestetsky [7] and Glass and Hibbert [382]. The conserved quantum numbers are now J the total angular momentum of the electron target atom collision wave function, M_J its z -component and π the total parity rather than L , S , M_L , M_S and π defined following (2.58). This leads to many more coupled channels which have to be included in the expansion of the collision wave function and to many more coupled integrodifferential equations which have to be solved. We consider in detail the extension of R -matrix collision theory to include the relativistic Breit–Pauli terms in the Hamiltonian in Sect. 5.4.2, having summarized the computer programs which implement this approach in Sect. 5.1.1. Then in Sect. 5.4.3 we consider a frame-transformation theory extension of this approach where the relativistic terms in the Breit–Pauli Hamiltonian are omitted in the high-energy spectrum in the internal R -matrix region but are included in the low-energy spectrum in the internal region and also in the external and asymptotic regions, with considerable saving in computational effort.

Finally, we observe that the above approaches for including relativistic effects using the Breit–Pauli Hamiltonian have been used with considerable success to treat electron collisions with a wide range of low and intermediate Z atoms and ions. However, in order to obtain accurate results for electron collisions with the heaviest atomic targets it is necessary to treat both the target and the collision wave function using the Dirac Hamiltonian. We present a detailed discussion of Dirac R -matrix theory of electron collisions with heavy atoms and ions in Sect. 5.5.

5.4.1 Transformation of the K - and S -Matrices

This approach is appropriate for light atomic or ionic targets where relativistic effects are small and hence the energy intervals between the fine-structure levels of the target are small compared with the energy intervals between the $LS\pi$ -coupled energy levels of the target and the energy of the scattered electron. K -matrices are first calculated, omitting all relativistic terms in the Hamiltonian, as described in Sect. 5.1. These K -matrices are then transformed to full intermediate coupling to yield cross sections corresponding to transitions between fine-structure levels of the target. This is the basis of a widely used computer program JAJOM, written by Saraph [810, 811] for electron–ion collisions. We also consider an extension of this approach using multichannel quantum defect theory by Griffin et al. [426] and Badnell and Griffin [34], which yields accurate transformed K - and S -matrices when some channels are closed.

For the situation where relativistic effects are not large, it is convenient to adopt the pair-coupling scheme defined by the equations

$$\mathbf{L}_i + \mathbf{S}_i = \mathbf{J}_i, \quad \mathbf{J}_i + \boldsymbol{\ell}_i = \mathbf{K}_i, \quad \mathbf{K}_i + \mathbf{s}_i = \mathbf{J}, \quad (5.116)$$

where \mathbf{L}_i , \mathbf{S}_i and \mathbf{J}_i are the orbital, spin and total angular momentum operators of the target atom or ion, ℓ_i and s_i are the orbital and spin angular momentum operators of the scattered electron, \mathbf{K}_i is an intermediate angular momentum operator and \mathbf{J} is the total angular momentum operator of the electron plus target atom or ion system which is conserved in the collision. This pair-coupling scheme can be related to the $LS\pi$ -coupling scheme adopted in Sect. 5.1 which is defined by the equations

$$\mathbf{L}_i + \ell_i = \mathbf{L}, \quad \mathbf{S}_i + s_i = \mathbf{S}, \quad \mathbf{L} + \mathbf{S} = \mathbf{J}. \quad (5.117)$$

The recoupling coefficient between these schemes can be simply expressed in terms of Racah coefficients, defined in Appendix A.2, as follows:

$$\begin{aligned} & \langle [(L_i S_i) J_i, \ell_i] K_i \frac{1}{2}; J M_J | (L_i \ell_i) L, (S_i \frac{1}{2}) S; J M_J \rangle \\ &= [(2L + 1)(2S + 1)(2J_i + 1)(2K_i + 1)]^{1/2} W(L \ell_i S_i J_i; L_i K_i) \\ & \quad \times W(L J S_i \frac{1}{2}; S K_i). \end{aligned} \quad (5.118)$$

We can then express the K -matrix $K_{\alpha\beta}^{J\pi}(E)$, defined in the pair-coupling scheme, in terms of the K -matrix $K_{ij}^{\Gamma}(E)$, determined in the $LS\pi$ -coupling scheme by the equation

$$\begin{aligned} K_{\alpha\beta}^{J\pi}(E) &= \sum_{LS} \langle [(L_i S_i) J_i, \ell_i] K_i \frac{1}{2}; J M_J | (L_i \ell_i) L, (S_i \frac{1}{2}) S; J M_J \rangle K_{ij}^{\Gamma}(E) \\ & \quad \times \langle (L_j \ell_j) L, (S_j \frac{1}{2}) S; J M_J | [(L_j S_j) J_j, \ell_j] K_j \frac{1}{2}; J M_J \rangle, \end{aligned} \quad (5.119)$$

where the summation goes over all LS values which contribute to the J value considered. Also the channel subscripts α and β on the K -matrix elements $K_{\alpha\beta}^{J\pi}(E)$ in (5.119) represent the quantum numbers

$$\alpha \equiv \alpha_i L_i S_i J_i \ell_i K_i \frac{1}{2}, \quad \beta \equiv \alpha_j L_j S_j J_j \ell_j K_j \frac{1}{2}. \quad (5.120)$$

It follows that the K -matrix must first be determined in $LS\pi$ -coupling for all significant $LS\pi$ values when relativistic terms in the Hamiltonian are omitted. Equation (5.119) is then used to transform the K -matrix from the $LS\pi$ -coupling scheme to the pair-coupling scheme for all relevant $J\pi$ values.

For atoms and ions where the term splitting¹ in the target due to relativistic effects is small compared with the term separation, the transformation involving the angular momentum variables given by (5.119) provides an accurate representation of the collision. However, with increasing nuclear charge number Z , relativistic effects increase in importance and the target Hamiltonian can no longer be treated as diagonal with respect to the target quantum numbers L_i and S_i . If relativistic effects are

¹ In this discussion a term corresponds to a target state belonging to the quantum numbers $\alpha_i L_i S_i \pi_i$ in the absence of relativistic effects (see, for example, [232]).

not large, it is appropriate to represent these effects by expanding the resultant target states in terms of the target states retained in the original $LS\pi$ -coupled expansion defined by (5.5) and (5.6) omitting relativistic effects. We first recouple the original $LS\pi$ -coupled target states as follows:

$$\begin{aligned} \Phi_i(\alpha_i L_i S_i J_i M_{J_i} \pi_i | \mathbf{X}_N) &= \sum_{M_{L_i} M_{S_i}} (L_i M_{L_i} S_i M_{S_i} | J_i M_{J_i}) \\ &\times \Phi_i(\alpha_i L_i S_i M_{L_i} M_{S_i} \pi_i | \mathbf{X}_N), \end{aligned} \quad (5.121)$$

where $(L_i M_{L_i} S_i M_{S_i} | J_i M_{J_i})$ are Clebsch–Gordan coefficients defined in Appendix A.1 and where we have explicitly denoted the dependence of the target states on the angular momentum quantum numbers, as in (2.14). We then expand the target states including relativistic effects in terms of these recoupled states according to

$$\Phi_i(\Delta_i J_i M_{J_i} \pi_i | \mathbf{X}_N) = \sum_{\alpha_i L_i S_i} f(\Delta_i J_i \pi_i; \alpha_i L_i S_i \pi_i) \Phi_i(\alpha_i L_i S_i J_i M_{J_i} \pi_i | \mathbf{X}_N), \quad (5.122)$$

where the summation goes over all the target states retained in the original $LS\pi$ -coupled expansion defined by (5.6) which can couple to $J_i M_{J_i} \pi_i$ and where we have introduced a parameter Δ_i which replaces α_i and which serves to distinguish different target states with the same total angular momentum and parity. The term-coupling coefficients $f(\Delta_i J_i \pi_i; \alpha_i L_i S_i \pi_i)$, defined by (5.122) [509, 510], can be obtained by diagonalizing the Breit–Pauli target Hamiltonian H_N^{BP} , which includes relativistic terms as described in Sect. 5.4.2, in this new basis for each $J_i \pi_i$ as follows:

$$\langle \Phi_i(\Delta_i J_i M_{J_i} \pi_i | \mathbf{X}_N) | H_N^{\text{BP}} | \Phi_j(\Delta_j J_j M_{J_j} \pi_j | \mathbf{X}_N) \rangle = e^{J_i \pi_i} \delta_{ij}, \quad i, j = 1, \dots, n_i, \quad (5.123)$$

where n_i is the number of target states with $J_i \pi_i$ symmetry represented by the parameters Δ_i and Δ_j . The K -matrix $K_{\mu\nu}^{J\pi}(E)$ in this “full intermediate coupling” representation is then given in terms of the original K -matrix $K_{\alpha\beta}^{J\pi}(E)$, defined by (5.119), by

$$K_{\mu\nu}^{J\pi}(E) = \sum_{\alpha_i L_i S_i} \sum_{\alpha_j L_j S_j} f(\Delta_i J_i \pi_i; \alpha_i L_i S_i \pi_i) K_{\alpha\beta}^{J\pi}(E) f(\Delta_j J_j \pi_j; \alpha_j L_j S_j \pi_j), \quad (5.124)$$

where the channel subscripts μ and ν on the K -matrix elements $K_{\mu\nu}^{J\pi}(E)$ in this equation represent the following quantum numbers:

$$\mu \equiv \Delta_i J_i \ell_i K_i \frac{1}{2}, \quad \nu \equiv \Delta_j J_j \ell_j K_j \frac{1}{2}. \quad (5.125)$$

The multichannel S -matrix and hence the T -matrix in the pair-coupling scheme are then obtained in terms of the K -matrices defined by (5.119) and (5.124) using

the procedure described in Sect. 2.5. The S -matrix is defined in terms of the K -matrix, in analogy with (2.112), by the matrix equation

$$\mathbf{S}^{J\pi} = \frac{\mathbf{I} + i\mathbf{K}^{J\pi}}{\mathbf{I} - i\mathbf{K}^{J\pi}}, \quad (5.126)$$

and the corresponding T -matrix is defined in analogy with (2.119) by

$$\mathbf{T}^{J\pi} = \mathbf{S}^{J\pi} - \mathbf{I}. \quad (5.127)$$

The cross sections and collision strengths for transitions between the fine-structure levels of the target can be obtained in this new coupling scheme, as described in Sect. 2.5. We obtain the following result for the total cross section

$$\sigma^{\text{Tot}}(i \rightarrow j) = \sum_{J\pi} \sigma^{J\pi}(i \rightarrow j), \quad (5.128)$$

where the partial wave cross sections

$$\sigma^{J\pi}(i \rightarrow j) = \frac{(2J+1)}{2k_i^2(2J_i+1)} \sum_{\ell_i \ell_j K_i K_j} |T_{ji}^{J\pi}|^2 \quad (5.129)$$

are given in units of πa_0^2 .

The transformation procedure using (5.119) and (5.124) is appropriate when all the channels included in (5.5) and (5.6) are open. However, a difficulty arises at low electron impact energies where some of these channels are closed. In this energy region, some of the terms included in the term coupling expansion (5.122) correspond to open channels and others correspond to closed channels. Consequently, the transformation of the K -matrix to full intermediate coupling, defined by (5.119) and (5.124), breaks down since the K -matrix, which has dimension $n_a \times n_a$, only includes the n_a open channels. The procedure usually adopted for dealing with this situation, using the Saraph computer program [810, 811], has been to set all the energy levels corresponding to a given term equal and to include after renormalization only those components of the term-coupling coefficients corresponding to open channels in the calculation. However, this procedure can lead to poor threshold energies, incorrect resonance structure and anomalous threshold effects in the cross sections as new terms are included in the calculation when the energy increases through the term thresholds.

In more recent electron–positive ion collision calculations by Griffin et al. [426] and Badnell and Griffin [34], the inconsistencies discussed in the previous paragraph have been removed using multichannel quantum defect theory (MQDT), discussed in Sect. 3.3.4. In this intermediate coupling frame transformation (ICFT) method, the unphysical K -matrices (\mathcal{K}) and S -matrices (χ), defined in Sect. 3.3.4, are first calculated on a coarse mesh in $LS\pi$ -coupling, neglecting relativistic effects.

These unphysical matrices are analytic functions of energy, which do not contain the threshold branch cuts, and have the dimension $n \times n$ at all energies, where n is the number of coupled channels. Hence they can be interpolated onto a fine energy mesh. The resultant unphysical matrices can then be transformed to full intermediate coupling using (5.119) and (5.124) for all required energies both above and below the thresholds. The physical K - and S -matrices in the open channels are then shown in Sect. 3.3.4 to be related to the unphysical K - and S -matrices as follows:

$$\mathbf{K}_{oo}^{J\pi} = \mathcal{K}_{oo}^{J\pi} - \mathcal{K}_{oc}^{J\pi} \frac{1}{\mathcal{K}_{cc}^{J\pi} + \tan(\pi \mathbf{v}_c)} \mathcal{K}_{co}^{J\pi} \quad (5.130)$$

and

$$\mathbf{S}_{oo}^{J\pi} = \mathcal{X}_{oo}^{J\pi} - \mathcal{X}_{oc}^{J\pi} \frac{1}{\mathcal{X}_{cc}^{J\pi} - \exp(-2\pi i \mathbf{v}_c)} \mathcal{X}_{co}^{J\pi}, \quad (5.131)$$

where \mathbf{v}_c is a diagonal matrix in the closed channels whose diagonal elements are defined by

$$v_i^2 = -\frac{(Z - N)^2}{k_i^2}, \quad i = n_a + 1, \dots, n, \quad (5.132)$$

where n_a is the number of open channels at the energy under consideration.

The T -matrix and cross sections for transitions between the fine-structure levels corresponding to the open channels are then given in terms of the open channel physical S -matrix $\mathbf{S}_{oo}^{J\pi}$ by (5.127), (5.128) and (5.129). Since the unphysical K - and S -matrices are smooth functions of energy, the fine-structure splitting of the energy levels of the target can be accurately included in the calculation. Also resonance structures which converge to all excited thresholds are included through the inverse terms in (5.130) and (5.131). In conclusion, this application of MQDT enables relativistic effects and resonance structures to be accurately included in electron–positive ion collisions for relatively light targets, by solving the time-independent Schrödinger equation in $LS\pi$ -coupling on a coarse mesh of energies using the non-relativistic R -matrix method, discussed in Sect. 5.1.

5.4.2 Breit–Pauli Hamiltonian

As the nuclear charge number Z increases relativistic effects must be included in the Hamiltonian used to determine both the target atom or ion wave function and the electron–target atom or ion collision wave function. This can be achieved, provided Z is not too large, by using the Breit–Pauli Hamiltonian (e.g. [7, 105, 382]).

The $(N + 1)$ -electron Breit–Pauli Hamiltonian can be written as

$$H_{N+1}^{\text{BP}} = H_{N+1}^{\text{NR}} + H_{N+1}^{\text{REL}}, \quad (5.133)$$

where H_{N+1}^{NR} , the non-relativistic Hamiltonian, is defined by (5.3) and H_{N+1}^{REL} consists of one- and two-body relativistic terms resulting from the reduction of the Dirac equation and the Breit interaction to Pauli form.

The one-body terms are defined by

$$H_{N+1}^{\text{MC}} = -\frac{1}{8}\alpha^2 \sum_{i=1}^{N+1} \nabla_i^4, \quad \text{relativistic mass-correction,} \quad (5.134)$$

$$H_{N+1}^{\text{D}_1} = -\frac{1}{8}\alpha^2 Z \sum_{i=1}^{N+1} \nabla_i^2 \left(\frac{1}{r_i} \right), \quad \text{one-body Darwin,} \quad (5.135)$$

$$H_{N+1}^{\text{SO}} = \frac{1}{2}\alpha^2 Z \sum_{i=1}^{N+1} r_i^{-3} (\boldsymbol{\ell}_i \cdot \mathbf{s}_i), \quad \text{spin-orbit,} \quad (5.136)$$

and the two-body terms are defined by

$$H_{N+1}^{\text{SOO}} = -\frac{1}{2}\alpha^2 \sum_{i \neq j=1}^{N+1} \left(\frac{\mathbf{r}_{ij}}{r_{ij}^3} \times \mathbf{p}_i \right) \cdot (\mathbf{s}_i + 2\mathbf{s}_j), \quad \text{spin-other orbit,} \quad (5.137)$$

$$H_{N+1}^{\text{OO}} = -\frac{1}{2}\alpha^2 \sum_{i < j=1}^{N+1} \left(\frac{\mathbf{p}_i \cdot \mathbf{p}_j}{r_{ij}} + \frac{\mathbf{r}_{ij}(\mathbf{r}_{ij} \cdot \mathbf{p}_i) \cdot \mathbf{p}_j}{r_{ij}^3} \right), \quad \text{orbit-orbit,} \quad (5.138)$$

$$H_{N+1}^{\text{SS}} = \alpha^2 \sum_{i < j=1}^{N+1} \frac{1}{r_{ij}^3} \left(\mathbf{s}_i \cdot \mathbf{s}_j - \frac{3(\mathbf{s}_i \cdot \mathbf{r}_{ij})(\mathbf{s}_j \cdot \mathbf{r}_{ij})}{r_{ij}^2} \right), \quad \text{spin-spin,} \quad (5.139)$$

$$H_{N+1}^{\text{D}_2} = \frac{1}{4}\alpha^2 \sum_{i < j=1}^{N+1} \nabla_i^2 \left(\frac{1}{r_{ij}} \right), \quad \text{two-body Darwin,} \quad (5.140)$$

$$H_{N+1}^{\text{SSC}} = -\frac{8\pi\alpha^2}{3} \sum_{i < j=1}^{N+1} (\mathbf{s}_i \cdot \mathbf{s}_j) \delta(\mathbf{r}_i \cdot \mathbf{r}_j), \quad \text{spin-spin contact.} \quad (5.141)$$

The Breit–Pauli Hamiltonian can then be rewritten as

$$H_{N+1}^{\text{BP}} = H_{N+1}^{\text{NR}} + H_{N+1}^{\text{FS}} + H_{N+1}^{\text{NFS}}, \quad (5.142)$$

where H_{N+1}^{FS} are fine-structure terms defined by

$$H_{N+1}^{\text{FS}} = H_{N+1}^{\text{SO}} + H_{N+1}^{\text{SOO}} + H_{N+1}^{\text{SS}}, \quad (5.143)$$

while H_{N+1}^{NFS} are non-fine-structure terms defined by

$$H_{N+1}^{\text{NFS}} = H_{N+1}^{\text{MC}} + H_{N+1}^{\text{D}_1} + H_{N+1}^{\text{OO}} + H_{N+1}^{\text{D}_2} + H_{N+1}^{\text{SSC}}. \quad (5.144)$$

The non-fine-structure terms commute with the operators \mathbf{L}^2 , \mathbf{S}^2 , L_z , S_z and π while the fine-structure terms only commute with the operators \mathbf{J}^2 , J_z and π . Thus it is necessary to use a representation which is diagonal in \mathbf{J}^2 , J_z and π . In practice, for electron collision calculations, the one-body terms defined by (5.134), (5.135) and (5.136) are found to be the most important and often only these terms in addition to H_{N+1}^{NR} are retained in calculations using the Breit–Pauli Hamiltonian H_{N+1}^{BP} . However, other terms, including in particular the spin–other orbit term (5.137), can also play a significant role and have been included in some recent R -matrix calculations.

We now consider the solution of the time-independent Breit–Pauli equation

$$H_{N+1}^{\text{BP}}\Psi = E\Psi. \quad (5.145)$$

As in non-relativistic R -matrix theory of electron collisions with atoms and atomic ions, we partition configuration space into three regions as illustrated in Fig. 5.1. We now discuss the solution in each of these regions in turn.

5.4.2.1 Internal Region Solution

In the internal region, corresponding to $0 \leq r \leq a_0$ in Fig. 5.1, the collision wave function can be written in analogy with (5.5) as

$$\Psi_{jE}^{JM_J\pi}(\mathbf{X}_{N+1}) = \sum_k \psi_k^{JM_J\pi}(\mathbf{X}_{N+1}) A_{kj}^{JM_J\pi}(E), \quad (5.146)$$

for each set of conserved quantum numbers J , M_J and π , where J is the total angular momentum quantum number, M_J is the corresponding magnetic quantum number and π is the parity. Also in (5.146) j labels the linearly independent solutions of (5.145), $\psi_k^{JM_J\pi}$ are energy-independent basis functions and $A_{kj}^{JM_J\pi}(E)$ are energy-dependent expansion coefficients which depend on the asymptotic boundary conditions satisfied by the wave function $\Psi_{jE}^{JM_J\pi}$ at the energy E . In analogy with (5.6) we expand the basis functions $\psi_k^{JM_J\pi}$ as follows:

$$\begin{aligned} \psi_k^{JM_J\pi}(\mathbf{X}_{N+1}) &= \mathcal{A} \sum_{i=1}^n \sum_{j=1}^{n_c} \overline{\Phi}_i^{JM_J\pi}(\mathbf{X}_N; \hat{\mathbf{r}}_{N+1}\sigma_{N+1}) r_{N+1}^{-1} u_{ij}^0(r_{N+1}) a_{ijk}^{J\pi} \\ &+ \sum_{i=1}^m \chi_i^{JM_J\pi}(\mathbf{X}_{N+1}) b_{ik}^{J\pi}, \quad k = 1, \dots, n_t, \end{aligned} \quad (5.147)$$

where n is the number of channel functions, n_c is the number of continuum orbitals retained in each channel, m is the number of quadratically integrable functions and $n_t = nn_c + m$ is the total number of linearly independent basis functions retained in this expansion. As noted earlier, the values of n , n_c , m and n_t are now considerably larger than the values corresponding to equivalent calculations using the non-relativistic expansion (5.6).

In order to determine the channel functions $\overline{\Phi}_i^{JM_J\pi}$ in (5.147) we commence with the target states $\Phi_i(\alpha_i L_i S_i M_{L_i} M_{S_i} \pi_i | \mathbf{X}_N)$ which diagonalize the non-relativistic target Hamiltonian H_N^{NR} as described in Sect. 2.2. We then recouple these states as in (5.121) to yield target states $\Phi_i(\alpha_i L_i S_i J_i M_{J_i} \pi_i | \mathbf{X}_N)$ belonging to the quantum numbers $L_i S_i J_i M_{J_i} \pi_i$. If relativistic effects in the target are not important then the channel functions are determined in the pair-coupling scheme defined by (5.116) as follows:

$$\begin{aligned} & \overline{\Phi}_i^{JM_J\pi}(\mathbf{X}_N; \hat{\mathbf{r}}_{N+1} \sigma_{N+1}) \\ &= \sum_{M_{J_i} m_{\ell_i} M_{K_i} m_i} (J_i M_{J_i} \ell_i m_{\ell_i} | K_i M_{K_i}) (K_i M_{K_i} \frac{1}{2} m_i | J M_J) \\ & \quad \times \Phi_i(\alpha_i L_i S_i J_i M_{J_i} \pi_i | \mathbf{X}_N) Y_{\ell_i m_{\ell_i}}(\theta_{N+1}, \phi_{N+1}) \chi_{\frac{1}{2} m_i}(\sigma_{N+1}). \end{aligned} \quad (5.148)$$

However, with increasing nuclear charge number Z the channel functions $\overline{\Phi}_i^{JM_J\pi}$ can no longer be accurately represented by eigenstates of the total orbital and spin angular momentum operators \mathbf{L}_i^2 and \mathbf{S}_i^2 , as assumed in (5.121) and (5.148). If the relativistic effects are not too large, then the target states can be represented by an expansion over the target states defined by (5.121) for each $J_i M_{J_i} \pi_i$ symmetry. Following our discussion in Sect. 5.4.1 we write

$$\Phi_i(\Delta_i J_i M_{J_i} \pi_i | \mathbf{X}_N) = \sum_{\alpha_i L_i S_i} f(\Delta_i J_i \pi_i; \alpha_i L_i S_i \pi_i) \Phi_i(\alpha_i L_i S_i J_i M_{J_i} \pi_i | \mathbf{X}_N), \quad (5.149)$$

where the summation in this equation goes over all target states retained in the original R -matrix expansion in (5.147) with the given $J_i \pi_i$ symmetry, and where we have introduced a level parameter Δ_i in this equation to distinguish different target states with the same $J_i M_{J_i} \pi_i$ symmetry. The term-coupling coefficients $f(\Delta_i J_i \pi_i; \alpha_i L_i S_i \pi_i)$ in (5.149) are determined by diagonalizing the target Breit–Pauli Hamiltonian H_N^{BP} in the basis $\Phi_i(\alpha_i L_i S_i J_i M_{J_i} \pi_i | \mathbf{X}_N)$ for each $J_i \pi_i$ symmetry as in (5.123) yielding the target energies $e_i^{J_i \pi_i}$. Equation (5.148), defining the channel functions, is then replaced by

$$\begin{aligned} & \overline{\Phi}_i^{JM_J\pi}(\mathbf{X}_N; \hat{\mathbf{r}}_{N+1} \sigma_{N+1}) \\ &= \sum_{M_{J_i} m_{\ell_i} M_{K_i} m_i} (J_i M_{J_i} \ell_i m_{\ell_i} | K_i M_{K_i}) (K_i M_{K_i} \frac{1}{2} m_i | J M_J) \\ & \quad \times \Phi_i(\Delta_i J_i M_{J_i} \pi_i | \mathbf{X}_N) Y_{\ell_i m_{\ell_i}}(\theta_{N+1}, \phi_{N+1}) \chi_{\frac{1}{2} m_i}(\sigma_{N+1}). \end{aligned} \quad (5.150)$$

Next the quadratically integrable functions $\chi_i^{JM_J\pi}$ in (5.147) can be obtained by recoupling the quadratically integrable functions χ_i^Γ retained in (5.6) in the absence of relativistic effects. In analogy with (5.121) we write

$$\chi_i^{JM_J\pi}(\alpha L S J M_J \pi | \mathbf{X}_{N+1}) = \sum_{M_L M_S} (L M_L S M_S | J M_J) \chi_i^\Gamma(\alpha L S M_L M_S \pi | \mathbf{X}_{N+1}). \quad (5.151)$$

Finally, the continuum basis orbitals $u_{ij}^0(r)$ in (5.147) can be determined using a similar approach to that described in Sect. 5.3.

Having defined the channel functions, quadratically integrable functions and continuum basis orbitals in (5.147), we can determine the coefficients $a_{ij}^{J\pi}$ and $b_{ik}^{J\pi}$ by diagonalizing $H_{N+1}^{\text{BP}} + \mathcal{L}_{N+1}$ in this basis as follows:

$$\langle \psi_k^{JM_J\pi} | H_{N+1}^{\text{BP}} + \mathcal{L}_{N+1} | \psi_{k'}^{JM_J\pi} \rangle_{\text{int}} = E_k^{J\pi} \delta_{kk'}, \quad k, k' = 1, \dots, n_t, \quad (5.152)$$

where the Bloch operator \mathcal{L}_{N+1} in this equation ensures that $H_{N+1}^{\text{BP}} + \mathcal{L}_{N+1}$ is hermitian in the space of functions satisfying arbitrary boundary conditions on the surface of the sphere of radius $r = a_0$ enveloping the internal region. It is defined by (5.8) since we will see that the relativistic terms in the Breit–Pauli Hamiltonian do not modify the form of the coupled second-order differential equations, given by (5.159), which are satisfied by the scattered electron on the boundary $r = a_0$ of the internal region, for the intermediate values of Z of interest in this section.

We then proceed using a straightforward extension of the approach adopted in non-relativistic electron collisions with atoms and atomic ions, described in Sect. 5.1.2. The reduced radial wave functions $F_{ij}^{J\pi}(r)$, describing the motion of the scattered electron in the i th channel, satisfy the equation

$$F_{ij}^{J\pi}(a_0) = \sum_{i'=1}^n R_{ii'}^{J\pi}(E) \left(a_0 \frac{dF_{i'j}^{J\pi}}{dr} - b_0 F_{i'j}^{J\pi} \right)_{r=a_0}, \quad i = 1, \dots, n, \quad (5.153)$$

where the elements of the R -matrix $R_{ii'}^{J\pi}(E)$ are defined by

$$R_{ii'}^{J\pi}(E) = \frac{1}{2a_0} \sum_{k=1}^{n_t} \frac{w_{ik}^{J\pi} w_{i'k}^{J\pi}}{E_k^{J\pi} - E}, \quad i, i' = 1, \dots, n, \quad (5.154)$$

the functions $F_{ij}^{J\pi}(r)$ are defined by

$$F_{ij}^{J\pi}(r_{N+1}) = \langle r_{N+1}^{-1} \overline{\Phi}_i^{JM_J\pi} | \Psi_{jE}^{JM_J\pi} \rangle', \quad i = 1, \dots, n \quad (5.155)$$

and the surface amplitudes $w_{ik}^{J\pi}$ are defined by

$$\begin{aligned}
w_{ik}^{J\pi} &= \langle r_{N+1}^{-1} \overline{\Phi}_i^{JM_J\pi} | \psi_k^{JM_J\pi} \rangle'_{r_{N+1}=a_0} \\
&= \sum_{j=1}^{n_c} u_{ij}^0(a_0) a_{ijk}^{J\pi}, \quad i = 1, \dots, n, \quad k = 1, \dots, n_t. \quad (5.156)
\end{aligned}$$

A Buttle correction to the R -matrix and wave function can be included as discussed for non-relativistic electron collisions in Sect. 5.3.2. We can also write down an alternative expression for the reduced radial wave functions $F_{ij}^{J\pi}(r)$ by substituting for $\Psi_{jE}^{JM_J\pi}$ from (5.146) into (5.155) giving

$$F_{ij}^{J\pi}(r_{N+1}) = \sum_{k=1}^{n_t} \langle r_{N+1}^{-1} \overline{\Phi}_i^{JM_J\pi} | \psi_k^{JM_J\pi} \rangle' A_{kj}^{JM_J\pi}(E), \quad i = 1, \dots, n. \quad (5.157)$$

As in (5.20), (5.21) and (5.22), the primes on the Dirac brackets in (5.155), (5.156) and (5.157) mean that the integrations are carried out over the space and spin coordinates of all $N + 1$ electrons in the internal region, except the radial coordinate r_{N+1} of the scattered electron, where the resulting integral is independent of the magnetic quantum number M_J . Finally, we note that (5.153) provides the boundary condition for the solution of the electron–atom collision problem in the external region.

5.4.2.2 External Region Solution

In the external region, corresponding to $a_0 \leq r \leq a_p$ in Fig. 5.1, electron exchange and correlation effects between the scattered electron and the target atom or atomic ion can be neglected and (5.147) reduces to

$$\Psi_{jE}^{JM_J\pi}(\mathbf{X}_{N+1}) = \sum_{i=1}^n \overline{\Phi}_i^{JM_J\pi}(\mathbf{X}_N; \hat{\mathbf{r}}_{N+1} \sigma_{N+1}) r_{N+1}^{-1} F_{ij}^{J\pi}(r_{N+1}), \quad r_{N+1} \geq a_0, \quad (5.158)$$

where j labels the linearly independent solutions. Also, the channel functions $\overline{\Phi}_i^{JM_J\pi}$ in (5.158) are defined by either (5.148) or (5.150), depending on the importance of relativistic effects in the target, and $F_{ij}^{J\pi}(r)$ are energy-dependent reduced radial wave functions, defined by (5.155). Following our discussion of non-relativistic collisions given in Sect. 5.1.3, the coupled equations satisfied by the reduced radial functions $F_{ij}^{J\pi}(r)$ in (5.158) are obtained by substituting (5.158) into the Breit–Pauli equation (5.145) and projecting onto the channel functions $\overline{\Phi}_i^{JM_J\pi}$. We find that the functions $F_{ij}^{J\pi}(r)$ satisfy the following set of coupled second-order differential equations:

$$\left(\frac{d^2}{dr^2} - \frac{\ell_i(\ell_i + 1)}{r^2} + \frac{2(Z - N)}{r} + k_i^2 \right) F_{ij}^{J\pi}(r) = 2 \sum_{i'=1}^n V_{ii'}^{J\pi}(r) F_{i'j}^{J\pi}(r), \quad i = 1, \dots, n, \quad r \geq a_0, \quad (5.159)$$

where ℓ_i is the orbital angular momentum of the scattered electron, k_i^2 is the square of the wave number of the scattered electron defined by

$$k_i^2 = 2 \left(E - e_i^{J_i \pi_i} \right), \quad i = 1, \dots, n \quad (5.160)$$

and the potential matrix $V_{ii'}^{J\pi}(r)$ is defined by

$$\begin{aligned} V_{ii'}^{J\pi}(r_{N+1}) = & \langle r_{N+1}^{-1} \overline{\Phi}_i^{JM_J\pi}(\mathbf{X}_N; \hat{\mathbf{r}}_{N+1} \sigma_{N+1}) \left| \sum_{k=1}^N \frac{1}{r_{kN+1}} - \frac{N}{r_{N+1}} \right| \\ & \times r_{N+1}^{-1} \overline{\Phi}_{i'}^{JM_J\pi}(\mathbf{X}_N; \hat{\mathbf{r}}_{N+1} \sigma_{N+1}) \rangle', \quad i, i' = 1, \dots, n, \end{aligned} \quad (5.161)$$

which replaces (2.66) when relativistic terms are retained in the Hamiltonian. Following our discussion in Sect. 2.3, this potential matrix can be written as a summation over inverse powers of r as follows:

$$V_{ii'}^{J\pi}(r) = \sum_{\lambda=1}^{\lambda_{\max}} \alpha_{ii'\lambda}^{J\pi} r^{-\lambda-1}, \quad r \geq a_0, \quad i, i' = 1, \dots, n, \quad (5.162)$$

where the long-range potential coefficients $\alpha_{ii'\lambda}^{J\pi}$ are defined, in analogy with (2.74), by the equation

$$\begin{aligned} \alpha_{ii'\lambda}^{J\pi} = & \langle r_{N+1}^{-1} \overline{\Phi}_i^{JM_J\pi}(\mathbf{X}_N; \hat{\mathbf{r}}_{N+1} \sigma_{N+1}) \left| \sum_{k=1}^N r_k^\lambda P_\lambda(\cos \theta_{kN+1}) \right| \\ & \times r_{N+1}^{-1} \overline{\Phi}_{i'}^{JM_J\pi}(\mathbf{X}_N; \hat{\mathbf{r}}_{N+1} \sigma_{N+1}) \rangle', \quad i, i' = 1, \dots, n, \\ & \lambda = 1, \dots, \lambda_{\max}. \end{aligned} \quad (5.163)$$

We derive explicit expressions for these coefficients in Appendix D.1; see (D.25) and (D.26).

The solution of (5.159) can be obtained by sub-dividing the external region into p sub-regions, as illustrated in Fig. 5.1, and propagating the R -matrix for each required energy from $r = a_0$ to a_p as described in Appendix E. Since the expression for the long-range potential coefficients, defined by (D.25) and (D.26), is diagonal in the quantum number K_i , defined following (5.116), then the set of second-order differential equations (5.159) sub-divide into two uncoupled sets of equations depending on whether $K_i = J - \frac{1}{2}$ or $K_i = J + \frac{1}{2}$. This enables more efficient R -matrix propagator methods to be used with considerable saving in computational effort, as discussed in Appendix E.6. This is analogous to the situation in non-relativistic collisions of electrons with atoms and atomic ions, discussed in Sect. 5.1.3, where the corresponding second-order differential equations sub-divide into two uncoupled sets of equations depending on whether the target spin $S_i = S - \frac{1}{2}$ or $S_i = S + \frac{1}{2}$.

5.4.2.3 Asymptotic Region Solution

The solution of the time-independent Breit–Pauli equation (5.145) in the asymptotic region, corresponding to $a_p \leq r \leq \infty$ proceeds as in non-relativistic electron collisions described in Sect. 5.1.4. In this region (5.147) again reduces to (5.158), where the reduced radial wave functions $F_{ij}^{J\pi}(r)$ satisfy the coupled second-order differential equations (5.159). As in Sect. 5.1.4 we assume that the radius a_p is chosen large enough that one of the asymptotic expansion methods discussed in Appendix F.1 gives an accurate solution of (5.159) in this region. We are then able to use these solutions to relate the $n_a \times n_a$ -dimensional K -matrix $\mathbf{K}^{J\pi}(E)$ to the $n \times n$ -dimensional R -matrix $\mathbf{R}^{J\pi}(E)$ at $r = a_p$, where n_a is the number of open channels at the energy under consideration. Finally, having determined the K -matrix we can determine the S -matrix and hence the T -matrix, as described in Sect. 5.1.4.

The total and partial wave cross sections for transitions between fine-structure levels of the target are then given by (5.128) and (5.129). We see that the definition of the cross section is formally the same as that given in Sect. 5.4.1, where the transformed K -matrices, defined by (5.119) and (5.124), are used to calculate the S - and T -matrices. However, using the Breit–Pauli Hamiltonian correctly accounts for the kinematics of the scattered electron and gives a consistent treatment of the collision above and below thresholds.

5.4.3 Frame-Transformation Theory

One computational difficulty, which arises as a result of using the Breit–Pauli Hamiltonian (5.133) rather than the non-relativistic Hamiltonian (5.3), is that the number of coupled channels included in the internal region expansion (5.147) is greatly increased for the same set of target states included in the non-relativistic expansion (5.6). This results in a corresponding increase in the size of the Hamiltonian matrices in (5.152) that must be diagonalized. For example in e^- –Fe II collisions, considered in Sect. 5.6.5, if all $LS\pi$ -coupled target states corresponding to the five target configurations

$$3d^64s, 3d^7, 3d^64p, 3d^54s^2, 3d^54s4p \quad (5.164)$$

are included in the expansion of the total wave function then, when relativistic effects are omitted, a maximum of 818 coupled channels are obtained for total spin state $S = 1$ and a maximum of 354 coupled channels are obtained for total spin state $S = 2$. On the other hand, if relativistic Breit–Pauli terms are included in the Hamiltonian then the calculation must be carried out in $J\pi$ -coupling which results in a maximum of 5,076 coupled channels. However, it is pointed out in Sect. 5.6.5 that converged results at low energies may require target states from additional configurations to be included in the R -matrix expansion. For example, we see from Table 5.2 that if target states from the 10 configurations, illustrated in Fig. 5.10, are included in the expansion then the maximum number of coupled channels increases

to 2,575 in $LS\pi$ -coupling and to 15,576 in $J\pi$ -coupling. In both the 5 and 10 target configuration cases, including relativistic terms in the Hamiltonian increases the time required to diagonalize the Hamiltonian matrices by more than two orders of magnitude, making the calculations much more demanding.

In order to address this computational difficulty we observe that for many low-energy electron–atom and electron–ion collision calculations, where relativistic effects play an important role, it is often appropriate to omit or partly omit the relativistic terms in the Hamiltonian in the internal region, although these terms must still be included in the external and asymptotic regions in order to obtain accurate threshold energies and hence accurate scattering amplitudes and cross sections. Also, we will see in Chap. 6, where we consider electron collisions at intermediate energies, that it is often necessary to include a large number of pseudostates to allow for inelastic effects above the ionization threshold. In this case, it is not necessary to include relativistic effects involving these pseudostates although these effects can still be important for the physical states included in the R -matrix expansion. In a similar way, it is not necessary to include relativistic effects in the higher continuum basis orbitals represented by the expansion over j in (5.147) which are included to give a converged R -matrix expansion.

In the frame-transformation theory (FTT) method, the relativistic Breit–Pauli terms in the Hamiltonian are omitted in the internal region in the high-energy spectrum, where they are dominated by the electron kinetic energy contribution to the total energy. However, they can be included in the internal region in the low-energy spectrum. These terms are then fully included in the external and asymptotic regions, where they give rise to the relativistic term splitting of the channels which plays an important role, particularly for low-energy electron collisions with atoms and near neutral ions. The corresponding partitioning of configuration space is illustrated in Fig. 5.3, which can be compared with Fig. 5.1 applicable when the FTT method is not used.

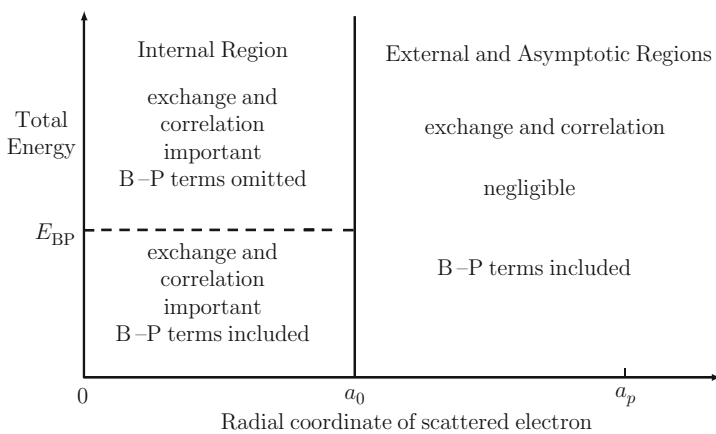


Fig. 5.3 Partitioning of configuration space in the FTT method showing the procedure for including relativistic Breit–Pauli (B–P) terms in the internal, external and asymptotic regions

In the FTT method the calculation is carried out in the following four steps:

- (i) The non-relativistic Hamiltonian H_{N+1} defined by (5.3) is first diagonalized in the internal region in the basis (5.6) for all $LS\pi$ values of importance. The R -matrices $\mathbf{R}^I(E)$ on the boundary $r = a_0$ of the internal region defined by (5.19) are calculated in the usual way, as described in Sect. 5.1.2. If required, this step of the calculation can be made more efficient by using the partitioned R -matrix method discussed in Sect. 5.3.4.
- (ii) The R -matrices $\mathbf{R}^I(E)$ at $r = a_0$ calculated in step (i) are transformed from the $LS\pi$ -coupling scheme to the pair-coupling scheme by transformation (5.119). Also, if relativistic effects in the target are important, a further transformation (5.124) of the R -matrices to full intermediate coupling is made using term-coupling coefficients, yielding the R -matrices $\mathbf{R}^{J\pi}(E)$ for each $J\pi$. This can be achieved using the computer program FINE discussed in Sect. 5.1.1.
- (iii) The R -matrices calculated in step (ii) are partitioned for each $J\pi$ into two sub-matrices $\mathbf{R}_A^{J\pi}(E)$ and $\mathbf{R}_B^{J\pi}(E)$ as follows:

$$\mathbf{R}^{J\pi}(E) = \mathbf{R}_A^{J\pi}(E) + \mathbf{R}_B^{J\pi}(E). \quad (5.165)$$

The sub-matrix $\mathbf{R}_A^{J\pi}(E)$ corresponds to the terms in the R -matrix expansion where the energies of the R -matrix poles E_k^I satisfy $E_k^I > E_{\text{BP}}$ and the sub-matrix $\mathbf{R}_B^{J\pi}(E)$ corresponds to the remaining terms in the R -matrix expansion where the energies of the R -matrix poles E_k satisfy $E_k^I \leq E_{\text{BP}}$, where the energy E_{BP} shown in Fig. 5.3 separates the high-energy spectrum from the low-energy spectrum in the internal region. The Breit–Pauli Hamiltonian H_{N+1}^{BP} , defined in (5.133), is then diagonalized in the internal region in the basis defined by the sub-matrix $\mathbf{R}_B^{J\pi}(E)$ for each $J\pi$, and the corresponding R -matrix $\mathcal{R}_B^{J\pi}(E)$ calculated. The R -matrix replacing (5.165) is then given by

$$\mathbf{R}_{\text{FTT}}^{J\pi}(E) = \mathbf{R}_A^{J\pi}(E) + \mathcal{R}_B^{J\pi}(E). \quad (5.166)$$

In some situations involving electron collisions with intermediate Z atoms and ions it is appropriate to choose E_{BP} so that $E_k^I > E_{\text{BP}}$ for all k . Hence, in this case step (iii) is omitted and

$$\mathbf{R}_{\text{FTT}}^{J\pi}(E) = \mathbf{R}_A^{J\pi}(E). \quad (5.167)$$

This approach has been used by Cassidy et al. [204] who carried out low-energy electron collision calculations for Ni II. In this calculation the non-relativistic program RMATRIXII was used to determine the surface amplitudes for the R -matrix $\mathbf{R}^I(E)$ on the boundary $r = a_0$ of the internal region. The program FINE, discussed in Sect. 5.1.1, was then used to transform these surface amplitudes to full intermediate coupling yielding the R -matrix $\mathbf{R}_{\text{FTT}}^{J\pi}(E)$ on the boundary $r = a_0$.

- (iv) Finally, the R -matrix $\mathbf{R}_{\text{FTT}}^{J\pi}(E)$ at $r = a_0$ provides the boundary condition at $r = a_0$ for determining the solution in the external and asymptotic regions using the Breit–Pauli Hamiltonian, as discussed in Sect. 5.4.2. As shown in Sect. 5.4.2 the corresponding coupled second-order differential equations subdivide into two uncoupled sets of equations depending on whether the quantum number $K_i = J - \frac{1}{2}$ or $J + \frac{1}{2}$ with considerable saving in computational effort. Finally, the K -matrix, S -matrix and T -matrix are determined for each energy E and $J\pi$, as described in Sect. 5.4.2, and the cross sections determined. We see in this way that the FTT method correctly accounts for the kinematics of the scattered electron giving a consistent treatment of the collision above and below thresholds.

In conclusion, we observe that the ICFT method, discussed in Sect. 5.4.1, can be regarded as a further approximation to the FTT method. In the ICFT method the R -matrices $\mathbf{R}^I(E)$ at $r = a_0$ resulting from step (i) are propagated outwards across the external region in $LS\pi$ -coupling, neglecting the relativistic terms in the Hamiltonian in this region. The transformation to full intermediate coupling is then carried out on the K -matrices in the asymptotic region, rather than on the R -matrices on the internal region boundary in the FTT method. Hence the FTT method includes the relativistic terms in the Hamiltonian fully in the external region. This can be important for neutral targets where the ICFT method, which uses multichannel quantum defect theory, is not applicable and for low-energy electron collisions with targets where the relativistic term splitting is large. However, both methods reduce the size of the very large Hamiltonian matrices which arise when relativistic terms in the Breit–Pauli Hamiltonian are fully included in the internal region and are therefore much less demanding computationally.

5.5 Dirac R -Matrix Theory

In this section we extend R -matrix theory to treat electron collisions with heavy atoms and atomic ions where the nuclear charge number Z is large and as a result relativistic effects must be included using the Dirac Hamiltonian. We commence in Sect. 5.5.1 by introducing the Dirac Hamiltonian describing electron collisions with an N -electron target atom or ion. We then summarize the historical background of work in this area commencing with the first introduction of Dirac R -matrix theory in nuclear physics and its first application in the study of electron–atom collisions. We conclude this section by summarizing recent theoretical developments and computer programs. Then in Sect. 5.5.2 we commence our detailed analysis of Dirac R -matrix theory by considering the solution of the time-independent Dirac equation in an internal region yielding the R -matrix on the boundary of this region. This analysis takes advantage of our discussion of the solution of the Dirac equation in potential scattering in Sect. 1.6 and our discussion of Dirac R -matrix theory in potential scattering in Sect. 4.6. We also consider the convergence of the

solution on the boundary of the internal region when radial continuum basis orbitals satisfying homogeneous boundary conditions are used; a problem which we also considered in non-relativistic potential scattering in Sect. 4.1. Having determined the R -matrix on the boundary of the internal region, we then consider the solution of the Dirac equation, or the equivalent Schrödinger equation, in the external region in Sect. 5.5.3 and in the asymptotic region in Sect. 5.5.4 which yields the K -matrix, S -matrix and collision cross sections. Finally, in Sect. 5.5.5 we consider the procedure usually adopted for calculating the radial continuum basis orbitals in the expansion of the wave function in the internal region. Since in many applications these orbitals satisfy homogeneous boundary conditions, similar to those adopted in many non-relativistic calculations, we conclude our analysis in Sect. 5.5.6 by describing the procedure for calculating a Buttle correction to the R -matrix which is required in this case.

5.5.1 Introduction and Computer Programs

The Dirac Hamiltonian describing electron collisions with N -electron target atoms or ions with nuclear charge number Z is given in atomic units by

$$H_{N+1}^D = \sum_{i=1}^{N+1} \left(\mathbf{c}\boldsymbol{\alpha} \cdot \mathbf{p}_i + \beta' c^2 - \frac{Z}{r_i} \right) + \sum_{i>j=1}^{N+1} \frac{1}{r_{ij}}, \quad (5.168)$$

where, adopting the notation introduced in potential scattering in Sect. 1.6, $\boldsymbol{\alpha}$ and $\beta' = \beta - I_4$ are 4×4 -dimensional Dirac matrices defined by (1.233) and (1.234). The solution of the time-independent Dirac equation

$$H_{N+1}^D \Psi = E \Psi \quad (5.169)$$

is then required for each set of conserved quantum numbers J , M_J and π , where J is the total angular momentum quantum number, M_J is the corresponding magnetic quantum number in some preferred direction and π is the total parity.

Dirac R -matrix theory was first introduced by Goertzel [385] who extended Wigner [968, 969] and Wigner and Eisenbud [972] R -matrix theory of nuclear reactions using the Dirac equation and a theory of electron–hydrogen atom collisions using the Dirac Hamiltonian was developed by Carse and Walker [203]. Dirac R -matrix theory of atomic collisions was first formulated by Chang [211–213] who wrote a computer program which he used to study electron collisions with Ne II and Ne photoionization. Later, Thumm and Norcross [926, 927] carried out low-energy electron–Cs collision calculations and Szmytkowski and Hinze [903–908] analysed the application of Dirac R -matrix theory in electron–atom collisions with emphasis on the convergence of the R -matrix expansion.

Recent work using Dirac R -matrix theory to study electron–atom collisions is based on the development of the general-purpose relativistic atomic structure program GRASP by Grant et al. [279, 408–410, 413–415, 514, 625, 718, 719]. As well

as calculating the target states used in electron–atom collision calculations described below, GRASP enables oscillator strengths and radiative decay rates for high Z atoms and ions to be determined. It also includes the facility for calculating corrections to the electron–electron interaction considered by Breit [131–133], as well as other quantum electrodynamic (QED) corrections.

Following the development of the relativistic atomic structure program GRASP, Norrington and Grant [696, 697] initiated the development of a general electron–atom Dirac atomic R -matrix collision program DARC which they used to study electron collisions with Ne II, Fe VII and Fe XXIII. Later further calculations were carried out by Wijesundera et al. [973–975], Ait-Tahar et al. [6] and other workers to study electron collisions with a wide range of heavy atoms and atomic ions and a detailed description of the program has been written by Norrington and Grant [698]. The theory and the DARC program have been further developed by Badnell [32] to treat electron collisions with atoms and atomic ions at intermediate energy, extending the analysis presented in Chap. 6, and recent developments of the theory have been discussed by Grant [411, 412].

5.5.2 Internal Region Solution

Following our discussion of non-relativistic R -matrix theory of electron–atom collisions in Sect. 5.1 we partition configuration space into an internal region, an external region and an asymptotic region, as shown in Fig. 5.1. We consider first the solution of the Dirac equation (5.169) in the internal region $0 \leq r \leq a_0$ for each set of conserved quantum numbers J , M_J and π . The first step is to determine the target states and pseudostates included in the expansion of the collision wave function. These states are defined in terms of four-component spinor basis functions $\phi_i(\mathbf{x})$ which can be written following (1.244) as

$$\phi_i(\mathbf{x}) = \frac{1}{r} \begin{pmatrix} P_i^a(r) \eta_{\kappa_i m_i}(\hat{\mathbf{r}}, \sigma) \\ i Q_i^a(r) \eta_{-\kappa_i m_i}(\hat{\mathbf{r}}, \sigma) \end{pmatrix}, \quad (5.170)$$

where the two-component spinors $\eta_{\kappa m}(\hat{\mathbf{r}}, \sigma)$ are defined by (1.245). Also in (5.170) the reduced radial orbitals $P_i^a(r)$ and $Q_i^a(r)$ are usually chosen to satisfy the orthonormality relations

$$\int_0^\infty [P_i^a(r) P_j^a(r) + Q_i^a(r) Q_j^a(r)] dr = \delta_{ij}, \quad \text{all } i \text{ and } j, \quad (5.171)$$

for each κ defined by (1.250) and Table 1.1. The radius a_0 of the internal region in Dirac R -matrix theory is then chosen so that the reduced radial orbitals $P_i^a(r)$ and $Q_i^a(r)$ satisfy

$$P_i^a(r) \approx 0, \quad Q_i^a(r) \approx 0, \quad r \geq a_0, \quad \text{all } i, \quad (5.172)$$

which ensures that electron exchange and correlation effects between the scattered electron and the target atom are negligible in the external and asymptotic regions, discussed below. The target states and pseudostates $\Phi_i^{J_i M_{J_i} \pi_i}(\mathbf{X}_N)$, which are constructed from these orbitals are then chosen to diagonalize the target Hamiltonian H_N^D as follows:

$$\langle \Phi_i^{J_i M_{J_i} \pi_i} | H_N^D | \Phi_j^{J_j M_{J_j} \pi_j} \rangle = e_i^{J_i \pi_i} \delta_{ij}, \quad (5.173)$$

for each $J_i M_{J_i} \pi_i$, where J_i is the total target angular momentum quantum number, M_{J_i} is the corresponding target magnetic quantum number, π_i is the target parity and $e_i^{J_i \pi_i}$ is the target energy.

Having determined the target states and pseudostates the collision wave function $\Psi_{jE}^{JM_J\pi}(\mathbf{X}_{N+1})$ at a total energy E can be expanded in analogy with (5.5) as follows:

$$\Psi_{jE}^{JM_J\pi}(\mathbf{X}_{N+1}) = \sum_k \psi_k^{JM_J\pi}(\mathbf{X}_{N+1}) A_{kj}^{J\pi}(E), \quad (5.174)$$

where j labels the linearly independent solutions of (5.169), $\psi_k^{JM_J\pi}$ are energy-independent basis functions and $A_{kj}^{J\pi}(E)$ are energy-dependent expansion coefficients, which depend on the asymptotic boundary conditions satisfied by the wave function $\Psi_{jE}^{JM_J\pi}$ at the energy E . We then expand the basis functions $\psi_k^{JM_J\pi}$ in (5.174) for each $JM_J\pi$ in analogy with (5.6) as follows:

$$\begin{aligned} \psi_k^{JM_J\pi}(\mathbf{X}_{N+1}) &= \mathcal{A} \sum_{i=1}^n \sum_{j=1}^{n_c} \overline{\Phi}_i^{JM_J\pi}(\mathbf{X}_N; \hat{\mathbf{r}}_{N+1} \sigma_{N+1}) r_{N+1}^{-1} u_{ij}^0(r_{N+1}) a_{ijk}^{J\pi} \\ &+ \sum_{i=1}^m \chi_i^{JM_J\pi}(\mathbf{X}_{N+1}) b_{ik}^{J\pi}, \quad k = 1, \dots, n_t, \end{aligned} \quad (5.175)$$

where n is the number of channels retained in the expansion, n_c is the number of continuum basis functions retained in each channel, m is the number of quadratically integrable functions and $n_t = nn_c + m$ is the total number of linearly independent basis functions in this expansion. The channel functions $\overline{\Phi}_i^{JM_J\pi}$ are defined by coupling the target states and pseudostates $\Phi_i^{J_i M_{J_i} \pi_i}(\mathbf{X}_N)$ with the relativistic spin-angle functions describing the scattered electron, as follows:

$$\begin{aligned} &\overline{\Phi}_i^{JM_J\pi}(\mathbf{X}_N; \hat{\mathbf{r}}_{N+1} \sigma_{N+1}) \\ &= \sum_{M_i m_i} (J_i M_i j_i m_i | JM_J) \Phi_i^{J_i M_i \pi_i}(\mathbf{X}_N) \phi_i^{j_i m_i}(\hat{\mathbf{r}}_{N+1}, \sigma_{N+1}), \end{aligned} \quad (5.176)$$

where the four-component spin-angle functions $\phi_i^{j_i m_i}(\hat{\mathbf{r}}, \sigma)$ describing the scattered electron are defined by

$$\phi_i^{j_i m_i}(\hat{\mathbf{r}}, \sigma) = \begin{pmatrix} \eta_{\kappa_i m_i}(\hat{\mathbf{r}}, \sigma) \\ i\eta_{-\kappa_i m_i}(\hat{\mathbf{r}}, \sigma) \end{pmatrix}. \quad (5.177)$$

As in (5.170), the spin–angle functions $\eta_{\kappa_i m_i}(\hat{\mathbf{r}}, \sigma)$ in this equation are two-component spinors defined by (1.245), where the angular momentum quantum number j_i is given in terms of the eigenvalue κ_i by (1.250). Finally, the radial motion of the scattered electron in the internal region is described by the two-component reduced radial continuum basis functions $u_{ij}^0(r)$ in (5.175) which are defined by

$$u_{ij}^0(r) = \begin{pmatrix} p_{ij}^0(r) \\ q_{ij}^0(r) \end{pmatrix}, \quad i = 1, \dots, n, \quad 0 \leq r \leq a_0, \quad (5.178)$$

where $p_{ij}^0(r)$ and $q_{ij}^0(r)$ are reduced radial continuum basis orbitals. Hence, in analogy with (1.244), we can rewrite (5.177) and (5.178) as a four-component spinor

$$r^{-1} u_{ij}^0(r) \phi_i^{j_i m_i}(\hat{\mathbf{r}}, \sigma) \equiv \frac{1}{r} \begin{pmatrix} p_{ij}^0(r) \eta_{\kappa_i m_i}(\hat{\mathbf{r}}, \sigma) \\ i q_{ij}^0(r) \eta_{-\kappa_i m_i}(\hat{\mathbf{r}}, \sigma) \end{pmatrix}, \quad i = 1, \dots, n, \quad 0 \leq r \leq a_0. \quad (5.179)$$

Following our discussion of Dirac R -matrix theory in potential scattering in Sect. 4.6, the reduced radial continuum basis orbitals $p_{ij}^0(r)$ and $q_{ij}^0(r)$ in (5.178) are chosen to vanish at the origin and to be non-zero on the boundary $r = a_0$ of the internal region. We describe a procedure in Sect. 5.5.5 which is often adopted for calculating these orbitals when they satisfy homogeneous boundary conditions at $r = a_0$.

Returning to (5.175), \mathcal{A} is the usual antisymmetrization operator defined by (2.46) which ensures that each term in the first expansion is antisymmetric with respect to interchange of the space and spin coordinates of any pair of the $N + 1$ electrons. Also, the functions $\chi_i^{JMj\pi}(\mathbf{X}_{N+1})$ are quadratically integrable functions which are constructed from the bound spinor basis functions $\phi_i(\mathbf{x})$ defined by (5.170) which are negligible by the boundary $r = a_0$ of the internal region. As in the non-relativistic expansion (5.6), these quadratically integrable functions are included in the expansion of the wave function for two reasons. First, for computational convenience the radial continuum basis orbitals $p_{ij}^0(r)$ and $q_{ij}^0(r)$ are usually constrained to be orthogonal to the physical orbitals used to construct the target states included in (5.175). Appropriate quadratically integrable functions constructed from these orbitals must therefore be included in the second expansion for completeness. The second reason for including the quadratically integrable functions is to represent short-range electron–electron correlation effects which are difficult to accurately represent by including a finite number of target states and pseudostates in the first expansion in (5.175).

We can determine the coefficients $a_{ijk}^{J\pi}$ and $b_{ik}^{J\pi}$ in (5.175) by diagonalizing the operator $H_{N+1}^D + \mathcal{L}_{N+1}^D$ as follows:

$$\langle \psi_k^{JM_J\pi} | H_{N+1}^D + \mathcal{L}_{N+1}^D | \psi_{k'}^{JM_J\pi} \rangle_{\text{int}} = E_k^{J\pi} \delta_{kk'}, \quad k, k' = 1, \dots, n_t, \quad (5.180)$$

where \mathcal{L}_{N+1}^D is a matrix Bloch operator, discussed below, and where the integrations in this equation are carried out over the space and spin coordinates of all $N + 1$ electrons, the radial integrals being confined to the internal region. It follows from the rotational symmetry of the Hamiltonian and the Bloch operator that the coefficients $a_{ijk}^{J\pi}$ and $b_{ik}^{J\pi}$ and the energy $E_k^{J\pi}$ depend on J and π but are independent of the magnetic quantum number M_J .

The matrix Bloch operator \mathcal{L}_{N+1}^D in (5.180), which operates only on the two-component space part of the scattered electron wave function, is introduced, as in (5.7), so that $H_{N+1}^D + \mathcal{L}_{N+1}^D$ is hermitian in the space of quadratically integrable functions $\psi^{(1)}$ and $\psi^{(2)}$ which vanish at the origin and satisfy arbitrary boundary conditions on the surface $r = a_0$ of the internal region. Hence, in analogy with (5.9), it follows that

$$\langle \psi^{(1)} | H_{N+1}^D + \mathcal{L}_{N+1}^D | \psi^{(2)} \rangle_{\text{int}} - \langle \psi^{(2)} | H_{N+1}^D + \mathcal{L}_{N+1}^D | \psi^{(1)} \rangle_{\text{int}} = 0, \quad (5.181)$$

where the integration is carried out over all $N + 1$ electronic space and spin coordinates which are confined to the internal region. Following our discussion of Dirac R -matrix theory in potential scattering given in Sect. 4.6, the required matrix Bloch operator, which is a generalization of (4.260), is given by

$$\mathcal{L}_{N+1}^D = \frac{1}{2}c \sum_{i=1}^{N+1} \begin{pmatrix} -b' & 1 \\ -1 & b'^{-1} \end{pmatrix} \delta(r_i - a_0), \quad (5.182)$$

where b' is an arbitrary constant. In the non-relativistic limit b' and hence b_r , introduced in Sect. 4.6, are related to the arbitrary constant b_0 in (5.8) by (4.257) and (4.258) which give

$$b' = \frac{b_r}{2a_0c} = \frac{1}{2a_0c} (b_0 + \kappa), \quad (5.183)$$

where κ is defined in terms of the orbital and total scattered electron angular momentum quantum numbers ℓ and j by (1.250) and Table 1.1. Hence b' and b_r will depend on the corresponding quantum numbers of the scattered electron in each channel.

We can now solve (5.169) in the internal region for each linearly independent solution defined by (5.174). In analogy with the procedure adopted in non-relativistic R -matrix theory in Sect. 5.1.2, we first include the Bloch operator term $\mathcal{L}_{N+1}^D \Psi$ on both sides of (5.169) giving

$$(H_{N+1}^D + \mathcal{L}_{N+1}^D - E) \Psi_{jE}^{JM_J\pi} = \mathcal{L}_{N+1}^D \Psi_{jE}^{JM_J\pi}. \quad (5.184)$$

Equation (5.184) then has the formal solution in the internal region given by

$$\Psi_{jE}^{JM_J\pi} = (H_{N+1}^D + \mathcal{L}_{N+1}^D - E)^{-1} \mathcal{L}_{N+1}^D \Psi_{jE}^{JM_J\pi}. \quad (5.185)$$

The spectral representation of the Green's function $(H_{N+1}^D + \mathcal{L}_{N+1}^D - E)^{-1}$ in (5.185) can be obtained in terms of the R -matrix basis functions $\psi_k^{JM_J\pi}$ defined by (5.175) and (5.180) giving

$$|\Psi_{jE}^{JM_J\pi}\rangle = \sum_{k=1}^{n_t} |\psi_k^{JM_J\pi}\rangle \frac{1}{E_k^{J\pi} - E} \langle \psi_k^{JM_J\pi} | \mathcal{L}_{N+1}^D | \Psi_{jE}^{JM_J\pi} \rangle. \quad (5.186)$$

We then project (5.186) onto the n channel functions $\overline{\Phi}_i^{JM_J\pi}(\mathbf{X}_N; \hat{\mathbf{r}}_{N+1}\sigma_{N+1})$, defined by (5.176), and substitute for the matrix Bloch operator \mathcal{L}_{N+1}^D defined by (5.182). We find using (5.174) and (5.175) that

$$F_{ij}^{J\pi}(r) = \frac{1}{2a_0} \sum_{i'=1}^n \sum_{k=1}^{n_t} \frac{v_{ik}^{J\pi}(r) [v_{i'k}^{J\pi}(a_0)]^T}{E_k^{J\pi} - E} B_{i'} F_{i'j}^{J\pi}(a_0), \\ i = 1, \dots, n, \quad 0 \leq r < a_0, \quad (5.187)$$

where the two-component reduced radial wave functions $F_{ij}^{J\pi}(r)$ are defined by

$$F_{ij}^{J\pi}(r_{N+1}) = \langle r_{N+1}^{-1} \overline{\Phi}_i^{JM_J\pi} | \Psi_{jE}^{JM_J\pi} \rangle', \quad i = 1, \dots, n, \quad (5.188)$$

and where the two-component functions $v_{ik}^{J\pi}(r)$ are defined by

$$v_{ik}^{J\pi}(r_{N+1}) = \langle r_{N+1}^{-1} \overline{\Phi}_i^{JM_J\pi} | \psi_k^{JM_J\pi} \rangle', \quad i = 1, \dots, n, \quad k = 1, \dots, n_t. \quad (5.189)$$

As in (5.20) and (5.21), the primes on the Dirac brackets in (5.188) and (5.189) mean that the integrations and summations are carried out over the space and spin coordinates of all $N + 1$ electrons in the internal region, except the radial coordinate r_{N+1} of the scattered electron. Also, as in (5.20) and (5.21), the contributions from the exchange terms and quadratically integrable functions in (5.175) to the integrals in (5.188) and (5.189) become negligibly small near the boundary $r = a_0$ of the internal region. Hence near the boundary $r = a_0$ the expression for $F_{ij}^{J\pi}(r)$ reduces to

$$F_{ij}^{J\pi}(r) = \sum_{k=1}^{n_t} v_{ik}^{J\pi}(r) A_{kj}^{J\pi}(E), \quad i = 1, \dots, n, \quad r \lesssim a_0, \quad (5.190)$$

where the functions $v_{ik}^{J\pi}(r)$ can be expanded in terms of the radial continuum basis functions $u_{ij}^0(r)$ in (5.178) as follows:

$$v_{ik}^{J\pi}(r) = \sum_{j=1}^{n_c} u_{ij}^0(r) a_{ijk}^{J\pi}, \quad i = 1, \dots, n, \quad k = 1, \dots, n_t, \quad 0 \leq r \leq a_0. \quad (5.191)$$

Finally in (5.187), the B_i , which arise from the Bloch operator \mathcal{L}_{N+1}^D defined by (5.182), are 2×2 matrices given by

$$B_i = a_0 c \begin{pmatrix} -b'_i & 1 \\ -1 & b'_{i-1} \end{pmatrix}, \quad i = 1, \dots, n, \quad (5.192)$$

where the elements b'_i in this matrix are defined in terms of the orbital and total scattered electron angular momentum quantum numbers in the i th channel by (5.183) and (1.250). Also in the above equations, $F_{ij}^{J\pi}(r)$, $v_{ik}^{J\pi}(r)$ and $u_{ij}^0(r)$ are two-component functions, where the radial continuum basis functions $u_{ij}^0(r)$ are defined by (5.178). We observe that when the number of channels $n = 1$, (5.187) reduces to (4.264) obtained in our discussion of Dirac R -matrix theory in potential scattering.

Following our discussion of Dirac R -matrix theory in potential scattering in Sect. 4.6, we now consider the convergence of expansion (5.187) as $r \rightarrow a_0$ from below when the continuum basis orbitals $p_{ij}^0(r)$ and $q_{ij}^0(r)$ satisfy homogeneous boundary conditions at $r = a_0$. We first rewrite the reduced radial wave functions $F_{ij}^{J\pi}(r)$ and the functions $v_{ik}^{J\pi}(r)$ in terms of their components as follows:

$$F_{ij}^{J\pi}(r) = \begin{pmatrix} P_{ij}^{J\pi}(r) \\ Q_{ij}^{J\pi}(r) \end{pmatrix}, \quad i = 1, \dots, n \quad (5.193)$$

and

$$v_{ik}^{J\pi}(r) = \begin{pmatrix} w_{ik}^{J\pi}(r) \\ y_{ik}^{J\pi}(r) \end{pmatrix} = \sum_{i'=1}^{n_c} \begin{pmatrix} p_{i'i}^0(r) \\ q_{i'i}^0(r) \end{pmatrix} a_{i'i'k}^{J\pi}, \quad i = 1, \dots, n, \quad k = 1, \dots, n_t. \quad (5.194)$$

Substituting these equations into (5.187) then yields the coupled equations

$$P_{ij}^{J\pi}(r) = \frac{1}{2a_0} \sum_{i'=1}^n \sum_{k=1}^{n_t} \frac{w_{ik}^{J\pi}(r)}{E_k^{J\pi} - E} C_{i'kj}, \quad i = 1, \dots, n, \quad 0 \leq r < a_0 \quad (5.195)$$

and

$$Q_{ij}^{J\pi}(r) = \frac{1}{2a_0} \sum_{i'=1}^n \sum_{k=1}^{n_t} \frac{y_{ik}^{J\pi}(r)}{E_k^{J\pi} - E} C_{i'kj}, \quad i = 1, \dots, n, \quad 0 \leq r < a_0, \quad (5.196)$$

where

$$C_{ikj} = a_0 c [w_{ik}^{J\pi}(a_0) y_{ik}^{J\pi}(a_0)] \begin{pmatrix} -b'_i & 1 \\ -1 & b'_{i-1} \end{pmatrix} \begin{pmatrix} P_{ij}^{J\pi}(a_0) \\ Q_{ij}^{J\pi}(a_0) \end{pmatrix}. \quad (5.197)$$

We now assume that the radial continuum basis orbitals $p_{ij}^0(r)$ and $q_{ij}^0(r)$ satisfy homogeneous boundary conditions at $r = a_0$ defined by

$$q_{ij}^0(a_0) = b'_i p_{ij}^0(a_0), \quad i = 1, \dots, n, \quad j = 1, \dots, n_c, \quad (5.198)$$

which corresponds to the boundary condition procedure often adopted in calculating these orbitals, described in Sect. 5.5.5. Hence it follows from (5.194) that

$$y_{ik}^{J\pi}(a_0) = b'_i w_{ik}^{J\pi}(a_0), \quad i = 1, \dots, n, \quad k = 1, \dots, n_t. \quad (5.199)$$

Substituting this result into (5.197) we find that (5.195) and (5.196) become

$$P_{ij}^{J\pi}(r) = \frac{1}{2a_0} \sum_{i'=1}^n \sum_{k=1}^{n_t} \frac{w_{ik}^{J\pi}(r) w_{i'k}^{J\pi}(a_0)}{E_k^{J\pi} - E} \left[2a_0 c Q_{i'j}^{J\pi}(a_0) - b_{ri'} P_{i'j}^{J\pi}(a_0) \right],$$

$$i = 1, \dots, n, \quad 0 \leq r < a_0 \quad (5.200)$$

and

$$Q_{ij}^{J\pi}(r) = \frac{1}{2a_0} \sum_{i'=1}^n \sum_{k=1}^{n_t} \frac{y_{ik}^{J\pi}(r) w_{i'k}^{J\pi}(a_0)}{E_k^{J\pi} - E} \left[2a_0 c Q_{i'j}^{J\pi}(a_0) - b_{ri'} P_{i'j}^{J\pi}(a_0) \right],$$

$$i = 1, \dots, n, \quad 0 \leq r < a_0, \quad (5.201)$$

where using (5.183) we have written

$$b_{ri} = b_0 + \kappa_i = 2a_0 c b'_i, \quad i = 1, \dots, n. \quad (5.202)$$

We see that when the number of channels $n = 1$ then (5.200), (5.201) and (5.202) reduce to (4.272), (4.273) and (4.258) which we obtained in Dirac R -matrix theory in potential scattering, where we remember that n_t in (5.200) and (5.201) is the total number of basis functions retained in expansion (5.175), which corresponds to n in (4.272) and (4.273).

The limit of (5.200) and (5.201) when $r \rightarrow a_0$ from below is then given by

$$P_{ij}^{J\pi}(a_0) = \sum_{i'=1}^n \mathcal{R}_{ii'}^{J\pi}(E) \left[2a_0 c Q_{i'j}^{J\pi}(a_0) - b_{ri'} P_{i'j}^{J\pi}(a_0) \right], \quad i = 1, \dots, n$$

$$(5.203)$$

and

$$Q_{ij}^{J\pi}(a_0) = b'_i \sum_{i'=1}^n \mathcal{R}_{ii'}^{J\pi}(E) \left[2a_0 c Q_{i'j}^{J\pi}(a_0) - b_{ri'} P_{i'j}^{J\pi}(a_0) \right], \quad i = 1, \dots, n,$$

$$(5.204)$$

where the $n \times n$ -dimensional R -matrix $\mathcal{R}_{ij}^{J\pi}(E)$ is defined by

$$\mathcal{R}_{ij}^{J\pi}(E) = \frac{1}{2a_0} \sum_{k=1}^{n_t} \frac{w_{ik}^{J\pi}(a_0) w_{jk}^{J\pi}(a_0)}{E_k^{J\pi} - E}, \quad i, j = 1, \dots, n \quad (5.205)$$

and where the surface amplitudes $w_{ik}^{J\pi}(a_0)$ are defined by (5.194). As in Dirac R -matrix theory in potential scattering considered in Sect. 4.6, see (4.274), (4.275),

and (4.276) and the following discussion, we can only find a trivial solution of both (5.203) and (5.204) given by

$$P_{ij}^{J\pi}(a_0) = Q_{ij}^{J\pi}(a_0) = 0, \quad i = 1, \dots, n, \quad (5.206)$$

when the R -matrix $\mathcal{R}_{ij}^{J\pi}(E)$ is non-singular. To see this we substitute for the summation on the right-hand side of (5.204) from (5.203) showing, after using (5.202), that the terms $[2a_0cQ_{ij}^{J\pi}(a_0) - b_{ri}P_{ij}^{J\pi}(a_0)]$ in both (5.203) and (5.204) are zero. However, at the poles of the R -matrix $\mathcal{R}_{ij}^{J\pi}(E)$ we obtain, after using (5.202), the non-trivial solution of (5.203) and (5.204) given by

$$Q_{ij}^{J\pi}(a_0) = b'_i P_{ij}^{J\pi}(a_0), \quad i = 1, \dots, n, \quad (5.207)$$

which corresponds to the homogeneous boundary condition (5.198) satisfied by the radial continuum basis orbitals.

We can understand this result by considering the non-relativistic limit of (5.203) and (5.204) as $r \rightarrow a_0$ from below. In analogy with our discussion of Dirac R -matrix theory in potential scattering following (4.274), we see that (5.203) reduces in the non-relativistic limit to the usual equation relating the reduced radial wave function to its derivative on the boundary $r = a_0$ of the internal region. On the other hand, (5.204) reduces in this limit to an expansion of the derivative of the wave function on the boundary of the internal region. However, when radial continuum basis orbitals satisfying homogeneous boundary conditions are adopted in the analysis, this expansion only converges to the exact solution at the poles of the R -matrix when (5.207) is satisfied. Hence, in this case, expansion (5.201) is not uniformly convergent on the boundary $r = a_0$ except at the poles of the R -matrix. A detailed analysis of the structure of the two-point boundary value problem for the Dirac operator by Grant [412] confirms that (5.203), where the R -matrix is defined by (5.205), provides the boundary condition at $r = a_0$ for integrating the coupled differential equations in the external region outwards from $r = a_0$, as discussed in Sect. 5.5.3.

Finally, we note that, as in non-relativistic collisions, in order to obtain accurate results when radial continuum basis orbitals satisfying homogeneous boundary conditions are adopted, a Buttler correction to the R -matrix must be included. We consider a procedure for calculating these continuum basis orbitals in Sect. 5.5.5 and for calculating a Buttler correction to the R -matrix in Sect. 5.5.6.

5.5.3 External Region Solution

We consider in this section the solution of the Dirac equation (5.169) in the external region, corresponding to $a_0 \leq r \leq a_p$ in Fig. 5.1. As in non-relativistic electron collisions, the radius a_0 is chosen so that the charge distribution of the target eigenstates and pseudostates retained in expansion (5.175) are negligible for $r \geq a_0$ and

hence electron exchange and correlation effects between the scattered electron and the target atom or atomic ion are negligible in this region. The expansion of the total wave function $\Psi_{jE}^{JM_J\pi}(\mathbf{X}_{N+1})$ defined by (5.174) and (5.175) then reduces to

$$\Psi_{jE}^{JM_J\pi}(\mathbf{X}_{N+1}) = \sum_{i=1}^n \overline{\Phi}_i^{JM_J\pi}(\mathbf{X}_N; \hat{\mathbf{r}}_{N+1}\sigma_{N+1}) r_{N+1}^{-1} F_{ij}^{J\pi}(r_{N+1}), \quad (5.208)$$

where j labels the linearly independent solutions. Also, the channel functions $\overline{\Phi}_i^{JM_J\pi}$ retained in expansion (5.208) are the same as those retained in the internal region expansion (5.175) and defined by (5.176). Finally, the reduced radial functions $F_{ij}^{J\pi}(r)$ in (5.208) can be written as energy-dependent two-component functions defined in terms of the reduced radial continuum orbitals $P_{ij}^{J\pi}(r)$ and $Q_{ij}^{J\pi}(r)$ by (5.193).

We obtain coupled first-order differential equations satisfied by the reduced radial continuum orbitals $P_{ij}^{J\pi}(r)$ and $Q_{ij}^{J\pi}(r)$ in the external region by substituting (5.208) into (5.169) and projecting onto the channel functions $\overline{\Phi}_i^{JM_J\pi}(\mathbf{X}_N; \hat{\mathbf{r}}_{N+1}\sigma_{N+1})$. This gives the following coupled first-order differential equations

$$\left(\frac{d}{dr} + \frac{\kappa_i}{r} \right) P_{ij}^{J\pi}(r) - \frac{1}{c} \left(2c^2 + \epsilon_i + \frac{z}{r} \right) Q_{ij}^{J\pi}(r) = -\frac{1}{c} \sum_{i'=1}^n V_{ii'}^{J\pi}(r) Q_{i'j}^{J\pi}(r),$$

$$i = 1, \dots, n \quad (5.209)$$

and

$$\left(\frac{d}{dr} - \frac{\kappa_i}{r} \right) Q_{ij}^{J\pi}(r) + \frac{1}{c} \left(\epsilon_i + \frac{z}{r} \right) P_{ij}^{J\pi}(r) = \frac{1}{c} \sum_{i'=1}^n V_{ii'}^{J\pi}(r) P_{i'j}^{J\pi}(r),$$

$$i = 1, \dots, n, \quad (5.210)$$

where $r \geq a_0$. Also in (5.209) and (5.210) $z = Z - N$, ϵ_i are the channel energies in atomic units and the potential matrix $V_{ii'}^{J\pi}(r)$, which has a similar form to (2.66) in non-relativistic electron collisions with atoms and atomic ions, is defined by

$$V_{ii'}^{J\pi}(r_{N+1}) = \langle r_{N+1}^{-1} \overline{\Phi}_i^{JM_J\pi}(\mathbf{X}_N; \hat{\mathbf{r}}_{N+1}\sigma_{N+1}) \left| \sum_{k=1}^N \frac{1}{r_{kN+1}} - \frac{N}{r_{N+1}} \right|$$

$$\times r_{N+1}^{-1} \overline{\Phi}_{i'}^{JM_J\pi}(\mathbf{X}_N; \hat{\mathbf{r}}_{N+1}\sigma_{N+1}) \rangle', \quad i, i' = 1, \dots, n, \quad (5.211)$$

where the prime on the Dirac bracket in (5.211) and later equations means that the integration is carried out over the space and spin coordinates of all $N + 1$ electrons except the radial coordinate r_{N+1} of the scattered electron. Also, the inclusion of the term $-N/r_{N+1}$ in the definition of $V_{ii'}^{J\pi}(r)$ means that the long-range Coulomb

potential experienced by the scattered electron is completely included on the left-hand side of (5.209) and (5.210). Also, as in non-relativistic electron collisions, the potential terms on the right-hand side of (5.209) and (5.210) can be simplified using (2.72). We obtain

$$V_{ii'}^{J\pi}(r) = \sum_{\lambda=1}^{\lambda_{\max}} \alpha_{ii'\lambda}^{J\pi} r^{-\lambda-1}, \quad r \geq a_0, \quad i, i' = 1, \dots, n, \quad (5.212)$$

where the long-range potential coefficients $\alpha_{ii'\lambda}^{J\pi}$ are defined, in analogy with (2.74) in non-relativistic collisions, by

$$\begin{aligned} \alpha_{ii'\lambda}^{J\pi} = & \langle r_{N+1}^{-1} \overline{\Phi}_i^{JM_J\pi}(\mathbf{X}_N; \hat{\mathbf{r}}_{N+1} \sigma_{N+1}) \left| \sum_{k=1}^N r_k^\lambda P_\lambda(\cos \theta_{kN+1}) \right| \\ & \times r_{N+1}^{-1} \overline{\Phi}_{i'}^{JM_J\pi}(\mathbf{X}_N; \hat{\mathbf{r}}_{N+1} \sigma_{N+1}) \rangle', \quad i, i' = 1, \dots, n, \\ & \lambda = 1, \dots, \lambda_{\max}, \end{aligned} \quad (5.213)$$

and where the upper limit λ_{\max} in the summation over λ in (5.212) results from the triangular relations satisfied by the angular momentum quantum numbers which arise in the integral in (5.213).

For low-energy electron collisions with atoms and atomic ions, where the ionic interaction potential $(Z - N)/r$ in the external region and the channel energies are both small compared with c^2 then the coupled differential equations (5.209) and (5.210) can be reduced to non-relativistic limiting form. Following our discussion of the Dirac equation in potential scattering, given in Sect. 1.6, these equations can be transformed to the non-relativistic limiting form given by

$$\left(\frac{d^2}{dr^2} - \frac{\kappa_i(\kappa_i + 1)}{r^2} + \frac{2(Z - N)}{r} + k_i^2 \right) P_{ij}^{J\pi}(r) = 2 \sum_{i'=1}^n V_{ii'}^{J\pi}(r) P_{i'j}^{J\pi}(r), \quad i = 1, \dots, n, \quad r \geq a_0, \quad (5.214)$$

where $k_i^2 = 2\epsilon_i$. In addition in the non-relativistic limit (5.203) reduces to

$$P_{ij}^{J\pi}(a_0) = \sum_{i'=1}^n \mathcal{R}_{ii'}^{J\pi}(E) \left(a_0 \frac{dP_{i'j}^{J\pi}}{dr} - b_0 P_{i'j}^{J\pi} \right)_{r=a_0}, \quad i = 1, \dots, n, \quad (5.215)$$

where we have used (5.183) and (5.202) to relate b_{ri} in (5.203) to b_0 in (5.215). Equations (5.214) and (5.215) are in standard non-relativistic form as discussed in Sect. 5.1.3. Hence, after the Buttler correction, discussed in Sect. 5.5.6, has been added to the diagonal elements of the R -matrix $\mathcal{R}_{ij}^{J\pi}(E)$, defined by (5.205), (5.214)

can be integrated outwards from $r = a_0$, subject to the boundary condition at $r = a_0$, defined by (5.215), to $r = a_p$ and fitted to an asymptotic expansion to yield the K -matrix and S -matrix, using the procedure discussed in Sects. 5.1.3 and 5.1.4.

However, for electron collisions with highly ionized ions, where $Z - N$ and hence the excitation energies are large, the use of (5.214) in the external and asymptotic regions can lead to error. For example, for electron collisions with the He-like ion Fe XXV, which has a residual charge of 24, an incident electron energy of ~ 500 Rydbergs is required to excite the target from the ground state [985]. For these incident electron energies the velocity v of the electron is approximately 0.16 c . Hence for ionic targets with high values of the effective charge $Z - N$, one possibility is to transform the coupled first-order differential equations (5.209) and (5.210) to coupled second-order differential equations with a first-order derivative term, analogous to (4.289) in potential scattering. The R -matrix can then be propagated outwards from $r = a_0$ to a_p , using the propagator method discussed in Appendix E.5. Alternatively, the original coupled first-order differential equations (5.209) and (5.210) can be integrated outwards from $r = a_0$ to a_p , using a standard approach for solving these equations (see, for example, [573]). In both cases a Buttler correction, discussed in Sect. 5.5.6, has to be added to the R -matrix $\mathcal{R}_{ij}^{J\pi}(E)$ defined by (5.205) if continuum basis orbitals satisfying homogeneous boundary conditions at $r = a_0$ are used in the internal region.

5.5.4 Asymptotic Region Solution

We now consider the solution of (5.209) and (5.210) in the asymptotic region, corresponding to $r \geq a_p$ in Fig. 5.1. We have seen in our discussion of the external region solution in Sect. 5.5.3 that for low-energy collisions, when the interaction potential $(Z - N)/r$ and the channel energies are small compared with c^2 , (5.209) and (5.210) can be reduced to non-relativistic form. In this case we can solve the resultant equations in the asymptotic region as discussed in Sect. 5.1.4 yielding the S -matrix, T -matrix and cross sections. However, for electron collisions with highly ionized ions it is necessary to determine the asymptotic region solution of (5.209) and (5.210) directly. In this analysis we assume that the channels are ordered so that the channel energies ϵ_i in (5.209) and (5.210) satisfy

$$\epsilon_1 \geq \epsilon_2 \geq \dots \geq \epsilon_n, \quad (5.216)$$

where the first n_a channels are open with $\epsilon_i \geq 0$ and the last n_b channels are closed with $\epsilon_i < 0$, where $n_a + n_b = n$. As in non-relativistic collisions, considered in Sect. 5.1.4, we define, in analogy with (5.37), $n + n_a$ linearly independent solutions of (5.209) and (5.210) satisfying the following asymptotic boundary conditions:

$$\begin{aligned}
p_{ij}(r) \underset{r \rightarrow \infty}{\sim} g_i \sin \theta_i \delta_{ij}, \quad q_{ij}(r) \underset{r \rightarrow \infty}{\sim} \frac{\epsilon_i}{k_i c} g_i \cos \theta_i \delta_{ij}, \\
i = 1, \dots, n, \quad j = 1, \dots, n_a, \\
p_{ij}(r) \underset{r \rightarrow \infty}{\sim} g_i \cos \theta_i \delta_{ij}, \quad q_{ij}(r) \underset{r \rightarrow \infty}{\sim} -\frac{\epsilon_i}{k_i c} g_i \sin \theta_i \delta_{ij}, \\
i = 1, \dots, n, \quad j = 1, \dots, n_a, \\
p_{ij}(r) \underset{r \rightarrow \infty}{\sim} \bar{g}_i \exp(-\phi_i) \delta_{ij}, \quad q_{ij}(r) \underset{r \rightarrow \infty}{\sim} \frac{\epsilon_i}{|k_i| c} \bar{g}_i \exp(-\phi_i) \delta_{ij}, \\
i = 1, \dots, n, \quad j = n_a + 1, \dots, n, \quad (5.217)
\end{aligned}$$

where

$$g_i = \left[\frac{1}{k_i} \left(1 + \frac{\epsilon_i}{2c^2} \right) \right]^{1/2}, \quad k_i = \left[\frac{\epsilon_i}{c} \left(\frac{\epsilon_i}{c} + 2c \right) \right]^{1/2}, \quad \bar{g}_i = \left[\frac{1}{|k_i|} \left(1 + \frac{\epsilon_i}{2c^2} \right) \right]^{1/2}. \quad (5.218)$$

Also in (5.217),

$$\theta_i = k_i r - \frac{1}{2}(\gamma_i - 1)\pi + y_i \ln 2k_i r + \psi_i - \arg \Gamma(\gamma_i + iy_i), \quad i = 1, \dots, n_a, \quad (5.219)$$

where

$$\gamma_i = \left(\kappa_i^2 - \frac{z^2}{c^2} \right)^{1/2}, \quad y_i = \frac{z}{k_i} \left(1 + \frac{\epsilon_i}{c^2} \right), \quad \psi_i = \frac{1}{2i} \ln \left(\frac{iz/k_i - \kappa_i}{\gamma_i - iy_i} \right) \quad (5.220)$$

and

$$\phi_i = |k_i| r - y_i \ln 2k_i r. \quad (5.221)$$

These asymptotic boundary conditions are discussed by Young and Norrington [985] who obtained asymptotic expansions for these solutions, analogous to the non-relativistic asymptotic expansions considered in Appendix F.1 [160, 356].

Following our discussion in Sect. 5.1.4, we can find n_a linearly independent solutions of the coupled differential equations (5.209) and (5.210) that vanish at the origin and are finite at infinity. The $n_a \times n_a$ -dimensional K -matrix is then defined in terms of the large components in the n_a open channels as follows:

$$\mathbf{P}^{J\pi}(r) \underset{r \rightarrow \infty}{\sim} \left[\frac{1}{\mathbf{k}} \left(\mathbf{I} + \frac{\boldsymbol{\epsilon}}{2c^2} \right) \right]^{1/2} \left[\sin \boldsymbol{\theta} + \cos \boldsymbol{\theta} \mathbf{K}^{J\pi} \right], \quad (5.222)$$

where the corresponding components in the n_b closed channels vanish asymptotically. By taking linear combinations of these solutions we can define a solution matrix $\mathbf{G}^{J\pi}(r)$ satisfying the asymptotic boundary conditions

$$\mathbf{G}^{J\pi}(r) \underset{r \rightarrow \infty}{\sim} \left[\frac{1}{\mathbf{k}} \left(\mathbf{I} + \frac{\boldsymbol{\epsilon}}{2c^2} \right) \right]^{1/2} [\exp(-i\boldsymbol{\theta}) - \exp(i\boldsymbol{\theta})\mathbf{S}^{J\pi}], \quad (5.223)$$

where the S -matrix, defined by this equation, and the corresponding T -matrix can be expressed in terms of the K -matrix by the usual matrix equations

$$\mathbf{S}^{J\pi} = \frac{\mathbf{I} + i\mathbf{K}^{J\pi}}{\mathbf{I} - i\mathbf{K}^{J\pi}}, \quad \mathbf{T}^{J\pi} = \mathbf{S}^{J\pi} - \mathbf{I}. \quad (5.224)$$

The cross sections can then be determined using the procedure described in Sect. 2.5. The partial cross section for a transition from an initial state $i \equiv \alpha_i J_i j_i$ to a final state $f \equiv \alpha_f J_f j_f$ corresponding to the conserved quantum numbers $J\pi$ is given by

$$\sigma^{J\pi}(i \rightarrow f) = \frac{2J + 1}{2k_i^2(2J_i + 1)} \sum_{j_i j_f} |T_{fi}^{J\pi}|^2, \quad (5.225)$$

where α_i and α_f distinguish target states with the same total angular momentum J_i and J_f , and where j_i and j_f are the initial and final angular momenta of the scattered electron. The total cross section is then defined by

$$\sigma^{\text{Tot}}(i \rightarrow f) = \sum_{J\pi} \sigma^{J\pi}(i \rightarrow f), \quad (5.226)$$

in units of πa_0^2 .

5.5.5 Continuum Basis Orbitals

We now consider the procedure usually adopted for calculating the reduced radial continuum basis orbitals $p_{ij}^0(r)$ and $q_{ij}^0(r)$ which are used in definition (5.178) of $u_{ij}^0(r)$ in the internal region. In most applications these orbitals have been chosen to satisfy homogeneous boundary conditions similar to those adopted in non-relativistic electron collisions, described in Sect. 5.3.1 and, as a result, a Buttler correction to the R -matrix, considered in Sect. 5.5.6, is required. However, as in non-relativistic electron-atom collisions and multiphoton ionization, arbitrary boundary condition methods, considered in Sect. 5.3.3, can also be used to determine the continuum basis orbitals.

In analogy with the coupled first-order differential equations (4.248), which arise in Dirac R -matrix theory in potential scattering, we consider here orbitals $p_{ij}^0(r)$ and $q_{ij}^0(r)$ which satisfy the following coupled first-order differential equations for each κ_i

$$\left(\frac{d}{dr} + \frac{\kappa_i}{r}\right)p_{ij}^0(r) - \frac{1}{c}[2c^2 + \epsilon_i - V_0(r)]q_{ij}^0(r) = -\frac{1}{c}\sum_k \lambda_{ijk} Q_k^a(r),$$

$$i = 1, \dots, n, \quad j = 1, \dots, n_c \quad (5.227)$$

and

$$\left(\frac{d}{dr} - \frac{\kappa_i}{r}\right)q_{ij}^0(r) + \frac{1}{c}[\epsilon_i - V_0(r)]p_{ij}^0(r) = \frac{1}{c}\sum_k \lambda_{ijk} P_k^a(r),$$

$$i = 1, \dots, n, \quad j = 1, \dots, n_c, \quad (5.228)$$

subject to the homogeneous boundary conditions, defined in analogy with (4.249) and (4.250), which can be written here as

$$\begin{pmatrix} p_{ij}^0(0) \\ q_{ij}^0(0) \end{pmatrix} = 0, \quad i = 1, \dots, n, \quad j = 1, \dots, n_c \quad (5.229)$$

and

$$q_{ij}^0(a_0) = b'_i p_{ij}^0(a_0), \quad i = 1, \dots, n, \quad j = 1, \dots, n_c. \quad (5.230)$$

Also in (5.227), (5.228), (5.229) and (5.230), n is the number of channels retained in the R -matrix expansion and n_c is the number of continuum basis functions retained in each channel. In the non-relativistic limit we have seen that b'_i in (5.230) is related to b_0 and κ_i by (5.183). Also the summations over k on the right-hand sides of (5.227) and (5.228) go over the reduced radial physical bound orbitals $P_k^a(r)$ and $Q_k^a(r)$ used to construct the target states retained in expansion (5.175) corresponding to the κ_i under consideration and the λ_{ijk} are Lagrange multipliers which are chosen so that the following orthogonality constraints

$$\int_0^{a_0} [p_{ij}^0(r)P_k^a(r) + q_{ij}^0(r)Q_k^a(r)]dr = 0, \quad i = 1, \dots, n \quad (5.231)$$

are satisfied for all j and k , for each κ_i . It follows that the reduced radial continuum basis orbitals $p_{ij}^0(r)$ and $q_{ij}^0(r)$ generated in this way are orthogonal and can be normalized so that

$$\int_0^{a_0} [p_{ij}^0(r)p_{ij'}^0(r) + q_{ij}^0(r)q_{ij'}^0(r)]dr = \delta_{jj'}, \quad i = 1, \dots, n \quad (5.232)$$

for all j and j' . For each κ_i , the reduced radial physical bound orbitals $P_k^a(r)$ and $Q_k^a(r)$, retained on the right-hand side of (5.227) and (5.228), together with the corresponding reduced radial continuum orbitals $p_{ij}^0(r)$ and $q_{ij}^0(r)$, generated by solving (5.227), (5.228), (5.229) and (5.230) subject to the orthonormality constraints

given by (5.231) and (5.232), form a complete set over the range $0 \leq r < a_0$ in the limit $n_c \rightarrow \infty$, for any value of b_r in (5.183) and zero-order potential $V_0(r)$.

In order to obtain rapid convergence of the R -matrix expansion (5.205), including the Buttler correction discussed below, the zero-order potential $V_0(r)$ in (5.227) and (5.228) should provide a good representation of the charge distribution of the target atom or ion. In practice, the static potential of the target atom or ion in its ground state is often adopted. Also, as in non-relativistic collisions, the inhomogeneous terms on the right-hand sides of (5.227) and (5.228) play the role of an exchange potential while at the same time ensuring that the continuum basis orbitals are orthogonal to the physical orbitals used to construct the target states.

5.5.6 Buttler Correction

When the reduced radial continuum basis orbitals $p_{ij}^0(r)$ and $q_{ij}^0(r)$ in definition (5.178) of $u_{ij}^0(r)$ satisfy the zero-order coupled differential equations (5.227) and (5.228) subject to homogeneous boundary conditions (5.229) and (5.230), then it is necessary to add a ‘‘Buttler correction’’ to the R -matrix to obtain accurate results. Our procedure, which is analogous to that adopted in non-relativistic collisions discussed in Sect. 5.3.2, corrects for the omission of the high-lying pole terms in expansion (5.205) of the R -matrix $\mathcal{R}_{ij}^{J\pi}(E)$. Also, as in non-relativistic electron collisions with atoms and ions, only the diagonal elements of the R -matrix usually need to be corrected.

The diagonal elements of the R -matrix $\mathcal{R}_{ij}^{J\pi}(E)$ are determined in terms of the solution of the coupled zero-order differential equations (5.227) and (5.228) used to calculate the reduced radial continuum basis orbitals $p_{ij}^0(r)$ and $q_{ij}^0(r)$. The diagonal elements of the zero-order R -matrix $\mathcal{R}_{ij}^0(E)$ at an arbitrary energy E are given, following (4.287), by

$$\mathcal{R}_{ii}^0(E) = p_i^0(a_0) \left[2a_0 c q_i^0(a_0) - b_{ri} p_i^0(a_0) \right]^{-1}, \quad i = 1, \dots, n, \quad (5.233)$$

where $p_i^0(r)$ and $q_i^0(r)$ are solutions of (5.227) and (5.228) at the energy E , subject to the boundary condition (5.229) at the origin and to the orthogonality constraints (5.231). The diagonal elements of the zero-order R -matrix can also be written in terms of the infinite set of eigensolutions $p_{ij}^0(r)$ of (5.227) and (5.228), subject to the boundary conditions (5.229) and (5.230) and the orthogonality and normalization constraints (5.231) and (5.232). We obtain

$$\mathcal{R}_{ii}^0(E) = \frac{1}{2a_0} \sum_{k=1}^{\infty} \frac{[p_{ik}^0(a_0)]^2}{E_k^0 - E}, \quad i = 1, \dots, n. \quad (5.234)$$

Finally, the Buttler correction to the diagonal elements of the R -matrix $\mathcal{R}_{ij}^{J\pi}(E)$, defined by (5.205), can be written as

$$\mathcal{R}_{ii}^{J\pi(\text{BC})}(E) = \frac{1}{2a_0} \sum_{k=n_i+1}^{\infty} \frac{[p_{ik}^0(a_0)]^2}{E_k^0 - E}, \quad i = 1, \dots, n. \quad (5.235)$$

Using (5.233) and (5.234) we then find that

$$\begin{aligned} \mathcal{R}_{ii}^{J\pi(\text{BC})}(E) &= p_i^0(a_0) \left[2a_0 c q_i^0(a_0) - b_{ri} p_i^0(a_0) \right]^{-1} \\ &\quad - \frac{1}{2a_0} \sum_{k=1}^{n_i} \frac{[p_{ik}^0(a_0)]^2}{E_k^0 - E}, \quad i = 1, \dots, n. \end{aligned} \quad (5.236)$$

The first term on the right-hand side of (5.236) is obtained by solving the coupled differential equations (5.227) and (5.228) at the energy E of interest and the second term is given in terms of the reduced radial continuum basis orbitals evaluated on the boundary $r = a_0$ of the internal region together with the corresponding eigenenergies. As in non-relativistic collisions, both terms in (5.236) can be rapidly calculated at a few energies and since the Buttle correction is smoothly varying in the low-energy region of interest it can be interpolated to give the correction at the required energies.

5.6 Low-Energy Electron Collision Calculations

Over the last 40 years a vast number of electron–atom and electron–ion collision calculations have been carried out using R -matrix computer programs which have implemented the theory reviewed in this chapter. These calculations have been undertaken both in support of experiment and also to provide data required in the analysis of applications, for example, in plasma physics, laser physics and astrophysics. In this section we consider low-energy electron–atom and electron–ion collision calculations where only elastic scattering and excitation processes are energetically allowed or are important, reserving a discussion of electron collisions at intermediate energies, where ionizing collisions are important, to Chap. 6. The examples that we present illustrate both the criteria necessary to obtain reliable cross sections and the accuracy now obtainable for low-energy electron collisions with atoms and atomic ions. However, we will see that difficulties are still experienced for heavier open d- and f-shell targets involving many coupled channels.

5.6.1 Electron Collisions with H

We begin by considering electron collisions with atomic hydrogen, the lightest one-electron target atom. This simplifies the collision calculation since the non-relativistic hydrogen atom wave functions are known exactly and hence we are not concerned with electron–electron correlation effects among the target electrons

which arise in more complex atomic targets. However, the Schrödinger equation for the electron–hydrogen atom system describes a three-body problem and is therefore not solvable exactly. The importance of obtaining accurate numerical solutions for this system is not only because of its intrinsic importance arising from the fact that atomic hydrogen is the most abundant atom in the universe, but also because these solutions illustrate features, such as resonances and threshold effects, which are common to multi-electron atomic targets. Hence calculations carried out for electron–hydrogen atom collisions provide a test of methods, such as the R -matrix method, which are applicable to general multi-electron targets.

We have pointed out in Sects. 2.2 and 2.3 that in order to obtain accurate low-energy electron–atom collision cross sections it is necessary to include target pseudostates in the expansion of the collision wave function to represent the long-range polarization of the target in the field of the scattered electron. In early calculations by Burke et al. [177] and Fon et al. [328] full account of the long-range polarization potential was taken by including the $2\bar{p}$ pseudostate defined by (2.23) as well as the $1s$ target eigenstate in the “close coupling with pseudostates” expansion (2.55). Differential cross sections for elastic scattering were calculated from 1 to 200 eV by Fon et al. [328] which compared well with absolute angular distribution measurements by Williams [977–979]. However, the $2\bar{p}$ state has an unphysical threshold at ~ 11.4 eV and the omission of physical excited states in the expansion meant that resonance and threshold effects in the 9–13.6 eV range were not accurately represented.

In order to obtain accurate elastic and inelastic e^- –H collision cross sections at low energies, including resonance and threshold effects, Bartschat et al. [72] carried out benchmark calculations using two independent R -matrix methods and also using the convergent close-coupling (CCC) method developed by Bray and Stelbovics [126, 127] and reviewed by Bray et al. [129, 130]. The two R -matrix methods, the R -matrix with pseudostates (RMPS) method and the intermediate energy R -matrix (IERM) method, which are described in detail in Chap. 6, are designed to obtain accurate collision cross sections close to and above the ionization threshold. However, both methods give convergent results at low energies. In the RMPS calculation eight S-states, eight P-states and three D-states were included in expansion (5.6), where the lowest six states corresponded to the exact $n = 1, 2$ and 3 non-relativistic H atom eigenstates, while the remaining 13 states were pseudostates, allowing for long-range polarization and short-range correlation effects. The corresponding IERM calculation also included the six $n = 1, 2$ and 3 H atom eigenstates as well as orbitals representing long-range polarization and short-range correlation effects. We show the results of these three calculations for the total elastic and $1s$ – $2s$ and $1s$ – $2p$ excitation cross sections between the $n = 2$ and 3 thresholds compared with the experimental data of Williams [980] in Fig. 5.4. We see that the agreement between theory and experiment is excellent, with theory accurately reproducing the resonance structure converging to the $n = 3$ threshold at 0.8889 Rydbergs and the $^1P^o$ resonance just above the $n = 2$ threshold, which had been analysed in detail by Macek and Burke [621]. We note that the $^1S^e$ resonance at ~ 0.862 Rydbergs has been discussed in Sect. 3.2.3 (see Fig. 3.5).

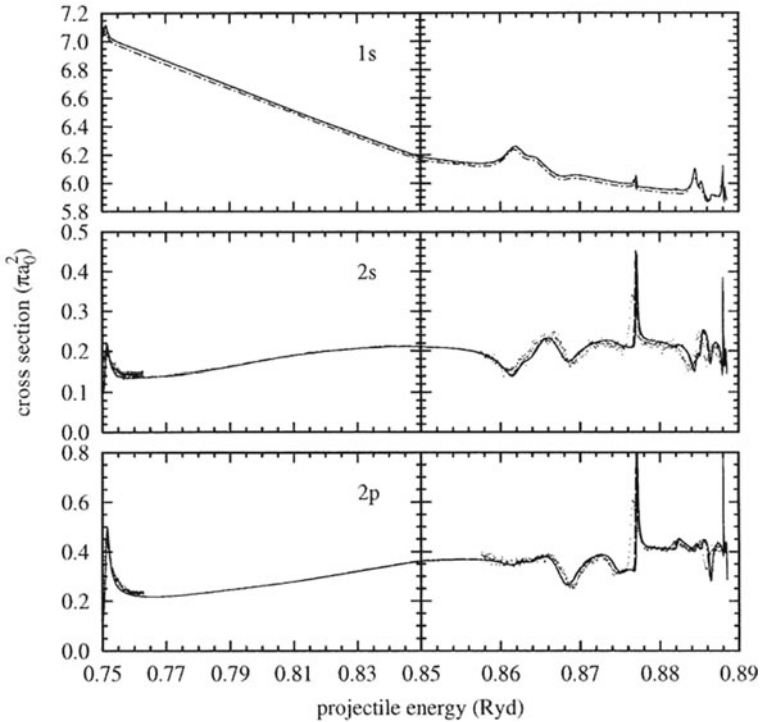


Fig. 5.4 Total electron–hydrogen atom 1s–1s elastic cross section and 1s–2s and 1s–2p excitation cross sections for collision energies between the $n = 2$ and 3 thresholds. *Full curve*, RMP; *broken curve*, IERM; *chain curve*, CCC. The *dots* represent the experimental data of Williams [980] (Fig. 4 from [72])

In conclusion, low-energy scattering amplitudes and cross sections for e^- –H collisions can be accurately calculated using the R -matrix method for low n states. However, there are still major computational problems remaining in order to obtain accurate low-energy excitation cross sections for high n states of atomic hydrogen which, for example, are of importance in some diffuse hydrogen clouds in the cold interstellar medium. This computational difficulty is due to the many coupled channels involved and the large extent of the corresponding target atom wave functions. We will return to this difficulty when we discuss electron collisions with hydrogen atoms at intermediate energies in [Chap. 6](#).

5.6.2 Electron Collisions with He

Results from electron–helium atom collision calculations have many applications. Helium is relatively easy to study in the laboratory, so many experiments have been performed providing stringent tests for theory. In astronomy, helium is the second

most abundant element in the universe, after atomic hydrogen, and helium lines associated with the excited $n = 2$, $n = 3$ and higher states are ubiquitous in spectra from many types of astronomical objects (see [709]). Since most emission line spectra observed in astronomy are produced by electron impact excitation or by radiative capture, followed by radiative decay of excited states, it is clear that there is a demand for high-quality atomic data to interpret these lines.

Also, helium is the simplest multi-electron atom and electron–helium collision calculations exhibit many features of calculations for more complex atomic targets. The most obvious difference from electron–hydrogen atom collisions is that the helium target wave function cannot be represented exactly; the system of nucleus plus two electrons being a three-body problem. Approximate target wave functions have to be used, usually employing configuration interaction expansions. Another difference is that the helium target can be in either a singlet or a triplet spin state rather than in just a doublet state as in the case of atomic hydrogen, which doubles the number of excited states for each principal quantum number n . Both of these differences result in increasing complexity in the corresponding collision calculations.

5.6.2.1 Elastic Scattering

The first low-energy e^- –He elastic scattering R -matrix calculations were carried out by Robb [792] using a static-exchange approximation where the target was represented by a configuration interaction expansion. These calculations were later extended by O'Malley et al. [705] who used an R -matrix eigenchannel method, discussed in Sect. 4.4.5. In this latter work, O'Malley et al. adopted a multiconfigurational helium ground-state wave function together with 1P and 1D pseudostates, constructed from the Hartree–Fock ground state $1s$ orbital and $2s$ – $4f$ pseudo-orbitals. These pseudo-orbitals were optimized to simultaneously minimize the ground-state energy and maximize the dipole and quadrupole polarizabilities of the target, as discussed by Vo Ky Lan et al. [941]. In this way they obtained 98% of the ground-state correlation energy as well as 99.8% of the dipole polarizability and approximately the correct quadrupole polarizability. The estimated error in the calculated total cross section below 8 eV was about 1% and this was born out by the excellent agreement with experiments by Kennerly and Bonham [530]. Both the total and momentum transfer cross sections were also in good agreement with variational calculations by Nesbet [677].

5.6.2.2 Inelastic Collisions

A series of R -matrix calculations have been carried out to determine the convergence of low-energy e^- –He excitation cross sections and resonance structure. In these calculations He target eigenstates were included in expansion (5.6) with progressively higher principal quantum number n . These were 5-state calculations by Berrington et al. [96] which included all eigenstates with $n \leq 2$, 11-state calculations by Freitas et al. [341] and Berrington et al. [99] which included all

eigenstates with $n \leq 3$, 19-state calculations by Berrington and Kingston [93] and Fon et al. [332] which included all eigenstates with $n \leq 4$, and 29-state calculations by Sawey et al. [815] and Fon et al. [333–335] which included all eigenstates with $n \leq 5$. The main conclusion from these calculations was that as the number of target eigenstates retained in the calculation increased, the cross sections converged at the lowest energies. However, the calculated cross sections were in error above the threshold of the highest eigenstate retained in the R -matrix expansion. That is the 5-state calculation had not converged above the $n = 2$ thresholds, the 11-state calculation had not converged above the $n = 3$ thresholds and so on. We will show in Chap. 6, when we discuss intermediate-energy collisions, that it is necessary to include pseudostates representing highly excited states and the ionization continuum in the R -matrix expansion, in order to obtain converged results close to and above the ionization threshold. We have also observed in Sect. 2.2.2 that, in order to obtain highly accurate results at low energies, it is necessary to include pseudostates in this expansion which represent long-range polarization effects and other virtual transitions via high-lying excited states and the continuum.

Recently, close to converged inelastic e^- -He R -matrix collision cross section calculations have been carried out and compared with experiment by Stepanović et al. [886] and by Lange et al. [570]. In the work of Stepanović et al. cross sections for exciting the 3^3S and 3^1S states of helium near threshold were studied. In the work of Lange et al. cross sections for exciting both the $n = 2$ and 3 states of helium were studied and were also compared with accurate calculations by Fursa and Bray [355] using the convergent close coupling method. We illustrate this work by showing in Fig. 5.5 the angle-integrated cross sections for excitation of helium to the 3^3S and 3^1S states. The calculations were carried out using the B-spline R -matrix (BSR) computer program written by Zatsarinsky [992], discussed in Sect. 5.1.1. The collision model adopted included 69 target states with S, P, D and F symmetries consisting of all target eigenstates with these symmetries up to $n = 5$, together with 42 pseudostates representing higher bound and continuum states. The experimental cross sections were obtained using a high-resolution electron impact spectrometer, in a crossed beam geometry, described in detail by Cvejanović et al. [240]. The experimental data were normalized to the theory, including a cascade contribution, at 23.20 eV for both the 3^3S and 3^1S states since the cross sections exhibit a smooth energy dependence in the neighbourhood of this energy and hence the experimental energy resolution does not play a significant role. The cascade contribution was found to be important only for the 3^3S excitation, whereas it was negligible for the 3^1S state. Overall the experimental cross sections shown in Fig. 5.5 are in good agreement with the optical excitation functions published by Heddle et al. [448]. The convoluted theoretical cross sections also exhibit remarkably good agreement with experiment although there are some discrepancies in the near-threshold region for excitation of the 3^3S state where theory predicts somewhat higher values for the resonance structure than observed experimentally. This may be due to the higher model sensitivity of the predicted resonance structure very close to threshold. A detailed analysis of this resonance structure is given by Lange et al. [570].

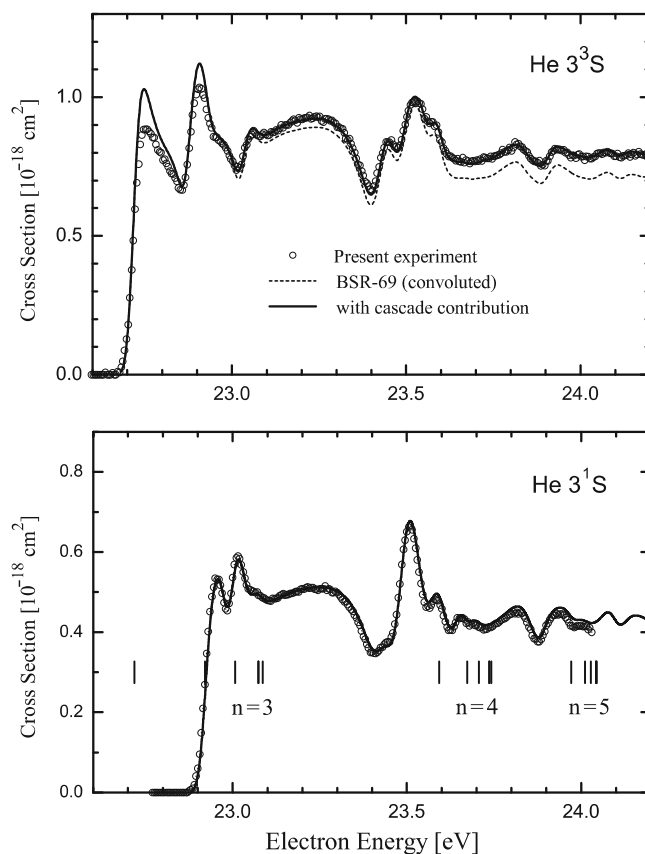


Fig. 5.5 Angle-integrated cross sections for electron impact excitation of the 3^3S and 3^1S states of helium. The experimental results are represented by *circles*. The theoretical *R*-matrix results without (*dashed line*) and with (*solid line*) cascade contributions were convoluted with a Gaussian of 37 meV (FWHM). The *vertical bars* in the *lower panel* represent the thresholds for the helium target states (Fig. 2 from [886])

Finally, we note that the results presented in both Figs. 5.4 and 5.5 show the important role that resonances play in determining low-energy electron–atom collision cross sections. In earlier work on He it was shown [175, 176] that two pronounced peaks which dominate the 1^1S – 2^3S collision strength close to threshold were due to 2^2P^o and 2^2D^e shape resonances, in agreement with angular distribution measurements by Ehrhardt and William [285] and Ehrhardt et al. [287]. Detailed elastic collision calculations below the 2^3S threshold also revealed the presence of a 2^2S^e resonance at ~ 19.31 eV, which was first observed by Schulz [835] and which has been discussed more recently by Hudson et al. [478]. We will see when we discuss further examples in this section that resonances are a common feature of all low-energy electron–atom and electron–ion collision cross sections.

5.6.3 *Electron Collisions with Ne*

We consider next low-energy electron collisions with neon atoms which are important both in fundamental studies and for their many applications. The latter include modelling applications in the lighting and lasing industry, in plasma processing and in the interpretation of astrophysical observations.

Elastic electron collisions with inert gases have been studied both experimentally and theoretically for many years. In particular, elastic scattering R -matrix calculations have been carried out by Fon and co-workers on He [329], Ne [327], Ar [330] and Kr [331], in which the ground state of the target together with a $^1P^o$ polarized pseudostate, representing the full dipole polarizability of the target, were included in the R -matrix expansion. In addition, elastic electron–neon collision calculations have been carried out by many other workers including McEachran and Stauffer [617], Dasgupta and Bhatia [250] and Saha [805], where in all these calculations good agreement with experiment was obtained. However, until recently the situation for inelastic collisions has been less satisfactory where, as shown by Khakoo et al. [533], none of the theoretical methods discussed in their paper were able to consistently reproduce the experimental data for angle-differential cross sections for excitation of the $2p^53s$ states, or their ratios.

However, more recent calculations carried out by Zatsarinny and Bartschat [998], using the B-spline R -matrix computer program BSR, have obtained very good agreement with experiments by Buckman et al. [146], which measured the cross section for exciting the $2p^53s\ ^3P_{0,2}^o$ states of neon from threshold to just above the $3p^53p$ thresholds. The sum of these two excitation cross sections had been used by Brunt et al. [141, 142] and Buckman et al. [146] to analyse the details of the resonance structure seen in these cross sections, discussed in the review of atomic negative ion resonances by Buckman and Clark [145].

Also, in later studies by Bömmels et al. [122] and Allan et al. [12], excellent agreement was obtained between R -matrix calculations and experiment for excitation of the $2p^53s$ states from threshold to above the $3p^53p$ thresholds. As an example, we show in Fig. 5.6 a comparison of calculated and experimental cross sections for excitation of the Ne $2p^53s\ ^3P_2, ^3P_1, ^3P_0$ and 1P_1 states reported by Allan et al. [12]. The experimental results were obtained using an electron scattering apparatus involving two-stage hemispherical analysers with an energy resolution (FWHM) of 9 meV [11]. Absolute cross sections reliable to $\pm 15\%$ were obtained by normalization to helium results. The R -matrix calculations were obtained including the $2p^6\ ^1S_0$ ground state of neon together with the $2p^53s$ and $2p^53p$ excited states in the R -matrix internal region expansion. This figure illustrates prominent resonance features just above the $2p^53s$ thresholds and a Wigner cusp together with a group of narrow resonances associated with the higher lying $2p^53p$ thresholds. The lower resonances can be assigned as core-excited shape resonances with the dominant configuration $2p^53s3p$ as discussed by Bömmels et al. [122], while further work is required to fully identify the resonances at the higher thresholds. Overall the excellent agreement between theory and experiment indicates that the main features of this collision process are accurately reproduced by the R -matrix calculation. Finally,

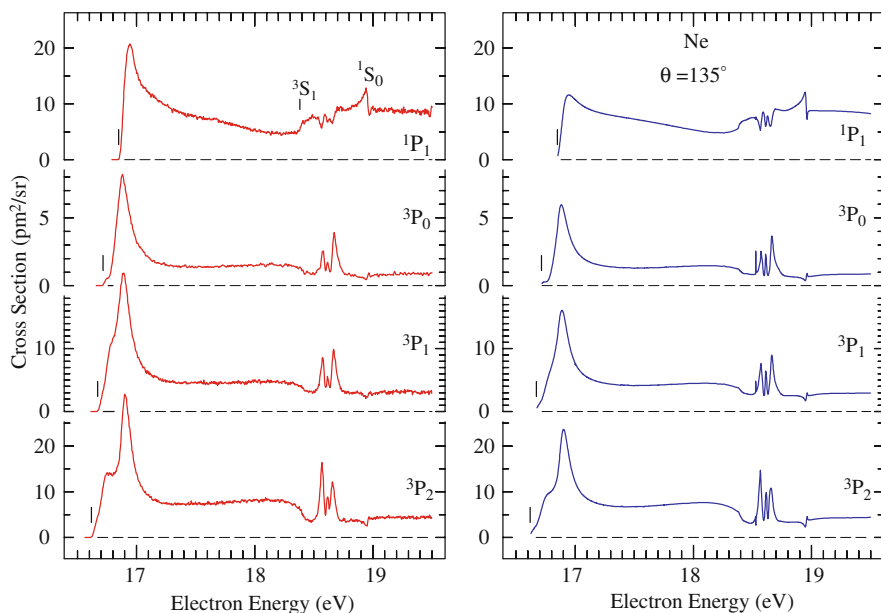
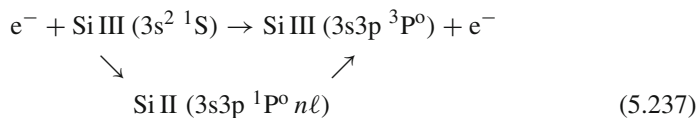


Fig. 5.6 Absolute cross sections (experiment in the *left panels* and *R-matrix calculations* in the *right panels*) for electron impact excitation of the $2p^5 3s$ states of Ne at a scattering angle $\theta = 135^\circ$. The *vertical bars* indicate the excitation thresholds including those of the $2p^5 3p$ 3S_1 and 1S_0 states of Ne (Fig. 2 from [12])

we note that the B-spline *R-matrix* computer program has been used to study a number of other electron–atom collision processes including low-energy electron collisions with argon [999], zinc [1000] and oxygen [1003].

5.6.4 Electron Collisions with Si III

As our next example we consider electron collisions with Si III (Si^{2+}). There is considerable demand for excitation rates for this ion, particularly in the study of laboratory plasmas and in the analysis of solar spectra where, for example, the intensity ratio of Si III lines have been used to determine the electron densities of quiet and active regions of the sun (e.g. [228]). Absorption lines of Si III have also been found in quasi-stellar objects [41]. Of particular importance is the following excitation process



which is dominated close to threshold by a Rydberg series of Feshbach resonances. These resonances are caused by capture of the incident electron into a bound

Rydberg state in the field of Si III in the excited $3s3p\ ^1P^o$ state, which decays leaving the target ion in its $3s3p\ ^3P^o$ first excited state. *R*-matrix calculations for this process have been carried out by Baluja et al. [46] and Griffin et al. [425], where the latter authors also studied transitions in the isoelectronic ion Ar VII (Ar^{6+}). In these calculations the 12 lowest target eigenstates of Si III were included in expansion (5.6), where each eigenstate was represented by a configuration interaction expansion. We present in Fig. 5.7 the collision strength for the $3s^2\ ^1S \rightarrow 3s3p\ ^3P^o$ transition calculated by Baluja et al. [46], compared with distorted wave results calculated by Blaha (quoted by Nicolas [684]). We see that at these low energies, the collision strength is dominated by resonance structure while the distorted wave results, which omit the intermediate resonance states in the collision, represent the much smaller non-resonant background. The importance of resonances for this transition is demonstrated in Table 5.1 where we compare the effective collision strength,

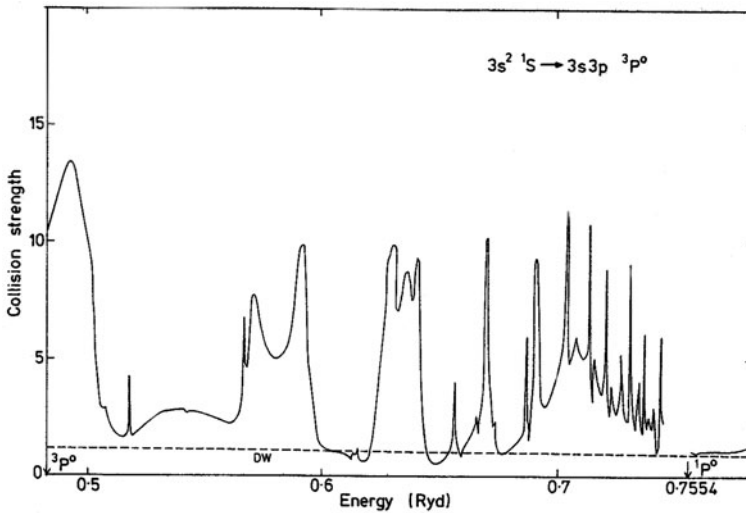


Fig. 5.7 Collision strength for the transition $3s^2\ ^1S \rightarrow 3s3p\ ^3P^o$ in Si III. *Full line*, *R*-matrix calculation [46]; *dashed line*, distorted wave calculation [684] (Fig. 1 from [46])

Table 5.1 Effective collision strength for the transition $3s^2\ ^1S \rightarrow 3s3p\ ^3P^o$ in Si III as a function of electron temperature for *R*-matrix and distorted wave calculations

Electron temp 10^4 K	<i>R</i> -matrix	Distorted wave
0.50	6.898	1.120
0.75	5.961	1.111
1.00	5.428	1.101
2.00	4.407	1.065
5.00	3.188	0.969
10.00	2.292	0.842
20.00	1.529	0.667

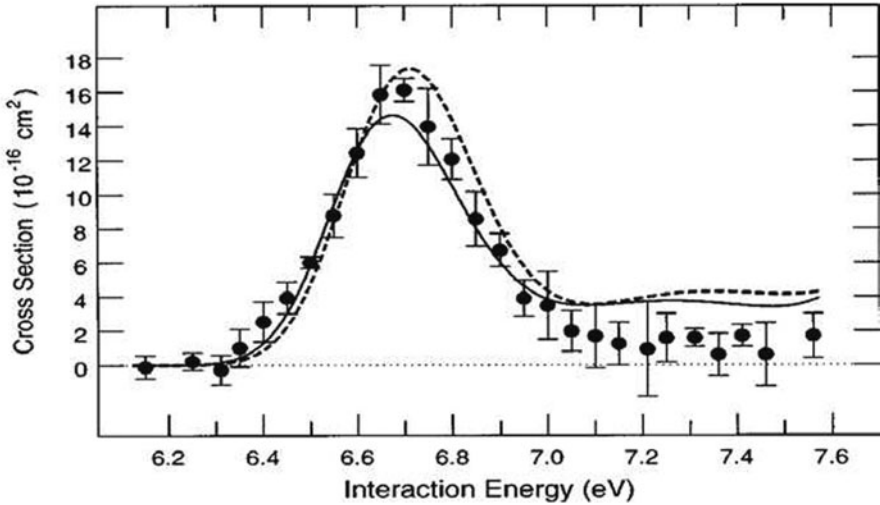


Fig. 5.8 Cross section for $3s^2\ ^1S \rightarrow 3s3p\ ^3P^o$ electron impact in Si III. Points represent average experimental values and bars give relative uncertainties at 90% confidence level. Dashed curve, *R*-matrix calculation [46]; solid curve, *R*-matrix calculation [425], both calculations convoluted with a Gaussian width 0.24 eV (Fig. 3 from [946])

defined by (2.153), for these two calculations for a range of electron temperatures. At 5,000 K the *R*-matrix result is larger by a factor of about 6 and even at 2×10^5 K it is still more than a factor of 2 higher.

More recently, absolute excitation cross sections for the $3s^2\ ^1S \rightarrow 3s3p\ ^3P^o$ and $^1P^o$ transitions in Si III were measured close to threshold by Wallbank et al. [946] using a merged electron-ion beams energy-loss technique. We show in Fig. 5.8 the measured cross section for the $3s^2\ ^1S \rightarrow 3s3p\ ^3P^o$ transition compared with the *R*-matrix calculation by Baluja et al. [46] and Griffin et al. [425]. The resonance peak close to the threshold seen in the *R*-matrix calculations is confirmed by experiment which is also in good agreement with its predicted magnitude. However, the agreement between the *R*-matrix calculations and experiment is less good at energies more than 1 eV above threshold, which Wallbank et al. believe may be due to the omission of backscatter electrons in the experiment.

In conclusion, the important experiment by Wallbank et al. [946] has shown that *R*-matrix theory can accurately predict low-energy cross sections for relatively light multi-electron ions. This work again demonstrates the crucial role that resonances play in enhancing low-energy electron-atom and electron-ion collision cross sections.

5.6.5 Electron Collisions with Fe II

Electron impact excitation cross sections and the related effective collision strengths for all ionization stages of iron peak elements are of crucial importance in the

quantitative analysis of many astronomical spectra, see, for example, [79]. As a result, for nearly two decades there has been a major effort as part of the international Iron Project [482] to calculate electron impact excitation data for all ionization stages of iron peak elements using R -matrix computer programs, and around 70 papers describing the results have been published in *Astronomy and Astrophysics*. Of particular importance is singly ionized iron where its high cosmic abundance, its relatively low ionization potential and its complex open d-shell atomic structure ensure that a very large number of electron impact excited lines are observed in objects as diverse as gaseous nebulae, active galactic nuclei, quasars, Seyfert galaxies and supernovae remnants. In addition, collisional data are required in the analysis of many laboratory plasmas which occur, for example, in laser plasma interactions and controlled thermonuclear fusion devices.

In the absence at present of experimental data for electron impact excitation cross sections for Fe II, this requirement for accurate collisional data can only be met by detailed and accurate calculations. However, there are a number of reasons why the calculation of collision cross sections for this and similar iron peak elements is difficult. First, the complexity of the open d-shell target means that large configuration interaction expansions, discussed in Sect. 2.2.1, are required to obtain accurate target wave functions and energies. Second, a very large number of coupled channels are required to accurately represent the collision wave function even for low-energy electron collisions. Third, the complex resonance structure which dominates the low-energy cross sections requires a very fine energy mesh to accurately resolve.

In order to illustrate the complexity of this problem we show in Fig. 5.9 the energy level diagram of Fe II below $30,000 \text{ cm}^{-1}$ ($\sim 3.72 \text{ eV}$), taken from the tables of Johansson [505] and Corliss and Sugar [232], with some forbidden infra-red and optical transitions observed in gaseous nebulae indicated. In this low-energy region there are 16 LS -coupled states of Fe II resulting in 46 fine-structure levels, where particular interest in earlier work has focused on transitions between the four lowest LS -coupled states, corresponding to the $3d^6 4s \text{ a}^6\text{D}$ ground state and the $3d^7 \text{ a}^4\text{F}$, $3d^6 4s \text{ a}^4\text{D}$ and $3d^7 \text{ a}^4\text{P}$ excited states. In order to obtain accurate excitation cross sections involving these states it is important to represent them by accurate configuration interaction expansions, as discussed in Sect. 2.2.1, and to adequately represent higher states that play an important role in the transitions as virtual states. In particular, these higher states give rise to resonances that lie in the energy range of interest which we will see below dominate the low-energy cross sections. We present in Fig. 5.10 an energy level diagram of Fe II which shows the range of energies of the LS -coupled states which could play an important role in low-energy electron collisions. As an indication of the size of the computation involved in including in the R -matrix expansion (5.6) all target states corresponding to the 10 lowest lying configurations $3d^6 4s$, $3d^7$, $3d^5 4s^2$, $3d^6 4p$, $3d^5 4s 4p$, $3d^6 5s$, $3d^6 4d$, $3d^6 5p$, $3d^6 4f$ and $3d^5 4p^2$, we give in Table 5.2 the maximum number of channels that can occur both in $LS\pi$ -coupling and in $J\pi$ -coupling including relativistic effects as an increasing number of these configurations are included in the calculation.

Over more than 25 years, a number of increasingly sophisticated e^- -Fe II collision calculations have been carried out. We summarize here some of the most

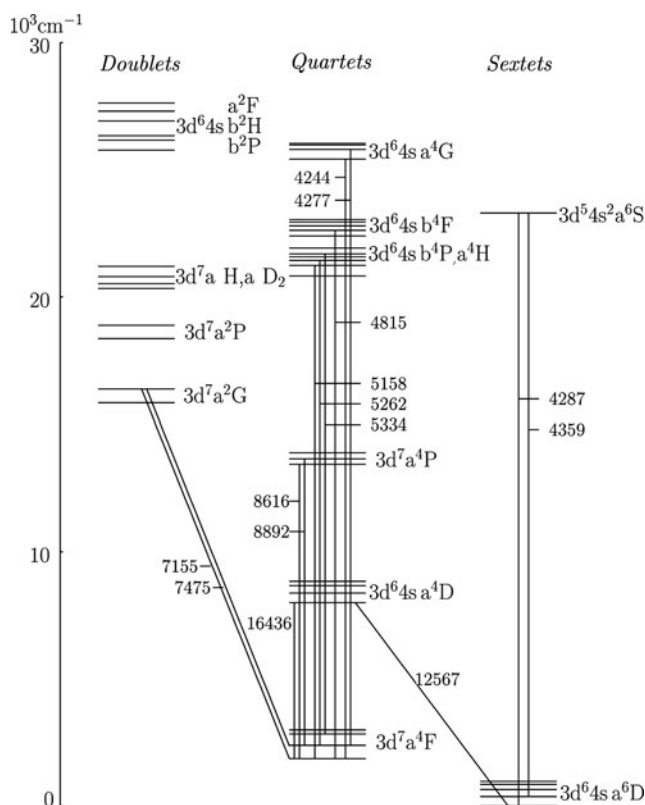


Fig. 5.9 The 16 LS -coupled states of Fe II below $30,000 \text{ cm}^{-1}$ showing the corresponding 46 fine-structure levels and some forbidden infra-red and optical transitions observed in gaseous nebulae, with their wavelengths given in Angstrom (Fig. 2 from [188])

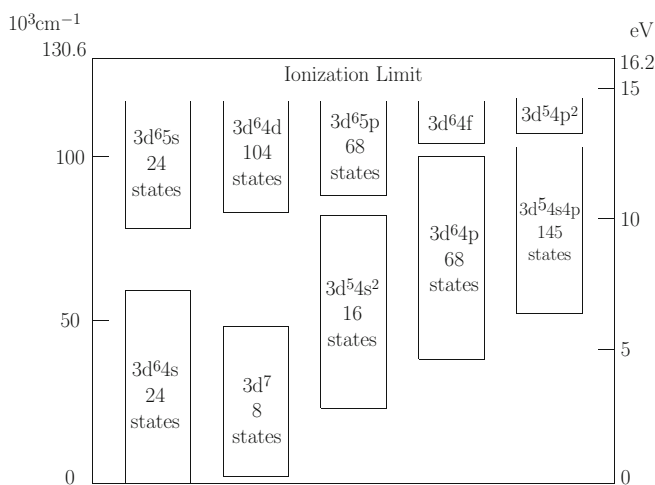


Fig. 5.10 Energy level diagram of Fe II showing the range of energies of the LS -coupled target states corresponding to the 10 lowest lying target configurations

Table 5.2 Maximum number of LS -coupled target states and coupled channels and the corresponding maximum number of fine-structure target states and coupled channels in an R -matrix expansion for e^- -Fe II collisions, where the numbers correspond to retaining in the calculation an increasing number of the target configurations illustrated in Fig. 5.10

No. of configs	$LS\pi$		$J\pi$	
	States	Channels	States	Channels
1	24	73	63	420
2	32	98	82	540
3	48	148	119	792
4	116	366	299	2,052
5	261	818	716	5,076
6	285	891	779	5,496
7	389	1,254	1,055	7,596
8	457	1,472	1,235	8,856
9	585	1,980	1,581	11,796
10	770	2,575	2,094	15,576

significant studies. The first detailed calculations were made by Nussbaumer and Storey [699], who included in their expansion of the collision wave function the four lowest LS -coupled states of Fe II shown in Fig. 5.9. However, these calculations were only carried out for three energies above all thresholds and hence no resonance structure was found. Later, Baluja et al. [48] extended this earlier work by adopting configuration interaction wave functions for the target and carrying out an R -matrix calculation including the four lowest LS -coupled states of Fe II using a finer energy mesh, which also included the resonance region below the highest threshold. It was found that even in the non-resonant region the excitation cross sections differed by a factor of 2 from the earlier results [699]. This work was further extended by Berrington et al. [101] who included relativistic terms from the Breit–Pauli Hamiltonian, discussed in Sect. 5.4.2, in the calculation of both the target and the collision wave functions, yielding effective collision strengths for transitions between the 16 fine-structure levels corresponding to the 4 lowest LS -coupled states of Fe II. The collision strengths obtained from this calculation were subsequently used by Keenan et al. [527] to obtain electron density-sensitive relative populations for the $3d^64s$ a⁶D fine-structure levels down to a temperature of 100 K and densities $N_c = 10^2$ – 10^6 cm⁻³ applicable to astrophysical plasmas, which were found to be a factor of 2 different from previous calculations.

With the rapid increase in computer power, Pradhan and Berrington [755] were able to carry out more sophisticated R -matrix calculations, which included all 38 quartet and sextet LS -coupled target states belonging to the $3d^64s$, $3d^7$ and $3d^64p$ configurations. It was found that the additional states belonging to the $3d^64p$ configuration, omitted in previous calculations, played an important role due to strong coupling with the $3d^64s$ states. Later, Zhang and Pradhan [1007] and Bautista and Pradhan [78] extended this LS -coupled calculation to yield collision strengths and effective collision strengths between the corresponding fine-structure levels, by recoupling the K -matrix elements using the pair-coupling scheme defined by (5.119). The rate coefficients for the transitions among the lowest 16 fine-structure levels were found to be substantially different from those predicted by Keenan

et al. [527] and by Nussbaumer and Storey [699], indicating that further work was required to obtain reliable rate coefficients.

In a series of more recent *R*-matrix calculations by Ramsbottom et al. [770–772] and by Zatsarinny and Bartschat [1001] all 113 quartet and sextet *LS*-coupled target states belonging to the lowest five configurations, $3d^64s$, $3d^7$, $3d^54s^2$, $3d^64p$ and $3d^54s4p$ in Fig. 5.10, were included in the expansion of the total wave function. This gave rise to a maximum of 354 channels for the total spin state $S = 2$ coupling the quartet and sextet target states. These calculations, carried out using two independent *R*-matrix computer programs RMATRXII and BSR, discussed in Sect. 5.1.1, were generally in good agreement although there were some differences in the low-energy region dominated by resonances caused by different representations of configuration interaction effects.

In order to calculate collision strengths and effective collision strengths for low-lying fine-structure forbidden transitions required in many astrophysical applications, Ramsbottom et al. [769, 773] also carried out Breit–Pauli *R*-matrix calculations including all fine-structure levels corresponding to the $3d^64s$, $3d^7$ and $3d^64p$ target configurations. It follows from Table 5.2 that this calculation included 262 coupled target states and a maximum of 1,800 coupled channels. We note that the target states and channels corresponding to the $3d^54s^2$ and $3d^54s4p$ configurations, which we see from Fig. 5.10 lie in the same energy range as the $3d^64p$ configuration, were not included in this calculation since their effect on the low-energy transitions of interest was expected to be small. We illustrate the results obtained in this calculation by showing in Fig. 5.11 the collision strength between the $3d^64s$ a ${}^6D_{9/2}^e$ and the

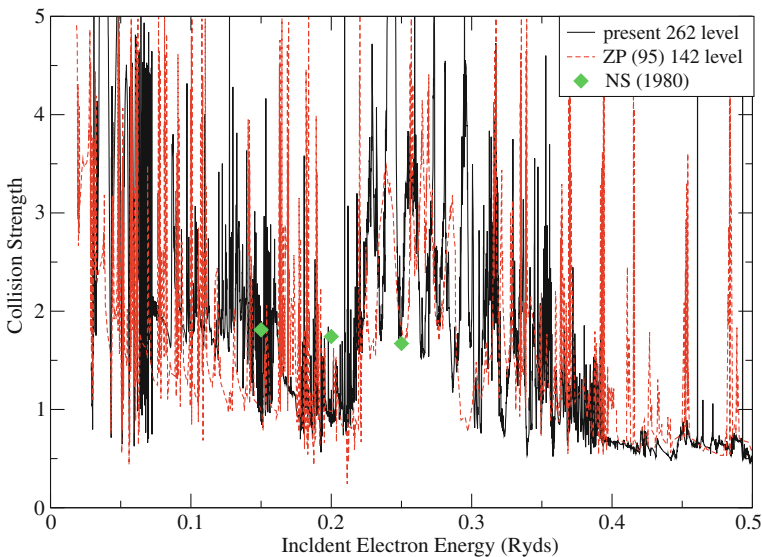


Fig. 5.11 Collision strengths for the $3d^64s$ a ${}^6D_{9/2}^e \rightarrow 3d^7$ a ${}^4F_{9/2}^e$ fine-structure transition in e^- -Fe II collisions. *Solid line*: Ramsbottom et al. 262-state calculation [773]; *dashed line*: Zhang and Pradhan 142-state calculation [1007]; *diamonds*: Nussbaumer and Storey calculation [699] (Fig. 3 from [773])

$3d^7 a^4F_{9/2}^e$ fine-structure levels, which are compared with the earlier calculations by Zhang and Pradhan [1007] and by Nussbaumer and Storey [699]. We see that the collision strength is dominated by resonances, which required the evaluation at 16,200 distinct energy values to accurately delineate, 16,000 being in the resonance region and 200 above this region. We also note that the agreement between the calculations by Ramsbottom et al. [773] and by Zhang and Pradhan [1007] is quite good, although the non-resonant background collision strength of the latter calculation appears lower at incident electron energies around 0.1 Rydbergs. The corresponding effective collision strength for this transition is shown in Fig. 5.12 for the temperature range from 30 to 100,000 K, which incorporates temperatures important in astrophysical and plasma applications. We see that the effective collision strengths predicted by Zhang and Pradhan [1007] lie between 10 and 15% higher than the Ramsbottom et al. [773] values. However, the single temperature value of Bautista and Pradhan [78] lies a factor of 3 lower than the Ramsbottom et al. [773] results. For this transition the early prediction of Berrington et al. [101] is in reasonably good agreement with the most recent results but the results of Keenan et al. [527] differ significantly from the most recent work [773]. It is thus clear from this figure that more work needs to be carried out to confirm the result for even this low-lying transition. Since there are no experimental measurements to compare these calculations with, accurate results can only be confirmed by systematically

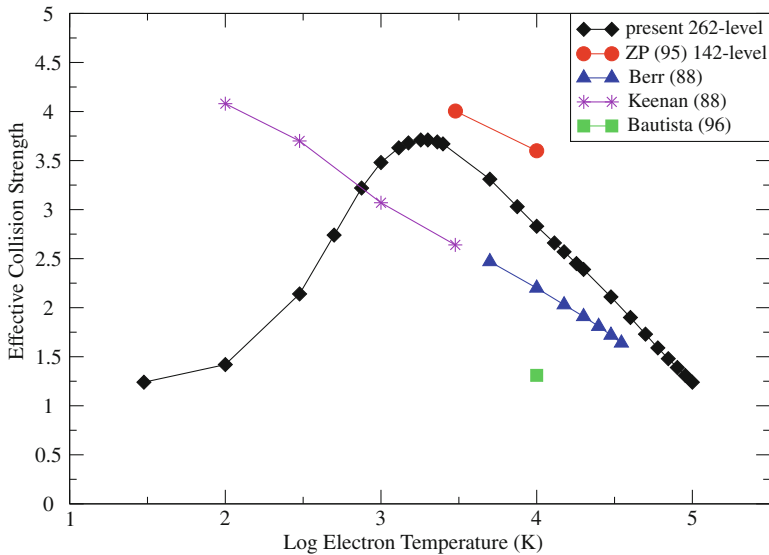


Fig. 5.12 Effective collision strengths as a function of log electron temperature in kelvin for the $3d^6 4s a^6D_{9/2}^e \rightarrow 3d^7 a^4F_{9/2}^e$ fine-structure transition in e^- -Fe II collisions. *Diamonds*: Ramsbottom et al. 262-state calculation [773]; *circles*: Zhang and Pradhan 142-state calculation [1007]; *triangles*: Berrington et al. [101]; *stars*: Keenan et al. [527]; *square*: Bautista and Pradhan [78] (Fig. 4 from [773])

increasing the number of configurations included in the target and in the collision wave functions until convergence is obtained.

In conclusion, we see by examining Fig. 5.10 that, in addition to configurations included in the recent calculations, target states belonging to higher and omitted configurations are expected to play an important role, particularly for transitions involving higher states of interest in applications. The role of the continuum, which could be represented by pseudostates discussed in Chap. 6, may also be important. We see from Table 5.2 that the inclusion of these additional target states greatly increases the number of coupled channels, particularly when collision strengths for transitions between fine-structure levels of the target are required. However, with the development of parallel R -matrix collision programs and the implementation of efficient methods for including relativistic terms in the calculation, discussed in Sects. 5.4 and 5.5, these objectives, while presenting a computational grand challenge [188], should be achievable in the near future.

5.6.6 Electron Collisions with Fe XV

We have observed in our discussion of electron collisions with Fe II in Sect. 5.6.5 that accurate calculations of collision strengths for many transitions of importance in the analysis of astronomical spectra will require the inclusion of relativistic effects in the Hamiltonian. We have also seen in Sects. 5.4 and 5.5 that there are several procedures for including these effects, whose accuracy depends on the nuclear charge number Z of the atomic nucleus, ranging from transforming the non-relativistic K -matrix for relatively small Z targets to solving the Dirac equation for large Z targets. An important question that arises is when can accurate results be obtained using the Breit–Pauli Hamiltonian, discussed in Sect. 5.4.2, and when is it necessary to use the Dirac Hamiltonian, discussed in Sect. 5.5. In this section we consider detailed R -matrix collision strength calculations for Mg-like Fe XV which addressed this question.

There have been a number of R -matrix calculations of electron impact excitation of Fe XV. These include Breit–Pauli R -matrix calculations by Eissner et al. [291] and Griffin et al. [427] and Dirac R -matrix calculations by Aggarwal et al. [3]. In this last work it was found that there were significant differences between the Breit–Pauli and the Dirac calculations and it was therefore suggested that a fully relativistic Dirac calculation is necessary in order to obtain accurate results for a 14 times ionized $Z = 26$ target.

In order to explain whether the differences in the calculations were due to the different treatment of the relativistic effects or to the approximations made in solving the resultant equations, Berrington et al. [103] carried out detailed calculations for electron collisions with Fe XV using both the Breit–Pauli computer program RMATRXI, discussed in Sect. 5.1.1, and the Dirac computer program DARC, discussed in Sect. 5.5.1, removing as far as possible any variation in algorithmic features, such as the energy mesh and the target states included in the expansion. In

both calculations 45 $J\pi$ target states were retained in the R -matrix expansion corresponding to the 9 configurations $3s^2$, $3s3p$, $3s3d$, $3s4s$, $3s4p$, $3s4d$, $3p^2$, $3p3d$ and $3d^2$. In addition, the configuration interaction representation of these target states was expanded in terms of the same set of configurations. In this way the possibility of pseudoresonances was avoided. Finally, in both calculations a fine energy mesh was adopted in order to fully resolve the resonance structure. As an example of the results obtained, the effective collision strengths for two double-electron transitions are shown in Fig. 5.13. We see that the Breit–Pauli and Dirac R -matrix results are in close agreement, with the variations between the calculations at lower temperatures being primarily attributed to the differences in the resonance positions determined by the Breit–Pauli and the Dirac target orbitals.

In conclusion, it was found that the average difference between the Breit–Pauli and Dirac R -matrix effective collision strengths for the 990 transitions considered between the 45 target states was only 6.14%. Furthermore, there is evidence from this work that the small differences that persist between the two calculations are due

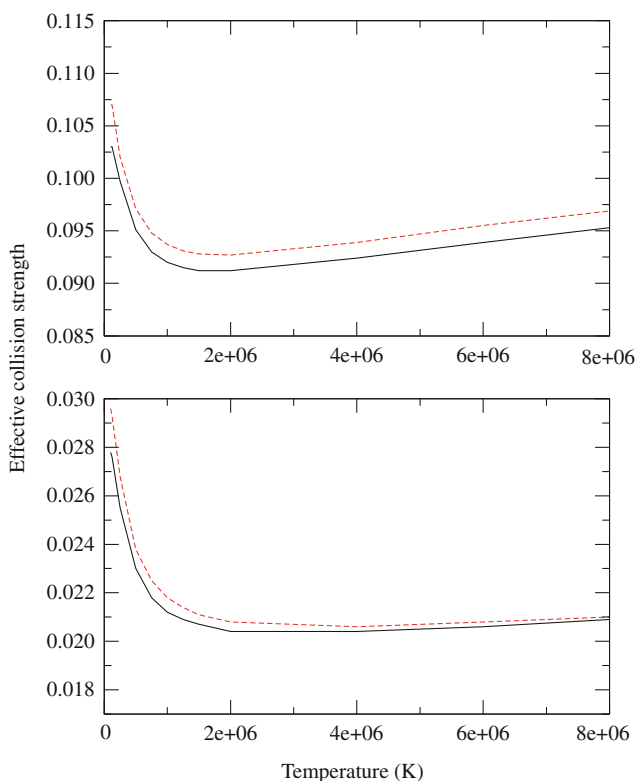


Fig. 5.13 Electron collisions with Fe XV. Effective collision strengths for the $3s^2 \ ^1S_0 \rightarrow 3p^2 \ ^1D_2$ (upper graph) and $3s^2 \ ^1S_0 \rightarrow 3p^2 \ ^3P_2$ (lower graph) transitions. Breit–Pauli R -matrix results are represented by solid lines and the Dirac R -matrix results are represented by dashed lines (Fig. 2 from [103])

primarily to variations in the target states rather than due to differences in collision theories. Consequently, this work shows that the Breit–Pauli Hamiltonian can be used with confidence in calculating transitions between the relatively low- Z iron peak elements.

5.6.7 Electron Collisions with Xe XXVII

As our last example in this chapter we consider Dirac R -matrix calculations of electron collisions with Ni-like Xe XXVII (Xe^{26+}) ions by Badnell et al. [37]. The spectra arising from electron impact excitation of heavier ions, such as ions

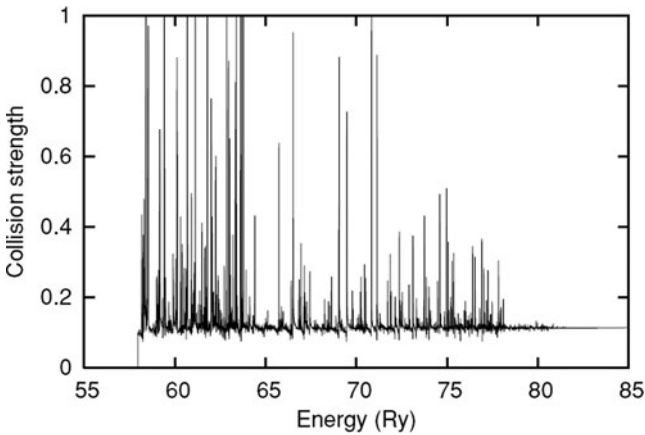


Fig. 5.14 Electron collisions with Xe^{26+} . Collision strength for the 129-state Dirac R -matrix $J = 0-0\ 3d^{10}\ 1S_0-3d^94d\ 1S_0$ transition (Fig. 2 from [37])

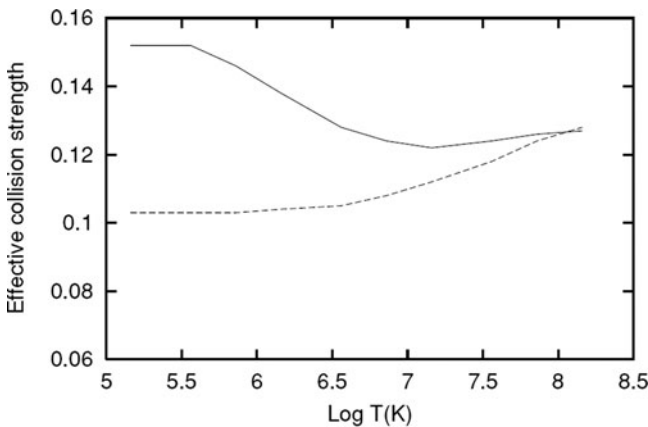


Fig. 5.15 Electron collisions with Xe^{26+} . Effective collision strength for the 129-state Dirac R -matrix $J = 0-0\ 3d^{10}\ 1S_0-3d^94d\ 1S_0$ transition. *Solid curve*: 129-state Dirac R -matrix calculation; *dashed curve*: plane wave Born approximation (Fig. 3 from [37])

of Xe, are important in many applications such as found in ITER (International Thermonuclear Experimental Reactor) and in the context of microlithographic light sources required to provide the next generation of etching for the semiconductor industry. In this work results for “feature photon emissivity coefficients”, which are important in these applications, were obtained for Xe^{26+} from the calculated collision strengths.

In order to obtain accurate results for this relatively heavy ion the Dirac R -matrix program DARC, discussed in Sect. 5.5.1, was used in the internal R -matrix region which was interfaced with an extended and parallelized version of the external region program, originally developed for the Opacity Project [100, 860], discussed in Sect. 8.3. The calculation included 129 states of Xe^{26+} arising from the configurations $3d^{10}$ and $3d^9n\ell$ for $n = 4$ and 5 and $\ell = 0$ to $n - 1$, which yield a maximum of 821 coupled channels. Also, 21 continuum basis orbitals were retained in each channel for $2J = 1-43$ and 16 continuum basis orbitals were retained for $2J = 44-71$, resulting in Hamiltonian matrices of rank 17,356 and 13,136, respectively. The contribution to the cross sections from $2J > 71$ (“top-up”) was obtained for dipole-allowed transitions using the sum rule proposed by Burgess [149] and for non-dipole transitions by assuming a geometric series in energy.

As an example of this study we show in Fig. 5.14 the results of the 129-state calculation of the strong $J = 0-0$ collision strength for the $3d^{10} \ ^1S_0-3d^94d \ ^1S_0$ transition, which populates the upper level of the lasing transition $3d^94d \ ^1S_0-3d^94p \ ^1P_1$ in Xe^{26+} . We see that over most of this energy range the collision strength is dominated by resonance structure which has to be included to obtain accurate results. To see this we compare the Maxwellian-averaged effective collision strength for this transition with plane wave Born approximation calculations in Fig. 5.15. We see that the Dirac R -matrix calculation is $\sim 18\%$ larger than the Born result at $\log T(K) = 6.8$, which corresponds to the temperature of peak fractional abundance for Xe^{26+} over a wide range of electron densities. We also see that at lower temperatures this discrepancy becomes even larger.

In conclusion, these calculations show that the Dirac R -matrix calculations give significantly different effective collision strengths from the Born approximation in the temperature range of interest. In addition, the resonance enhancement of the effective collision strength plays a crucial role in obtaining accurate results. In general, the Dirac R -matrix method will play an essential role in obtaining accurate electron collision strengths for the heaviest atomic targets at energies and temperatures of importance in many applications.